Targeted liposomes for drug delivery across the blood-brain barrier

ISBN: 978-90-39355220

Cover design: Mikenzo Communicatie, Utrecht, The Netherlands
Printed by: Ipskamp Drukkers B.V., Enschede, The Netherlands

Printing of this thesis was financially supported by:

Utrecht Institute for Pharmaceutical Sciences, Utrecht, The Netherlands
J.E. Jurriaanse Stichting, Rotterdam, The Netherlands
Phospholipid Research Center, Heidelberg, Germany
BD Biosciences, Franklin Lakes, USA

Targeted liposomes for drug delivery across the blood-brain barrier

Liposomen voor gericht geneesmiddeltransport
over de bloed-hersenbarrière
(met een samenvatting in het Nederlands)

PROEFSCHRIFT

ter verkrijging van de graad van doctor aan de Universiteit Utrecht
op gezag van de rector magnificus, prof.dr. G.J. van der Zwaan, ingevolge
het besluit van het college voor promoties in het openbaar te verdedigen
op maandag 18 april 2011 des middags te 2.30 uur

door

Inge van Rooy

geboren op 20 december 1982 te Waalre

Promotoren:	Prof.dr.ir. W.E. Hennink Prof.dr. G. Storm
Co-promotoren:	Dr. E. Mastrobattista Dr. R.M. Schiffelers

Beyond the line of blue -
The boundary of the star
Which turneth at the view
Of thy barrier and thy bar -
Of the barrier overgone
By the comets who were cast
From their pride, and from their throne
To be drudges till the last -
To be carriers of fire
(The red fire of their heart)
With speed that may not tire
And with pain that shall not part -

Edgar Allan Poe

Table of contents

Chapter 1

General introduction

The blood-brain barrier

In 1885, Paul Ehrlich intravenously injected organic dyes into animals [1]. He found that the dyes would leak out of the capillaries and stain all organs, except for the brain. At that time, Ehrlich concluded that the brain simply had no affinity for the dyes. In 1913, his student Edwin Goldmann did the opposite and injected the dyes directly into the cerebro-spinal fluid of the brain [2]. He found that only the brain was stained, and the rest of the body was not. These experiments showed the existence of a barrier between the blood and the brain, which is today known as the blood-brain barrier (BBB).

This barrier protects the brain by strictly regulating transport in and out of the brain, thereby maintaining brain homeostasis. The downside of this tightly controlled barrier is that it also limits the transport of therapeutics into the brain. Drugs to treat central nervous system (CNS) disorders are often unable to penetrate into the brain to perform their actions. Approximately 98% of the small molecule drugs, and nearly 100% of the large molecule pharmaceutics (e.g. peptides, proteins and nucleic acids) cannot substantially cross this barrier [3].

At the same time, treatment is needed for serious CNS diseases, including depression, schizophrenia, epilepsy, Alzheimer's disease, Parkinson's disease, brain cancer, and cerebrovascular diseases. Furthermore, the incidence of CNS disorders increases with age. As the proportion of people aged over 60 years keeps growing, neuropharmaceuticals will become more important in the future [4]. Therefore, research is needed to optimize delivery of CNS drugs across the blood-brain barrier.

Morphology of the blood-brain barrier

The blood-brain barrier is mainly formed by the endothelial cells surrounding the brain capillaries (Figure 1). Features that distinguish cerebral endothelial cells from other endothelial cells include the lack of fenestrae, the presence of tight junctions and adherens junctions between the cells, reduced vesicular transport, and increased numbers of mitochondria [5]. The endothelial cells are completely covered by a basal lamina (Figure 1), which consists of type IV collagen, fibronectin and laminin. In this membrane pericytes are embedded, covering about 20-30% of the endothelial cells. The basal lamina is surrounded by astrocyte end-feet [6].

Pericytes

The pericytes embedded in the basal lamina entangle the capillaries with claw-like appendices [7]. They have important functional properties: they mediate inflammatory processes, regulate the activity of the brain endothelial cells, and induce capillary-like structures to which they rapidly associate [8]. Pericytes regulate BBB-specific gene

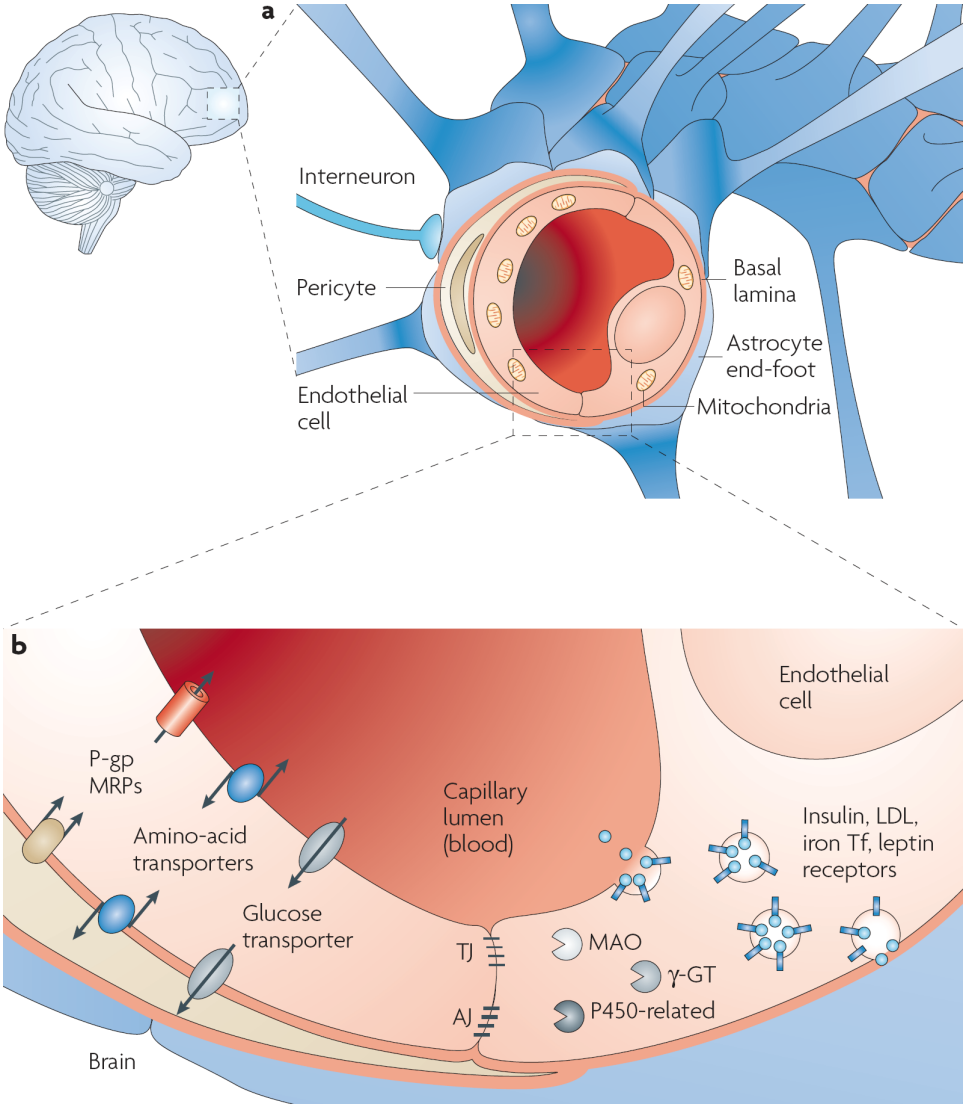

Figure 1. (***a***) *The blood–brain barrier (BBB) is formed by endothelial cells of the cerebral capillaries. These endothelial cells interact with perivascular elements such as basal lamina, astrocytic end-feet processes, and pericytes to form a functional BBB.* (***b***) *Cerebral endothelial cells form complex tight junctions (TJ) and adherens junctions (AJ). In addition, the presence of intracellular and extracellular enzymes such as monoamine oxidase (MAO), γ-glutamyl transpeptidase (γ-GT), and several cytochrome P450 enzymes endow this dynamic interface with metabolic activity. Specific receptors such as the insulin, low-density lipoprotein (LDL), iron transferrin (Tf) and leptin receptors are involved in brain transport of large molecules. Efflux transporters include P-gp (P-glycoprotein) and MRPs (multidrug resistance-associated protein family). Reprinted by permission from Macmillan Publishers Ltd: Nat Rev Drug Discov. [6], copyright (2007).*

expression patterns in endothelial cells, thereby decreasing endothelial transcytosis. Furthermore, they induce polarization of astrocyte end-feet surrounding the capillaries [9].

Astrocytes

Astrocytes of the grey matter are characterized by many thick cytoplasmic appendices and large nuclei. The endings of these appendices form cap-like structures, known as end-feet (Figure 1). These tightly attach to neurons on one side and to capillaries on the other, thereby mediating direct interaction between these cells [7]. Astrocytes are able to secrete a range of growth factors and cytokines, including transforming growth factor-β (TGFβ), glial-derived neurotrophic factor (GDNF), basic fibroblast growth factor (bFGF) and angiopoetin 1 (ANG1). These factors strongly contribute to the BBB phenotype of endothelial cells, leading to tighter tight junctions, and the expression and polarized localization of specific enzymes and transporters such as P-glycoprotein and GLUT-1 [10].

Tight junctions and adherens junctions

Tight junctions between cerebral endothelial cells are characterized by fusion of the outer leaflets of adjacent plasma membranes at intervals along the intercellular space between the cells [5]. These fusions prevent the paracellular transport of molecules between the endothelial cells [7]. Tight junctions consist of three integral membrane proteins: claudin, occludin and junctional adhesion molecules (JAMs). They are supported by cytoplasmic accessory proteins including ZO-1, ZO-2, ZO-3, cingulin and others, which link the plasma membrane proteins to the actin cytoskeleton (Figure 2). Claudins are the major components of tight junctions. They are 22 kDa phosphoproteins with 4 transmembrane domains. They bind to other claudins on adjacent endothelial cells to form the primary fusion. The carboxy terminal of claudins bind intracellularly to the ZO proteins [11]. The second component of the tight junctions, occludin, is a 65 kDa protein. Like claudin, it has 4 transmembrane regions and its cytoplasmic carboxy terminal interacts directly with the ZO proteins. Two extracellular loops of occludin and claudin on neighboring cells form the paracellular component of the BBB. The third group of proteins involved in tight junction formation is the JAMs. These proteins are members of the immunoglobulin superfamily with masses around 40 kDa. They contain a single transmembrane domain coupled to two extracellular 'immunoglobulin-like' loops [5].

Besides tight junctions, brain capillary endothelial cells are also joined by adherens junctions. They are located near the basolateral side of the endothelial cells, and consist of cadherins that interact with each other when calcium ions are present. Cadherins are linked to the actin cytoskeleton by catenins. Evidence suggests that ZO-1 and catenins cooperate, which implicates that tight junctions and adherens junctions both are needed to form the BBB [7,12].

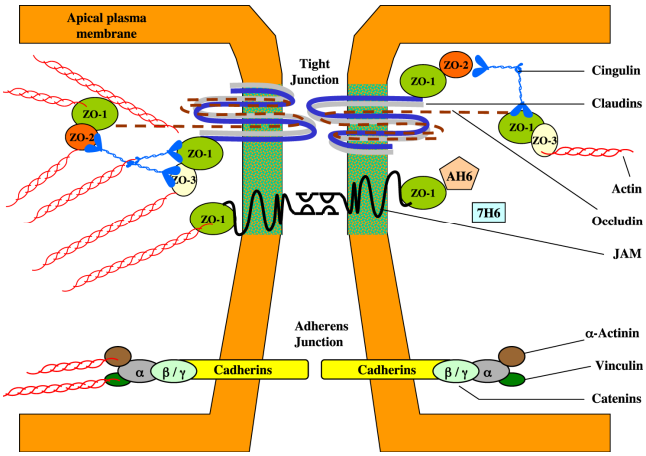

Figure 2. *Proposed locations of the major proteins associated with tight junctions at the BBB are shown. The tight junction is embedded in a cholesterol-enriched region of the plasma membrane (shaded). With kind permission from Springer Science+ Business Media [5], figure 4, modified from [12].*

Transport across the BBB

There are several transport pathways for molecules to enter the brain. They include transcellular lipophilic diffusion, paracellular hydrophilic diffusion, carrier mediated transcytosis, adsorptive mediated endocytosis, and receptor mediated endocytosis (see Figure 1 of chapter 2).

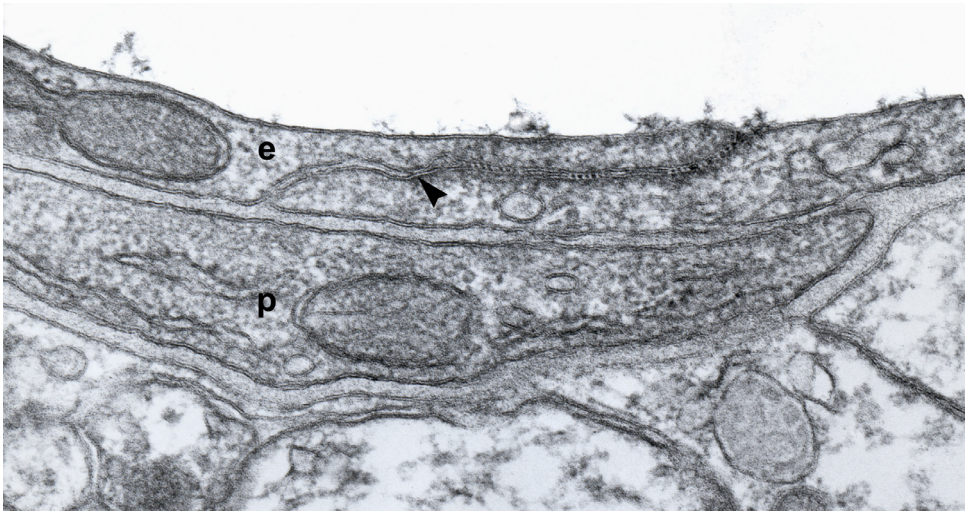

Figure 3. *Segment of normal cerebral cortical capillary wall consists of endothelium (e) and a pericyte (p) separated by basement membrane. This rat was injected with ionic lanthanum, which has penetrated the interendothelial space up to the tight junction (arrowhead). ×70,000. With kind permission from Springer Science+Business Media [5], figure 1.*

The paracellular hydrophilic diffusion pathway may be used by small water soluble molecules that can diffuse through the tight junctions [14]. However, most of these molecules can penetrate the interendothelial space just up to the tight junctions, and not beyond (Figure 3). Lipophilic diffusion can be used by lipid soluble molecules with molecular weights below 400 Da, and most of the current CNS therapeutics enter the brain via this pathway [15].

Carrier-mediated transcytosis is used by small molecules such as glucose, amino acids, and purine bases to provide the brain with nutrients. These carriers are membrane-bound structures and are highly selective.

The final transport route is through receptor or adsorptive-mediated endocytosis. This is the only way for larger molecules such as antibodies and proteins, and structures such as nanoparticles to be transported into the brain [16]. Adsorptive-mediated transcytosis is initiated by the binding of polycationic substances to the negatively charged endothelial cell membranes by non-specific electrostatic interactions [14]. Receptor-mediated endocytosis involves binding of a ligand to a specific receptor, and is therefore more specific compared to adsorptive-mediated endocytosis, and consequently used more often for targeting purposes. Brain entry through receptor-mediated endocytosis consists of the following steps [17]:

1. *Binding of the ligand to the receptor*. This induces a modification of the receptor protein, either by cross-linking or by a conformational change of the receptor molecule. An endocytic event is triggered in the membrane surrounding the receptor, leading to formation of pits in the membrane, which are coated on the intracellular site with clathrin.
2. *Endocytosis*. The coated pits invaginate and form vesicles. The pits lose their clathrin coat and fuse with endosomes. The vesicle acidifies, causing the ligand to dissociate from the receptor.
3. *Movement through the endothelial cell.* The ligand-containing endosome may fuse with a lysosome, leading to degradation of its content. Alternatively, the endosome is transported towards the basolateral side of the cell.
4. *Exocytosis.* If the vesicle and its contents are not degraded, the transcytosed vesicle will ultimately be exocytosed at the basolateral side of the cell membrane.

Brain drug delivery

For drugs that do not easily penetrate the BBB, many attempts have been made to facilitate brain entry. These include the use of invasive methods, and the use of the above mentioned transport pathways.

Delivery by invasive methods

Traditional methods to get drugs into the brain completely circumvent the BBB or its associated endogenous transport pathways. These methods include intracerebroventricular (icv) injection, intracerebral (ic) injection, and permeability enhancement. These methods are much more invasive than oral or intravenous administration.

Upon icv injection, the drug is injected into the cerebrospinal fluid (CSF). At this point, the drug has to diffuse from the CSF to the brain parenchyma via the ependymal barrier, which is particularly accessible for compounds with a molecular weight smaller than 5000 Da [14]. However, the drug concentration in the brain parenchyma decreases exponentially with the distance from the ependymal surface [18]. Additionally, the CSF pool has a turn-over time of 4-5 hours, and the drugs are cleared from the CSF via this flow. Because of the rapid clearance of the CSF and the slow diffusion rate of drugs, there is generally insufficient diffusion of drugs into the brain parenchyma. However, icv injection can be effective when local administration of drugs is needed (e.g. treatment of tumors) or when the target receptor lies in close proximity to the ependymal surface [19].
Another invasive injection method is ic injection. With this method, drugs are injected straight into the brain parenchyma. However, this has turned out to be ineffective because of insufficient diffusion of the injected drugs from the site of injection [20].
A third invasive method to enhance drug uptake into the brain is by increasing the permeability of the BBB by osmotic disturbance [21]. This can be achieved by infusion of a hypertonic agent (e.g. mannitol 25%) in the carotid artery for 30 seconds. This opens the BBB for about 30 minutes, presumably by shrinking the endothelial cells and disrupting the tight junctions, so that the drugs can freely diffuse into the brain [22]. In this way, large molecules can be delivered. However, the opening of the BBB makes it possible for harmful substances in the circulation (e.g. neurotransmitters and toxins) to enter the brain as well, impeding clinical use [21]. This problem is also present when bradykinin or other cytokines (e.g. histamine) are used to open the tight junctions of the BBB, possibly restricting their use to terminal patients with brain tumors [23].

Delivery by carrier-mediated transcytosis

For a drug to cross the BBB by carrier-mediated transport, it has to mimic the structure of the endogenous ligand of the carrier. As the expression of these carriers is often polarized, knowledge of the stereochemical transport requirements of these carriers has been used to develop drugs that cross the BBB by carrier-mediated transport [24]. Examples include L-DOPA and gabapentin (using the large neutral amino acid transporter, LAT), mepyramine and lidocaine (using the organic cation transporter, OCT) and glycosylated morphine (using the glucose transporter, GLUT-1) [22].

Disadvantages of the use of carrier systems are competition of drugs with endogenous ligands, and the narrow substrate specificity. This prevents the use of carriers as transporters for many large molecules and nanoparticles [25].

Delivery by adsorptive-mediated endocytosis

Adsorptive-mediated endocytosis is hardly used for drug targeting to the brain, because this process also occurs to a large extent in other organs of the body (e.g. liver, kidneys), which decreases brain specificity [26]. Furthermore, the cationic charge may lead to aggregate formation in the circulation. Brain targeting using adsorptive-mediated endocytosis has been accomplished though, by using cationized human serum albumin (cHSA) as a transport vector. This charged protein coupled to ^{3}H-biotin was able to cross the BBB in significant amounts [27].

Delivery by receptor-mediated endocytosis

Receptor-mediated endocytosis uses targeting ligands that specifically bind to receptors expressed on the brain endothelial cells. The drug of interest can be either directly conjugated to the ligand, or the drug can be encapsulated into nanoparticles which are coupled to the ligand on the outside of the particle [28]. Particles that have been used for this purpose include liposomes, solid lipid nanoparticles, nanogels, dendrimers, albumin nanoparticles, and polymeric particles such as poly(lactic-co-glycolic acid) (PLGA) and poly(butyl cyanoacrylate) (PBCA) nanoparticles. Ligands include peptides, proteins, and antibodies.

The most studied receptor used for drug targeting to the BBB is the transferrin receptor (TfR). The natural ligand for this receptor is iron-bound transferrin (holo-transferrin), a plasma protein which transports iron in the circulation [29]. The receptor is highly expressed on immature erythroid cells, placental tissue, and rapidly dividing cells [30]. Furthermore it is expressed on hepatocytes and endothelial cells of the blood–brain barrier. In contrast to apo-transferrin, holo-transferrin has a high affinity for the TfR. Therefore holo-transferrin has been used to target drugs to the brain [31,32]. However, this application is limited *in vivo*, because endogenous levels of transferrin are high, resulting in nearly saturated transferrin receptors [14]. Nevertheless, successful brain targeting using transferrin as a targeting ligand has been accomplished. For example, the fusion of transferrin to mouse-human chimeric IgG3 showed significant uptake into the brain parenchyma [33]. In another study, nanocapsules coated with transferrin increased the delivery of encapsulated azidothymidine to the brain [31].

A strategy to circumvent endogenous competition of transferrin while targeting the transferrin receptor, is by using antibodies directed against the TfR. The most studied TfR-targeted antibody is the mouse anti-rat monoclonal antibody OX26. This antibody does not bind to the transferrin binding site on the TfR, but uses another epitope. Therefore binding does not interfere with normal transferrin transport, and there is no competition with endogenous transferrin [28]. Several compounds have been successfully targeted to the brain using this approach. Brain-derived neurotrophic factor (BDNF) showed significant uptake in rat brain tissues when conjugated to OX26 [34], and a biotinylated vasoactive intestinal peptide analog was taken up successfully in the brain after conjugation with OX26 [35].

The main disadvantage of OX26 is that the antibody is directed against the rat TfR and does not bind the TfR of other species, limiting the applicability to rats. For the use in mouse models, other monoclonal antibodies have been investigated, including 8D3 [36] and RI7217 [37]. When directly compared, brain uptake of 8D3 is higher (3.1 %ID/g) than uptake of RI7217 (1.6 % ID/g) [38]. However, RI7217 is more selective for the brain, as it is poorly taken up by the liver and kidney, in contrast to 8D3 [38].

Another widely characterized receptor on the BBB is the insulin receptor. Its endogenous ligand is insulin, however, insulin itself cannot be used as a ligand for targeting because high doses of insulin would have to be administered to be effective. This could lead to overdosing of insulin, causing hypoglycemia [28]. Therefore, also for this receptor, antibodies have been used for targeting, like the murine 83-14 monoclonal antibody [39].

Other receptors that have been used for drug delivery to the brain include the low-density lipoprotein receptor (LDLR) and the LDLR-related protein (LRP).These receptors can bind multiple ligands, including low-density lipoprotein (LDL), receptor associated protein (RAP), lactoferrin, melanotransferrin (P97), and apolipoproteins. Melanotransferrin has been successfully conjugated to chemotherapeutic agents to increase brain uptake for the treatment of brain tumors [40].

Also apolipoproteins have been successfully used as targeting ligands. Loperamide-loaded nanoparticles covalently attached to apolipoprotein E exerted analgesic effects in the brain, while non-modified control nanoparticles loaded with loperamide did not. Also, apolipoprotein E3 (a high receptor binding affinity apolipoprotein E) coupled loperamide loaded nanoparticles induced analgesic effects, whereas nanoparticles coupled to apolipoprotein E2 (a low receptor binding affinity apolipoprotein E) did not [41].

Phage display to identify targeting ligands

Besides using known ligands to target to known receptors, a different approach can be used in order to identify new ligands that have selectivity for the brain without requiring knowledge on the nature of the receptor. One possible approach is the technique of phage display, which was first described by Smith in 1985 [42]. The method starts with the creation of a bacteriophage library. DNA of a wild-type phage is modified with a foreign genetic insert that encodes for a peptide, protein, or antibody. Most often random peptide libraries are used. The library is created in such a way that the expressed foreign peptide is fused to either the minor or the major coat protein of the phage (Figure 4). In a random peptide library, the diversity of peptides should be as high as possible. Usually, libraries with a diversity of 10^8-10^9 different peptides are created [43].

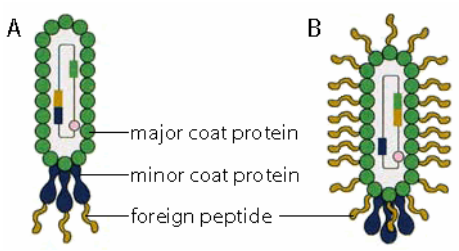

Figure 4. *Schematic representation of the bacteriophage. A foreign peptide can be displayed at the phage surface, fused to either the minor coat protein (**A**) or the major coat protein (**B**). With kind permission from Springer Science+Business Media: Plant Mol Biol, Phage display: practicalities and prospects, 50, 2002, 837-54, W.G. Willats, fig. 1 [43].*

Phage display selection can be described as a cycle (Figure 5). After the library has been created, it is incubated with the desired target, to select the phage out of the library with the proper characteristics to bind to the target. This process is called panning. The target can be a protein, a cell, a tissue, or even *in vivo* panning is possible (biopanning) by perfusing organs with phage or by iv injection of phage [45]. In the next step, the unbound phage are washed away and bound phage are eluted or isolated. The isolated phage are amplified in bacteria and additional panning cycles are performed to enrich the pool with high target-affinity phage. After three to four cycles, individual clones showing high selectivity and affinity to the target may be obtained [43]. The peptide sequence of the obtained phage can be analyzed by isolating and sequencing the phage DNA.

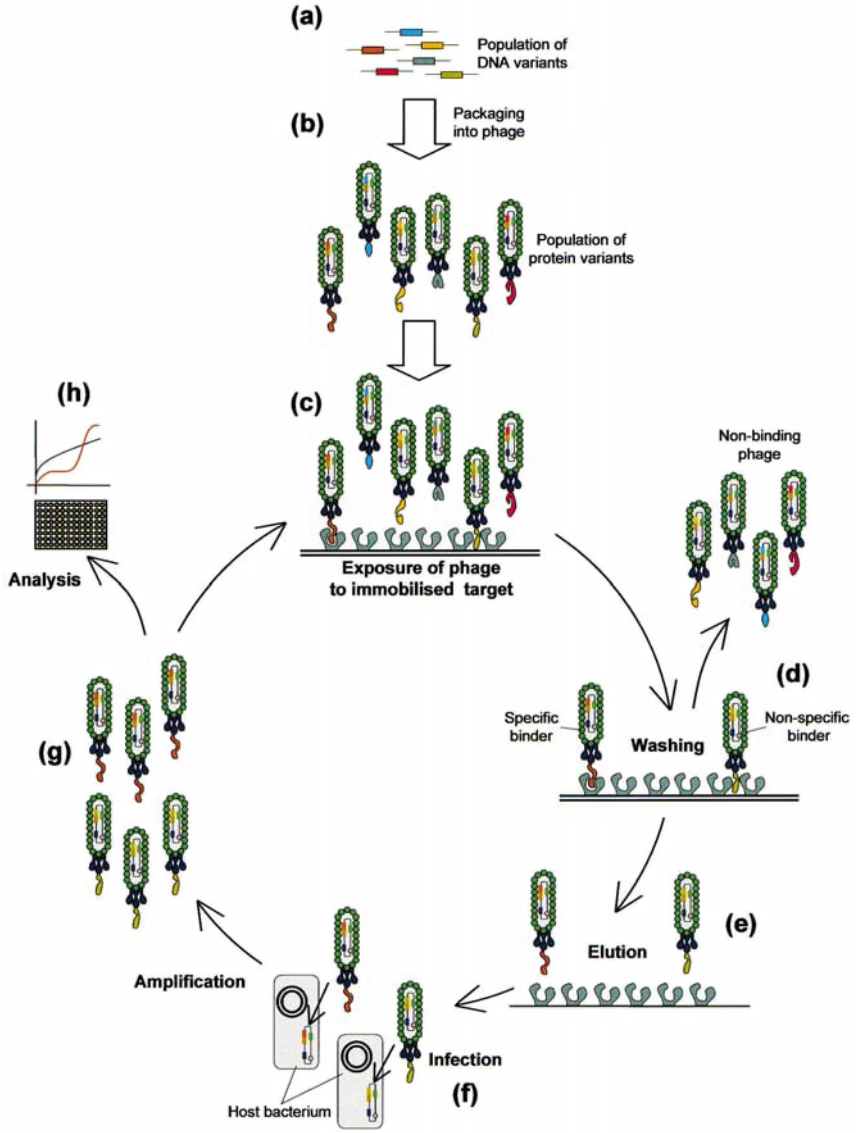

Figure 5. *The phage display cycle (**a**) A library of DNA sequences is created and (**b**) cloned into phage genomes. (**c**) The phage library is exposed to target molecules. (**d**) Non binding phage are washed off. (**e**) Bound phage are eluted. (**f**) Eluted phage are infected into host bacterial cells and thereby amplified. (**g**) This amplified phage population is in effect a secondary library that is greatly enriched in phage displaying peptides or proteins that bind to the target. (**h**) After several rounds of panning phage populations may be selected and analyzed. With kind permission from Springer Science+Business Media: Plant Mol Biol, Phage display: practicalities and prospects, 50, 2002, 837-54, W.G. Willats, fig. 2 [44].*

A successful phage display selection *in vivo* has been performed by Kolonin *et al.* [46]. Murine muscle, bowel, uterus, kidney, brain and pancreas were screened with a phage library by intravenously injecting the library, thereby distributing the phage throughout the body. The specific organs were taken out and phage that bound to the organs were isolated, leading to identification of several new organ-specific ligands. Additionally, several other studies have shown that phage display can be a very useful technique in the discovery of novel targeting ligands [45,47-49].

Liposomes for brain drug delivery

Liposomes have been widely used for brain delivery *in vivo* [50-53]. Liposomes are self-assembling colloidal structures consisting of lipid bilayers surrounding an aqueous compartment, and are able to encapsulate a wide variety of hydrophilic drugs within this compartment [54]. Lipophilic drugs can be incorporated into the lipid bilayer. Cholesterol is usually included in the bilayer to modify the permeability and stability of the liposome. To increase the circulation time *in vivo*, liposomes can be coated with polyethylene glycol (PEG). A great advantage is the ability to fine-tune the lipid composition, the surface charge, and the size. Brain-targeting ligands can be conjugated to the surface. One method to accomplish this is by a maleimide-thiol reaction. Phospholipid-maleimide conjugates or phospholipid-PEG-maleimide conjugates can be incorporated into the bilayer of the liposome. Thiolated ligands can be subsequently coupled by a thioether bond. The thiol groups of the ligands can either be intrinsically present in peptides or proteins (i.e. cysteine) or synthetically introduced into the molecule, for example via a N-succinimidyl-S-acetylthioacetate (SATA) modification (Figure 6) [55].

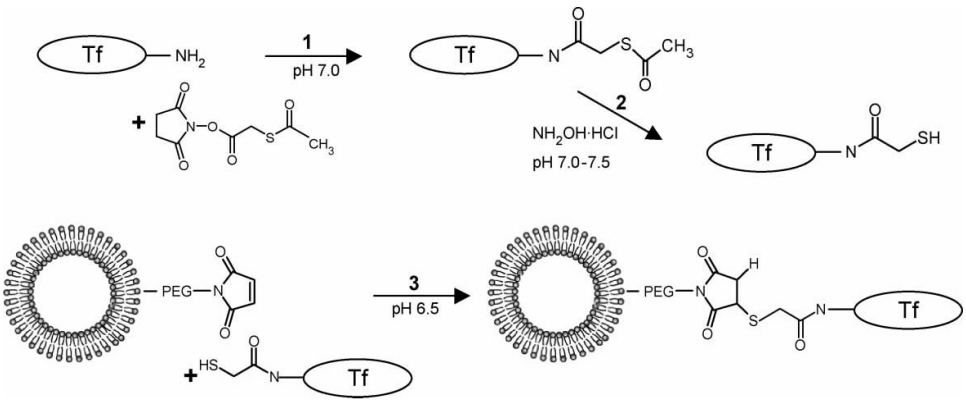

Figure 6. *Reaction scheme of the thiolation of transferrin (Tf) with N-succinimidyl-S-acetylthioacetate (SATA, step 1), the activation of thiolated Tf with hydroxylamine HCl (step 2) and the conjugation of Tf to liposomes, bearing maleimide-PEG-DSPE (step 3). Journal of drug targeting by Visser CC [55]. Copyright 2004 by Informa medical and pharmaceutical science – journals. Reproduced with permission.*

Aim and outline of this thesis

Nearly every neuron in the brain is connected to a capillary, with an average distance from neuron to capillary of 8–20 µm [56]. Therefore, the vascular route is the most promising to achieve a wide brain distribution of drugs. However, for drugs to be effective in the brain, they have to cross the BBB. Although many strategies have been attempted, and several preclinical successes have been achieved, a good brain delivery system is still lacking today. The aim of this thesis is to investigate the potential of ligand-modified liposomes to target drugs across the BBB.

Brain uptake is often studied using *in vitro* models. However, in this thesis, *in vivo* experiments are also performed to determine the uptake of liposomes into the mouse brain. Measuring brain uptake *in vivo* is easier said than done. Therefore, in **chapter 2**, current methods to study brain uptake are reviewed. Next to traditional methods to study the uptake of small molecules into the brain, this review focuses on methods to study the uptake of nanoparticles, for which different techniques have been applied.

After this technical exploration, matters are taken into our own hands, and the search for a brain-targeting ligand begins. First, in **chapter 3**, five different targeting ligands that have been described in literature are being evaluated. Liposomal formulations modified with the selected ligands are tested for their brain-targeting potential *in vitro* and *in vivo*. To differentiate between liposomes internalized by the brain endothelial cells, and liposomes that have crossed into the brain parenchyma, a brain capillary depletion technique is used to separate these fractions.

Brain-targeting ligands that have been described in literature are far from ideal. Nearly all targeted receptors are not only expressed on brain endothelial cells, but also on other sites in the body, making it difficult for high quantities of targeted formulations to reach the brain. Taking this into account, the search for an ideal ligand continues. In **chapter 4**, an attempt is being made to find a new specific brain-targeting peptide ligand, using the aid of phage display. A 15-amino acid peptide library is perfused through mouse brain capillaries *in situ*. The phage are infused via the heart, which makes them pass multiple endothelial sites (i.e. aorta and carotid arteries) before reaching the brain, allowing for a negative selection of ubiquitous endothelial-binding phage. After three panning rounds *in situ*, the phage are tested for cross-reactivity with human endothelial cells *in vitro*, and the best binders are selected.

After this selection, the 15-amino acid peptides displayed by the phage are synthetically produced to test their function as targeting ligands. In **chapter 5**, the peptides are

coupled to liposomes, and their brain-targeting potential is investigated *in vitro* and *in situ*. Additionally, measures to increase the functionality of these peptides are explored.

In above mentioned chapters, liposomes are tested for their targeting capacity. The ultimate clinical aim is to encapsulate CNS drugs into the liposomes, in order to transport the drugs into the brain. In **chapter 6**, liposomal formulations of two new neurotensin-degrading enzyme inhibitors are prepared. These CNS drugs hold great potential for treating psychotic disorders, however, they show poor brain uptake *in vivo*. As a liposomal formulation could increase the uptake, the preparation of such a formulation is investigated. Parameters tested include the association of the drugs with liposomes, liposomal stability, and compound release in the presence of albumin.

Finally, in **chapter 7**, the findings of this thesis are summarized and future perspectives for brain drug targeting are discussed.

References

[1] P. Ehrlich. Das Sauerstoff-Bedurfnis des Organismus: Eine Farbenanalytische Studie. (1885).

[2] E.E. Goldmann. Vitalfarbung am Zentralnervensystem, Abh. Preuss. Akad. Wiss. Phys. Math. K1 1 (1913) 1-60.

[3] W.M. Pardridge. Blood-brain barrier delivery, Drug Discovery Today. 12 (2007) 54-61.

[4] W.M. Pardridge. Why is the global CNS pharmaceutical market so under-penetrated? Drug Discov.Today. 7 (2002) 5-7.

[5] S. Nag, Morphology and molecular properties of cellular components of normal cerebral vessels, in: Nag S (Ed.), The Blood-Brain Barrier: Biology and Research Protocols, 1st ed., Humana Press, Totowa, New Jersey, 2003, pp. 3-36.

[6] R. Cecchelli, V. Berezowski, S. Lundquist, M. Culot, M. Renftel, M.P. Dehouck, et al. Modelling of the blood-brain barrier in drug discovery and development, Nat.Rev.Drug Discov. 6 (2007) 650-661.

[7] J. Bernacki, A. Dobrowolska, K. Nierwinska, A. Malecki. Physiology and pharmacological role of the blood-brain barrier, Pharmacol.Rep. 60 (2008) 600-622.

[8] J.A. Kim, N.D. Tran, Z. Li, F. Yang, W. Zhou, M.J. Fisher. Brain endothelial hemostasis regulation by pericytes, J.Cereb.Blood Flow Metab. 26 (2006) 209-217.

[9] A. Armulik, G. Genové, M. Mäe, M.H. Nisancioglu, E. Wallgard, C. Niaudet, et al. Pericytes regulate the blood-brain barrier, Nature. 468 (2010) 557-561.

[10] S. Nakagawa, M.A. Deli, H. Kawaguchi, T. Shimizudani, T. Shimono, A. Kittel, et al. A new blood-brain barrier model using primary rat brain endothelial cells, pericytes and astrocytes, Neurochem.Int. 54 (2009) 253-263.

[11] M. Furuse, H. Sasaki, S. Tsukita. Manner of interaction of heterogeneous claudin species within and between tight junction strands, J.Cell Biol. 147 (1999) 891-903.

[12] K. Matter, M.S. Balda. Signalling to and from tight junctions, Nat.Rev.Mol.Cell Biol. 4 (2003) 225-236.

[13] J.D. Huber, R.D. Egleton, T.P. Davis. Molecular physiology and pathophysiology of tight junctions in the blood-brain barrier, Trends Neurosci. 24 (2001) 719-725.

[14] A.G. de Boer, P.J. Gaillard. Drug Targeting to the Brain, Annu Rev Pharmacol Toxicol. 47 (2007) 323-355.

[15] B. Pavan, A. Dalpiaz, N. Ciliberti, C. Biondi, S. Manfredini, S. Vertuani. Progress in drug delivery to the central nervous system by the prodrug approach, Molecules. 13 (2008) 1035-1065.
[16] W.M. Pardridge. The blood-brain barrier: bottleneck in brain drug development, NeuroRx. 2 (2005) 3-14.
[17] U. Bickel, T. Yoshikawa, W.M. Pardridge. Delivery of peptides and proteins through the blood-brain barrier, Adv.Drug Deliv.Rev. 46 (2001) 247-279.
[18] R.G. Blasberg, C. Patlak, J.D. Fenstermacher. Intrathecal chemotherapy: brain tissue profiles after ventriculocisternal perfusion, J.Pharmacol.Exp.Ther. 195 (1975) 73-83.
[19] W.M. Pardridge. Drug targeting to the brain, Pharm.Res. 24 (2007) 1733-1744.
[20] L.K. Fung, M. Shin, B. Tyler, H. Brem, W.M. Saltzman. Chemotherapeutic drugs released from polymers: distribution of 1,3-bis(2-chloroethyl)-1-nitrosourea in the rat brain, Pharm.Res. 13 (1996) 671-682.
[21] Brasnjevic, H.W.M. Steinbusch, C. Schmitz, P. Martinez-Martinez. Delivery of peptide and protein drugs over the blood-brain barrier, Progress in Neurobiology. 87 (2009) 212-251.
[22] D.J. Begley. Delivery of therapeutic agents to the central nervous system: the problems and the possibilities, Pharmacol.Ther. 104 (2004) 29-45.
[23] D.F. Emerich, R.L. Dean, C. Osborn, R.T. Bartus. The development of the bradykinin agonist labradimil as a means to increase the permeability of the blood-brain barrier: from concept to clinical evaluation, Clin.Pharmacokinet. 40 (2001) 105-123.
[24] W.M. Pardridge. CNS drug design based on principles of blood-brain barrier transport, J.Neurochem. 70 (1998) 1781-1792.
[25] S. Ohtsuki, T. Terasaki. Contribution of carrier-mediated transport systems to the blood-brain barrier as a supporting and protecting interface for the brain; importance for CNS drug discovery and development, Pharm.Res. 24 (2007) 1745-1758.
[26] Beduneau, P. Saulnier, J. Benoit. Active targeting of brain tumors using nanocarriers, Biomaterials. 28 (2007) 4947-4967.
[27] Y.S. Kang, W.M. Pardridge. Brain delivery of biotin bound to a conjugate of neutral avidin and cationized human albumin, Pharm.Res. 11 (1994) 1257-1264.
[28] Jones, E. Shusta. Blood–Brain Barrier Transport of Therapeutics via Receptor-Mediation, Pharmaceutical Research. 24 (2007) 1759-1771.
[29] P. Ponka, C.N. Lok. The transferrin receptor: role in health and disease, Int.J.Biochem.Cell Biol. 31 (1999) 1111-1137.
[30] C.C. Visser, S. Stevanovic, L.H. Voorwinden, L.v. Bloois, P.J. Gaillard, M. Danhof, et al. Targeting liposomes with protein drugs to the blood-brain barrier in vitro, European Journal of Pharmaceutical Sciences. 25 (2005) 299-305.
[31] V. Mishra, S. Mahor, A. Rawat, P.N. Gupta, P. Dubey, K. Khatri, et al. Targeted brain delivery of AZT via transferrin anchored pegylated albumin nanoparticles, J.Drug Target. 14 (2006) 45-53.
[32] K. Ulbrich, T. Hekmatara, E. Herbert, J. Kreuter. Transferrin- and transferrin-receptor-antibody-modified nanoparticles enable drug delivery across the blood-brain barrier (BBB), European Journal of Pharmaceutics and Biopharmaceutics. 71 (2009) 251-256.
[33] S.U. Shin, P. Friden, M. Moran, T. Olson, Y.S. Kang, W.M. Pardridge, et al. Transferrin-antibody fusion proteins are effective in brain targeting, Proc.Natl.Acad.Sci.U.S.A. 92 (1995) 2820-2824.
[34] Y. Zhang, W.M. Pardridge. Blood-brain barrier targeting of BDNF improves motor function in rats with middle cerebral artery occlusion, Brain Res. 1111 (2006) 227-229.
[35] D. Wu, W.M. Pardridge. Central nervous system pharmacologic effect in conscious rats after intravenous injection of a biotinylated vasoactive intestinal peptide analog coupled to a blood-brain barrier drug delivery system, J.Pharmacol.Exp.Ther. 279 (1996) 77-83.

[36] K. Kissel, S. Hamm, M. Schulz, A. Vecchi, C. Garlanda, B. Engelhardt. Immunohistochemical localization of the murine transferrin receptor (TfR) on blood-tissue barriers using a novel anti-TfR monoclonal antibody, Histochem.Cell Biol. 110 (1998) 63-72.
[37] J. Lesley, R. Hyman, R. Schulte, J. Trotter. Expression of transferrin receptor on murine hematopoietic progenitors, Cell.Immunol. 83 (1984) 14-25.
[38] H.J. Lee, B. Engelhardt, J. Lesley, U. Bickel, W.M. Pardridge. Targeting Rat Anti-Mouse Transferrin Receptor Monoclonal Antibodies through Blood-Brain Barrier in Mouse, J Pharmacol Exp Ther. 292 (2000) 1048-1052.
[39] W.M. Pardridge. Blood-brain barrier delivery of protein and non-viral gene therapeutics with molecular Trojan horses, Journal of Controlled Release. 122 (2007) 345-348.
[40] D. Karkan, C. Pfeifer, T.Z. Vitalis, G. Arthur, M. Ujiie, Q. Chen, et al. A unique carrier for delivery of therapeutic compounds beyond the blood-brain barrier, PLoS One. 3 (2008) e2469.
[41] K. Michaelis, M.M. Hoffmann, S. Dreis, E. Herbert, R.N. Alyautdin, M. Michaelis, et al. Covalent linkage of apolipoprotein e to albumin nanoparticles strongly enhances drug transport into the brain, J.Pharmacol.Exp.Ther. 317 (2006) 1246-1253.
[42] G.P. Smith. Filamentous fusion phage: novel expression vectors that display cloned antigens on the virion surface, Science. 228 (1985) 1315-1317.
[43] G.P. Smith, V.A. Petrenko. Phage Display, Chem. Rev. 97 (1997) 391-410.
[44] W.G.T. Willats. Phage display: practicalities and prospects, Plant Molecular Biology. 50 (2002) 837-854.
[45] R. Pasqualini, E. Ruoslahti. Organ targeting In vivo using phage display peptide libraries, Nature. 380 (1996) 364-366.
[46] M.G. Kolonin, J. Sun, K. Do, C.I. Vidal, Y. Ji, K.A. Baggerly, et al. Synchronous selection of homing peptides for multiple tissues by in vivo phage display, FASEB J. 20 (2006) 979-981.
[47] W. Arap, R. Pasqualini, E. Ruoslahti. Cancer Treatment by Targeted Drug Delivery to Tumor Vasculature in a Mouse Model, Science. 279 (1998) 377-380.
[48] Sadanandam, M.L. Varney, L. Kinarsky, H. Ali, R.L. Mosley, R.K. Singh. Identification of functional cell adhesion molecules with a potential role in metastasis by a combination of in vivo phage display and in silico analysis, OMICS. 11 (2007) 41-57.
[49] M. Zahid, B.E. Phillips, S.M. Albers, N. Giannoukakis, S.C. Watkins, P.D. Robbins. Identification of a cardiac specific protein transduction domain by in vivo biopanning using a M13 phage peptide display library in mice, PLoS One. 5 (2010) e12252.
[50] N. Shi, Y. Zhang, C. Zhu, R.J. Boado, W.M. Pardridge. Brain-specific expression of an exogenous gene after i.v. administration, Proc.Natl.Acad.Sci.U.S.A. 98 (2001) 12754-12759.
[51] Y. Xie, L. Ye, X. Zhang, W. Cui, J. Lou, T. Nagai, et al. Transport of nerve growth factor encapsulated into liposomes across the blood-brain barrier: in vitro and in vivo studies, J.Control.Release. 105 (2005) 106-119.
[52] Schnyder, S. Krahenbuhl, J. Drewe, J. Huwyler. Targeting of daunomycin using biotinylated immunoliposomes: pharmacokinetics, tissue distribution and in vitro pharmacological effects, J.Drug Target. 13 (2005) 325-335.
[53] E. Afergan, H. Epstein, R. Dahan, N. Koroukhov, K. Rohekar, H.D. Danenberg, et al. Delivery of serotonin to the brain by monocytes following phagocytosis of liposomes, J.Control.Release. 132 (2008) 84-90.
[54] V.P. Torchilin. Recent advances with liposomes as pharmaceutical carriers, Nat.Rev.Drug Discov. 4 (2005) 145-160.
[55] C.C. Visser, L.H. Voorwinden, L.R. Harders, M. Eloualid, L. van Bloois, D.J.A. Crommelin, et al. Coupling of Metal Containing Homing Devices to Liposomes via a Maleimide Linker: Use of TCEP to Stabilize Thiol-groups without Scavenging Metals, Journal of Drug Targeting. 12 (2004) 569-573.

[56] K.E. Schlageter, P. Molnar, G.D. Lapin, D.R. Groothuis. Microvessel organization and structure in experimental brain tumors: microvessel populations with distinctive structural and functional properties, Microvasc.Res. 58 (1999) 312-328.

Chapter 2

In vivo methods to study uptake of nanoparticles into the brain

Inge van Rooy
Serpil Cakir-Tascioglu
Wim E Hennink
Gert Storm
Raymond M Schiffelers
Enrico Mastrobattista

Pharmaceutical Research 28 (3):456-71 (2011)

Abstract

Several *in vivo* techniques have been developed to study and measure the uptake of CNS compounds into the brain. With these techniques various parameters can be determined after drug administration, including the blood to brain influx constant (K_{in}), the permeability-surface area (PS) product, and the brain uptake index (BUI). These techniques have been mostly used for drugs that are expected to enter the brain via transmembrane diffusion or by carrier-mediated transcytosis. Drugs that have limitations in entering the brain via such pathways have been encapsulated in nanoparticles (based on lipids or synthetic polymers) to enhance brain uptake. Nanoparticles are different from CNS compounds in size, composition and uptake mechanisms. This has led to different methods and approaches to study brain uptake *in vivo*. Here we discuss the techniques generally used to measure nanoparticle uptake in addition to the techniques used for CNS compounds. Techniques include visualization methods, behavioral tests, and quantitative methods.

Introduction

Essentially none of the large-molecule pharmaceutics (e.g. peptides, proteins and nucleic acids) can enter the brain, and over 98% of small molecule drugs cannot enter the brain either [1]. In the past years, several methods to study brain uptake of drugs have been developed. To enhance brain uptake, nanoparticles have been used to target drugs to the brain. Nanoparticles are different from CNS compounds in size, composition and uptake mechanisms. This has led to different methods and approaches to study brain uptake *in vivo*. Here we discuss the techniques generally used to measure nanoparticle uptake in addition to the techniques used for CNS compounds.

Drug transport at the blood-brain barrier

Transport from the blood to the brain is limited by the blood-brain barrier (BBB). The BBB is formed by brain endothelial cells that line the cerebral microvessels. It is supported by other cell types surrounding the endothelium, such as astrocytes and pericytes [2]. These surrounding cells contribute to the induction of many barrier characteristics of the endothelium, such as tight junctions, that closely join the endothelial cells together. Next to being a "physical barrier", the BBB is also a "transport barrier". This aspect is formed by specific transport proteins and transcytosis mechanisms that mediate the uptake and efflux of molecules. Thirdly, a "metabolic barrier" is formed by the expression of metabolizing enzymes such as peptidases, cytochrome P450 enzymes, and monoamine oxidases [3-5]. All of these barrier functions control and regulate both inward and outward transfer of molecules between blood and the brain.

There are several routes for the transport of molecules across the BBB (Figure 1). Paracellular transport of hydrophilic molecules is highly restricted by the tight junctions present between brain endothelial cells.
Lipid soluble molecules with molecular weights below 400 Da are able to cross by transcellular lipophilic diffusion, provided that they are not bound to plasma proteins to a high extent, or form a substrate for a transport system at the BBB. Based on physicochemical properties such as molecular weight and hydrogen bonding, predictions can be made whether a compound can cross the BBB via this route [6,7].

For a variety of molecules that are essential for brain function, such as amino acids, glucose, peptides, and proteins, specific endogenous BBB transporters exist. These are expressed at both the luminal and the basolateral membranes of the endothelium [8]. These transporters can be either defined as carriers or receptors.

Carriers are membrane-restricted systems. They are generally responsible for the transport of small molecules with a fixed size and mass smaller than 600 Da. Carrier-mediated transcytosis is used for the delivery of nutrients such as glucose, amino acids, and purine bases to the brain. It is substrate selective, and only drugs that closely mimic the endogenous carrier substrates will be taken up [9].

Endocytosis at the BBB is effectuated through adsorption or receptor binding. Adsorptive-mediated endocytosis is initiated by the binding of polycationic substances to negative charges on the plasma membrane [9]. Receptor-mediated endocytosis is initiated by the binding of a receptor-specific ligand. Following adsorption or binding, the substance is internalized and transported via the early endosome to the lysosome, or transcytosed to the plasma membrane. The only way for larger molecules and particles such as antibodies, lipoproteins, proteins and nanoparticles to be transported into the brain is via receptor or adsorptive-mediated endocytosis [10], which is different from small molecular weight CNS drugs. When compared to the peripheral endothelium, the cerebral endothelium has a much lower endocytotic and transcytotic activity, making BBB-passage of larger molecules difficult even when endocytosis is possible. In pathological conditions, the transport mechanism at the BBB might be up or down regulated [1].

Next to these influx systems, many efflux mechanisms exist at the BBB as well. These include P-glycoprotein, MDR-related protein, ABC transporters, and several others [1].They restrict entry of molecules into the brain by promoting luminal release of compounds, and are important in removing harmful substances from the brain, thereby reducing toxic side effects of CNS drug metabolites. Substrates for efflux transporters include peptides, lipids, cholesterol, hormones, CNS drugs, and metabolites [11].

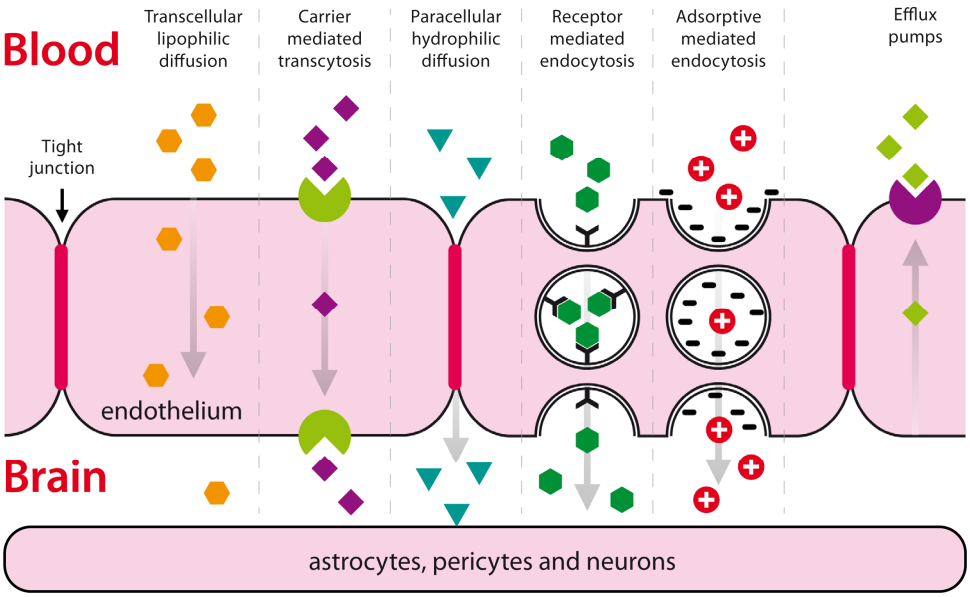

Figure 1. *Pathways across the blood-brain barrier [9,12].*

After *in vivo* administration, most CNS drugs will enter the brain in their free form via transcellular diffusion. However, many compounds with psychopharmacological activity do not posses the right physicochemical characteristics to be able to cross the BBB. One possible way to mask these characteristics is to package these compounds in nanoparticles. Nanoparticles are, of course, much larger and are only able to enter the brain endothelial cells via adsorptive or receptor-mediated endocytosis. Subsequent transcytosis to the basal side of the brain endothelial cells is required to enter into the brain parenchyma [2]. After a drug or nanoparticle formulation has been administered, the concentration that can be measured in the brain depends on several factors. These include: the plasma concentration-time curve, the extent of plasma protein binding, the permeability across the BBB, the efflux out of the brain by efflux transporters, the metabolic conversion by enzymes, the binding to membranes or intracellular sites in the brain, and the continual secretion and drainage of cerebrospinal fluid (CSF) and brain interstitial fluid (ISF) [5,13].

Many processes are thus involved in uptake and processing of drugs or particles at the BBB. From a pharmaceutical point of view, it is interesting to know at what rate and to what extent uptake occurs. Here we discuss the different techniques that have been used to measure uptake of molecules versus methods to asses uptake of nanoparticles.

In vivo techniques to measure compound permeation into the brain

A number of *in vivo* techniques have been developed to measure the uptake of CNS drugs into the brain. These techniques are routinely performed in rats or mice. Most of these assays capture the unidirectional uptake phase of a drug, without assumptions about the fate of the drug after it has entered the brain (e.g. cellular binding, degradation, and efflux) [14]. Two main parameters for the rate of brain penetration are often determined: K_{in} and PS product. K_{in} is the unidirectional influx constant from blood to brain. The PS product (alternatively also referred to as PA product) is the permeability-surface area product and is a measure of unidirectional clearance from blood to brain [15]. It represents that volume of plasma which gives up its content of the particular solute to interstitial fluid per unit time [16]. Both K_{in} and PS product are expressed in ml/min/g brain They are most commonly determined after intravenous injection or after *in situ* perfusion of the compound. They can also be determined in a specific brain region. In addition to K_{in} and PS, other pharmacokinetic parameters can be determined, for example by intracerebral microdialysis. Finally, brain specific parameters like the brain uptake index and the brain/plasma ratio can be determined. The methods to obtain these parameters are described below.

K_{in} and PS product determination by intravenous injection

The intravenous injection technique is regarded as the gold standard for brain uptake studies, because it involves fully physiological conditions [14,17]. With this technique, a (radiolabeled) compound is injected intravenously. Blood is sampled at various time points. A single brain tissue sample can be obtained at the terminal time point. K_{in} can be obtained using the following equation:

$$K_{in} = Q_{br} / AUC_{(0 \rightarrow T)}$$

- K_{in}: unidirectional influx constant from blood to brain (ml/min/g brain).
- Q_{br}: quantity of compound in the brain, without intravascular content (mass/g brain).
- $AUC_{(0 \rightarrow T)}$: integral of plasma concentration from t=0 to t=T.

Note that Q_{br} should represent the brain concentration without intravascular content [14]. The higher the drug concentration at the terminal time point, the more this will contribute to the concentration that is measured for the total brain. One way to remove the intravascular content is by extensively flushing the brain with a (heparinized) buffer before the brain is taken out. Alternatively, the intravascular volume can be determined by

co-administration of a vascular marker together with the drug. The marker is a substance that does not penetrate the blood-brain barrier, e.g. radiolabeled sucrose. When such a vascular marker has been included, Q_{br} can be calculated using the following equation:

$$Q_{br} = Q_{tot} - V_v C_{p(T)}$$

- Q_{tot}: total quantity of compound in the brain, including vascular content (mass/g brain).
- V_v: brain vascular volume (ml/g)
- $C_{p(T)}$: concentration of compound in the blood at time point T (mass/ml)

K_{in} and PS product determination by *in situ* perfusion

The *in situ* perfusion method complements the iv injection method. It has been originally developed for rats, but it has been expanded for mice, guinea pigs, and rabbits [18-20]. In the original rat method developed by Takasato *et al.* [21], the animal is anesthetised, and after a series of artery ligations, the perfusion fluid is infused up the common carotid artery (Figure 2). Perfusion can be stopped at a predetermined time point. Similar to the iv injection method, the perfusion fluid remaining in the brain can be flushed out, or a vascular marker can be included in the fluid. The brain is taken out for analysis of the compound. K_{in} can be obtained using the following equation:

$$K_{in} = Q_{br} / C_{pf} T$$

- Q_{br}: quantity of compound in the brain, without intravascular content (mass/g)
- C_{pf}: concentration of compound in the perfusion fluid (mass/ml)
- T: perfusion time

If a vascular marker has been included, Q_{br} can be calculated similar to the iv injection technique, using the following equation:

$$Q_{br} = Q_{tot} - V_v C_{pf}$$

- Q_{tot}: total quantity of compound in the brain, including vascular content (mass/g brain)
- V_v: brain vascular volume (ml/g brain)
- C_{pf}: concentration of compound in the perfusion fluid (mass/ml)

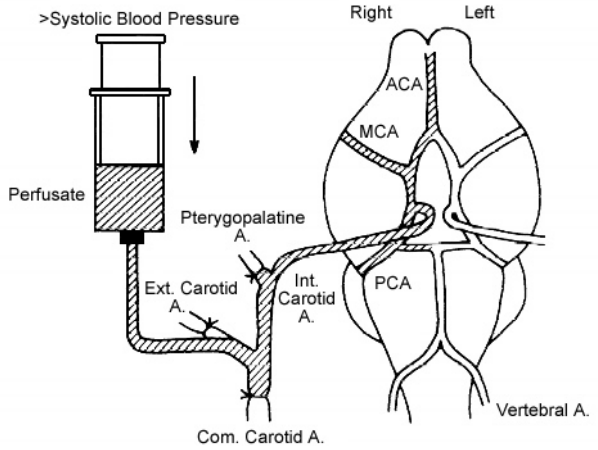

Figure 2. *Schematic representation of* in situ *brain perfusion. ACA = anterior cerebral artery. MCA = middle cerebral artery. PCA = posterior cerebral artery. Takasato* et al. *Am J Physiol. 1984 [21]. Am Physiol Soc, with permission.*

The main advantages of the iv injection method are the ease of injection, the possibility to simultaneously measure pharmacokinetics, and the fully physiological conditions, enabling all transporters, junction proteins, and enzymes to be present at their physiological concentration. The main advantages of the *in situ* perfusion method are the ability to tailor the perfusion fluid, the constant infusion concentration, and the absence of compound metabolism in other organs [17,22]. The K_{in} from both the iv injection and the *in situ* perfusion method can be converted into the cerebrovascular permeability-surface area product. From the PS product, permeability P can be calculated, given that the capillary surface area S is known. However, usually only the PS product is reported. PS calculation can be done using the Renkin-Crone equation:

$$PS = -F \ln(1 - K_{in} / F)$$

- PS: permeability-surface area product (ml/min/g brain).
- F: cerebral blood or perfusion flow rate (ml/min/g brain) [23]

Examples of PS product values obtained *in vivo* range from 0.0003 ml/min/g for sucrose, a compound that is considered BBB impermeable, to 1.2 ml/min/g for caffeine which has a high permeability [24].

Brain uptake index (BUI)

The brain uptake index (BUI), represents the relative uptake of a drug compared to a reference substance [25,26]. The reference is freely diffusible across the BBB, such as ^{14}C-butanol. The test compound is also radiolabeled, for example with ^{3}H. A small volume of buffer containing both the test compound and the reference is rapidly injected into the common carotid artery of anesthetised animals (e.g. in the rat 0.2 ml in less than 0.5 s).The bolus passes through the brain in less than 2 seconds after injection. After 5-15 seconds, the brain is isolated, and the radioactivity in brain tissue and injected buffer is determined. The BUI can be calculated using the following equation:

$$BUI = \frac{^{3}H \text{ brain} / ^{14}C \text{ brain}}{^{3}H \text{ injected} / ^{14}C \text{ injected}}$$

The BUI can be expressed as a percentage by multiplying it by 100. The BUI represents the net uptake of the drug normalized by the net uptake of the reference compound. It is therefore a direct function of the single-pass extraction (E) [27]. If the extraction of the reference is known (for example 100% for butanol [28]), the extraction of the drug can be calculated:

$$E_{drug} = E_{reference} \times BUI$$

The BUI can be related to the PS product using the Renkin-Crone equation:

$$E = 1 - e^{-PS/F}$$

The main advantage of the BUI technique is that it is fast while its main disadvantage is the low sensitivity. Additionally, drugs that are taken up slowly cannot be studied with this method [14]. Examples of BUI values obtained *in vivo* are 1.4% for sucrose, and 90% for caffeine [24].

Quantitative autoradiography

Quantitative autoradiography can be used to determine the amount of radioactive test compound in specific regions of the brain, such as stroke-affected areas [29] or brain tumors [30], following oral, intravenous or subcutaneous administration to small animals. Blood is sampled at various time points, and the brain is taken out at the terminal time point. The brain is subsequently sectioned into 20-µm thick sections, and exposed to X-ray film along with radioactive standards. Intravascular volume can be determined in a separate experiment using a BBB impermeable marker, such as radiolabeled sucrose. K_{in}

and PS product can be calculated with equations similar to those used for the intravenous injection method. The strength of quantitative autoradiography lies in the high spatial resolution in the micrometer range [14,31].

Microdialysis

Intracerebral microdialysis involves the implantation of a microdialysis probe in the brain. The probe, which consists of a semipermeable membrane, is continuously perfused with a physiological solution. The test drug is administered to the animal by the desired route (e.g. oral, intravenous or subcutaneous). Drugs that cross the BBB and enter the brain interstitial fluid, can traverse the semipermeable membrane by diffusion into the physiological buffer. The buffer is sampled from the probe, and drug concentration is measured. The concentration in the sample reflects the concentration of free drug in the brain. The main advantage of microdialysis is that brain levels, as well as blood levels of the drug can be determined at many time points in one animal. From these data, pharmacokinetic parameters can be obtained. Drawbacks include the technical difficulties of the implantation, and the fact that highly lipophilic compounds are generally difficult to recover [32].

Brain/plasma ratio

Commonly used in the pharmaceutical industry is the brain/plasma ratio [33]. The test drug is administered to the animal by the desired route. At a predetermined time point, the blood is sampled and the brain is taken out. The brain is homogenized and the drug concentration is determined in both brain and plasma. If multiple animals were used for multiple time points, the AUC of both the brain and plasma can be obtained. The brain concentration is then divided by the plasma concentration. This can be the ratio of one time point or the ratio of the AUCs [34]. The ratio provides a measure of the extent of brain penetration, not of the rate of brain penetration. Usually, the presence of drug remaining in the brain vasculature is not taken into account.

External detection methods

The techniques described so far involve sampling from the brain. Next to these invasive techniques, several non-invasive external imaging techniques exist, including positron emission tomograpy (PET), and single photon emission computed tomograpy (SPECT). It has been shown that PET can be used to quantitatively measure the PS product [35]. However, PET and SPECT are in general used for imaging of transporters, receptors, inflammation, or tumors in the brain, and not for the uptake of compounds [36-38].

More in-depth information on the advantages and disadvantages of each of the above mentioned techniques can be found in references [14] and [39].

CNS compounds versus nanoparticles

As the vast majority of potential CNS compounds have limited brain uptake, they may benefit from the use of advanced delivery systems in order to cross the BBB. Nanoparticles have been widely used as drug carriers to increase uptake of such drugs into the brain. The drug is encapsulated in, or associated to the particle, thereby masking its physiochemical characteristics. Particles that have been used include liposomes, solid lipid nanoparticles, nanogels, dendrimers, albumin nanoparticles, and polymeric particles such as poly(lactic-co-glycolic acid) (PLGA) and poly(butyl cyanoacrylate) (PBCA) nanoparticles. In many cases, they are combined with targeting ligands on the particle surface to enhance uptake. Ligands can include peptides, proteins, and antibodies. An overview of recent studies that used nanoparticles to target to the brain *in vivo*, is given in table I.

The brain uptake methods described above are excellent methods to determine the brain uptake of compounds that are expected to be brain permeable and are taken up by transcellular diffusion, or for small molecules that are taken up by carrier-mediated transcytosis [9]. However, brain uptake of nanoparticles occurs differently from such small molecules. For most nanoparticles it has been demonstrated that brain uptake is initiated by adsorptive or receptor mediated endocytosis into brain endothelial cells. This process is considerably slower than drug permeation, and therefore less compatible with some of the methods described above, like the BUI technique [14]. Of all distribution and kinetic parameters that can be obtained after drug administration, the PS product is in many reviews referred to as the best measure of BBB permeability [5,39]. The PS product has been determined for many substances, including CNS compounds [19], neurotrophic factors [40], and amino acids [41]. However, for nanoparticle formulations, this parameter is not commonly used. Unlike the BUI method that measures permeability after seconds, the iv injection method to measure the PS product allows time points to be selected according the researcher's own desire, making the PS product compatible with nanoparticles, or any other substance for that matter. The reason why this 'gold standard' is not used often in BBB nanoparticle studies, may be because the parameter has been developed for drug molecules. When the PS product of a drug has been determined, this is often compared to a brain impermeable compound (e.g. sucrose), to a permeable compound (e.g. butanol), or to another drug. In this way, permeabilities of different drugs can be ranked. When studies are performed using nanoparticles, uptake is usually not compared to other drugs. The goal will rather be to compare free vs particulate drug, or to compare targeted vs non-targeted particles, regardless of any encapsulated drug. Only 2 out of 29 studies shown in table I included the PS product in their *in vivo* experiments, either the PS product of the particle itself [42], or the PS product of a loaded drug [43].

Species	Administration	vasc corr	Time points	Particle type	Ligand	Particle size (nm)	Method	Data representation	Times increase	%ID brain	%ID blood	Ref
mice	iv jugular & femoral	none	24, 48, 72h	lipo	8D3 Mab	-	β-gal plasmid staining, microsc	images	-	-	-	[44]
rats	iv femoral	vasc wash	0.25, 0.5, 1h	lipo	RMP-7	-	Evans blue lipo, abs	ug/100 mg	Non-targ vs targ 4.9 fold	Non-targ 0.002%. Targ 0.012% /brain*	-	[45]
rats	perfusion & iv tail	vasc wash	perf 2, 5, 15 min. iv 2h	lipo	OX26	150	FM	images	-	-	-	[46]
rats	iv femoral	vasc wash	0.5h	lipo	RMP-7	70	^{125}I-NGF lipo	ng/g PK data	Non-targ vs targ 3.19 fold	Non-targ 0.11% Targ 0.32% /brain*	Non-targ 49% Targ 58% total*	[47]
rats	iv jugular	vol marker	1h	lipo	OX26	150	^{3}H-Daunomycin lipo	%ID/g PS product	Non-targ vs targ 2 fold	Non-targ 0.005% Targ 0.01% /gram	Both 0.9% /ml	[43]
rats	iv tail	vasc wash	RA 4, 24h FM 4h	lipo	-	170	^{3}H lipid and ^{14}C serotonin. FM	%(dpm/g tissue) /dose	Free vs lipo 2-fold	Free drug 0.068%. Lipo drug 0.138% /gram	Both 1% /ml	[48]
mice	iv tail	none	0.5, 1, 2h	lipo	Lf	130	Coumarin-6 lipo, HPLC.	ug/g PK data	Non-targ vs targ 2.3 fold	npc	PK data	[49]
mice	iv tail	none	0.25, 0.5, 1, 2, 4, 8, 12, 24, 48, 72h	SLN	-	76	Prodrug DO-FUdR NP, HPLC	ug/g PK data	Non-targ vs targ 0.25h 1.3fold	Free drug 2.08% SLN drug 2.66% /gram*	Free 8.1% SLN 11.3% /ml*	[50]

Species	Administration	vasc corr	Time points	Particle type	Ligand	Particle size (nm)	Method	Data representation	Times increase	%ID brain	%ID blood	Ref
mice rats	perfusion & iv tail	vasc wash	Rats 45, 60, 90, 120s. Mice 2, 6h	SLN	thiamine	67	^{3}H-hexadecanol and ^{3}H-thiamine NP	mice %ID Rats PS, K_{in}	no increase	2h and 6h both 0.5% /brain	Non-targ 65% Targ 80% /total	[42]
rats	iv	none	0.5, 2, 4, 6, 24h	BSA NP	Tf	120	AZT NP, HPLC.	%ID PK data	Non-targ vs targ 2.3 fold	Non-targ 9.3% Targ 21.1 % /brain	Both 25% /total*	[51]
mice	iv	n.a.	15, 30, 45, 60, 90 120 min	HSA NP	ApoE or tween80	340	Loperamide NP, tail-flick test	% MPE	-	-	-	[52]
mice	iv jugular	vasc wash	15, 30 min	HSA NP	ApoE	200 to 250	EM	images	-		-	[53]
mice	iv tail	n.a.	15, 30, 45, 60, 120, 180, 210 min	HSA NP	OX26, R17217, Tf	170	Loperamide NP, tail-flick test	% MPE	-	-	-	[54]
mice	iv tail	none	0.5, 1, 2, 4, 8, 24, 72, 168h	PMMA NP	poloxamer 407 or 908 or tween80	107	^{14}C-polymer	ng/mg brain PK data	Non-targ vs targ 11 fold	Non-targ 0.088% Targ 0.99% /gram*	30min: targ 60% /ml	[55]
mice	iv tail	none	biodistr 2h. vivo imag 120 min. pEGFP 48h.	PAMAM NP	Angio-pep-2	-	^{125}I-PAMAM. pEGFP NP, FM. Vivo imaging	% ID/g images	Non-targ vs targ 8.4 fold	Non-targ 0.03% Targ 0.25% /gram	-	[56]
mice	iv tail	none	TEM 1h. vivo im 4h. DNA FM 2d	PAMAM NP	Lf	-	GFP-DNA NP, FM, EM, vivo imaging	images	-	-	-	[57]
mice	iv tail	none	1h	nanogel	-	64 to 94	^{3}H-ODN and ^{3}H-nanogel	% ID/g	Free vs nanogel 15 fold	2.67% /gram	Nanogel 2.81% /gram	[58]

Species	Administration	vasc corr	Time points	Particle type	Ligand	Particle size (nm)	Method	Data representation	Times increase	%ID brain	%ID blood	Ref
rats	perfusion & iv femoral	vasc wash	perf 3-4 min. iv 1h	PLGA NP	opioid peptides	200	PLGA-rhodamine and fluorescine, FM	images	-	-	-	[59]
rats	iv tail	none	15, 30, 45, 60, 90, 120, 240, 360, 420 min	PLGA NP	g7 opoid peptide	150	Loperamide and rhodamine NP, hot plate test, FM	%MPE images	-	-	-	[60]
mice	iv tail	vasc wash	1, 3, 6h 1, 7, 14, 28d	PLGA NP	TAT	320	^{3}H-ritonavir NP. FM	ug/g	Non-targ vs targ 6.5 fold	Non-targ 1.08% Targ 7.1% /gram*	1h: both 1% and remain low/ml*	[61]
mice	iv tail	vasc wash	0.25, 0.5, 1, 2, 4, 8, 12, 24h	PLGA NP	catBSA	150	6-coumarin NP, HPLC. FM	ng/g PK data images	Non-targ vs targ 2.3 fold	npc	PK data	[62]
rats	iv jugular, carotid, & tail	vasc wash	1h	PLGA NP	-	290	Superoxide dismutase NP. 6-coumarin NP, HPLC	% ROS damage	-	Non-targ carot 1.8% jugul 0.13% tail 0.11% /brain	-	[63]
rats	iv tail	none	0.25, 0.5, 1, 1.5, 4, 5, 24h	PLGA NP	g7 opoid peptide	160	Rhodamine NP, HPLC. Loperamide NP, hot plate test	ug/g (text also %ID/g)	npc	Non-targ low % Targ 15% /gram	0.25h: Non-targ undetec Targ ~6% /gram*	[64]

Species	Administration	vasc corr	Time points	Particle type	Ligand	Particle size (nm)	Method	Data representation	Times increase	%ID brain	%ID blood	Ref
rats	iv tail	none	1, 1.5, 3, 5, 24h	PLGA NP	g7 opoid peptide	180	Rhodamine NP, HPLC. FM. Loperamide NP, hot plate test	%MPE %ID/g	npc	Non-targ low % Targ 14.3% /gram	-	[65]
rats	ip	vasc wash	10, 20, 60 min	PLA NP	-	250	Tacrine-NP. Histological brain damage	ECoG profiles. Brain damage	-	-	-	[66]
mice	iv tail	n.a.	15, 45, 90, 120, 180 min	PBCA NP	apo AII, B, CII, E, or J	300	Dalargin or loperamide NP, tail-flick test	% MPE	-	-	-	[67]
rats	iv tail	vasc wash	90 min	PBCA NP	-	145	PMI fluo dye NP, FM	images	dependent on conc	-	-	[68]
mice	iv	none	15, 45, 90 min, 24h	PBCA NP	tween80	250	NGF NP, NGF ELISA kit and behavior	pg/mg	Non-targ vs targ 3 fold	Non-targ 8% Targ 24% /brain*	-	[69]
mice	iv tail	none	2, 5, 15, 30, 60, 120, 240 min	PBCA NP	tween80	50	^{125}I-clioquinol NP, behaviour. Vivo imaging	%ID/g images	Free vs NP 2.3 fold	Free drug 1% NP drug 2.3% /gram	Free 9.2% NP 12% /gram	[70]

Table I. *Methods and partial results of several in vivo brain targeting studies of the past decade. Underlined time points indicate time points of best results and of %ID in table, unless indicated otherwise. NP = nanoparticle. SLN = solid lipid nanoparticle. Lipo = liposome. FM = fluorescence microscopy. EM = electron microscopy. Vasc wash = vascular washout. n.a. = not applicable. npc = not possible to calculate by the authors of this review. Tf = transferrin. Lf = lactoferrin. Non-targ = non-targeted particles. Targ = targeted particle. * = percentage was calculated by the authors of this review from the data in the referenced article, these values represent estimations. In case multiple particles were tested in one study, result of the best performing particle is shown.*

In vivo techniques to measure nanoparticle uptake into the brain

The design of brain uptake studies of free drugs is generally different from the design of brain uptake studies of nanoparticles, because the size, physicochemical properties, and uptake mechanisms are different. This results in different approaches. The methods that have been used for brain targeting studies using nanoparticles in the past decade are described here.

Visualization methods

Microscopy is the most widely used qualitative method to study BBB uptake of nanoparticles *in vivo*. Fluorescence microscopy is often used for its sensitivity. It requires loading of the nanoparticles with a fluorescent dye [62], or covalent coupling of the particle building blocks to a dye [59]. Commonly used fluorescent dyes include rhodamine-123, fluorescein, and 6-coumarin. Particles are usually injected iv, and after sectioning the brain, they can be localized using fluorescence microscopy. The brain endothelium can be visualized by using an endothelium staining marker such as lectin. If such a marker is included in the staining procedure, a distinction can be made between particles that are associated with the brain endothelium, and particles that have crossed into the brain parenchyma [68]. If gene delivery to the brain is of interest, a plasmid expressing a fluorescent protein can be incorporated into the particle, and gene expression can be assessed by visualizing protein fluorescence in the brain sections [57].
Next to fluorescence microscopy, electron microscopy is commonly used. With this technique, single particles can be visualized in specific regions of the brain. For example, Zensi *et al*. [53] showed that human serum albumin nanoparticles could be detected by electron microscopy in murine brain sections after iv administration. In the electron microscopic pictures, a distinction can be seen between particles in the capillary lumen, particles within the endothelial cells (Figure 3), and particles that have been taken up into neuronal cells.

Besides microscopic section imaging, *in vivo* fluorescence imaging can be used to visualize uptake of particles into the brain [56,57]. *In vivo* fluorescence imaging involves labeling of the particles with a fluorophore. A sensitive camera detects the fluorescence emission in the whole body of a living small animal. Fluorescent labels that absorb in the near-infrared region are generally preferred, because they limit tissue autofluorescence [71,72]. Fluorescence intensity in the brain area can be compared between different nanoparticle formulations, to determine which formulation shows the highest brain accumulation [73].

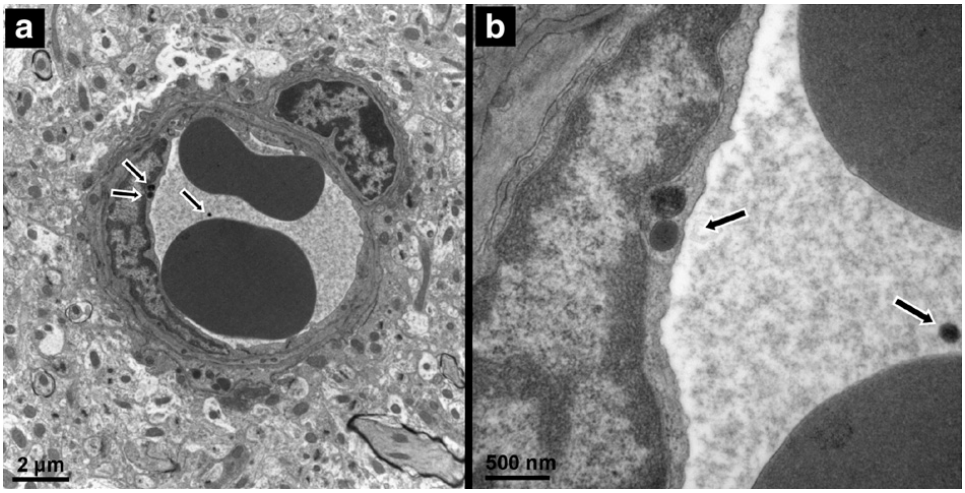

Figure 3. *Micrographs of the cortex region of mice after injection of Apo E-modified HSA nanoparticles. 15 min after intravenous injection the nanoparticles (dark spheres indicated by arrows) could be seen inside the endothelial cells. (**a**) shows a cross section of a blood vessel with two nanoparticles in the endothelial cell and one nanoparticle still in the lumen of the vessel. (**b**) shows a higher magnification of the same micrograph. Reprinted from Journal of Controlled Release [53]. Copyright (2009), with permission from Elsevier.*

Although *in vivo* imaging is a rapidly progressing field, detection is at present not sensitive enough to visualize the particles within the microenvironment of the brain, or to provide quantitative information on the usually low concentrations that have accumulated in the brain.

Behavioral tests

Some drugs that act on the CNS are unique compared to drugs that act on any other organ, because of their ability to interfere with brain signaling, and to induce specific behavioral effects. This gives rise to the possibility of not only detecting the level of compound that reaches the brain, but also to determine whether the compound has a pharmacodynamic effect. Drugs that normally do not enter the brain can be encapsulated into nanoparticles, to be transported over the BBB. The effect of the drug in the brain, can be read out by monitoring the behavior of the animal, with specifically designed behavioral tests.

These tests do not register the whole particle inside the brain, but only the free drug that has been released from the particle, as only the free drug will be able to exert an effect. Drug release from nanoparticles at the site of interest is crucial, therefore behavioral tests are of great value.

Nociceptive tests

A common model drug that has been used in combination with nanoparticles, is the opiate antagonist loperamide. Intracerebral administration of loperamide causes antinociceptive effects. However, after iv injection of loperamide, these effects are not seen. This is due to the efflux membrane transporter P-glycoprotein [74]. Loperamide molecules that reach the endothelial cells of the blood-brain barrier are rapidly transported back to the blood circulation. Therefore, loperamide is not able to enter into the brain parenchyma, making it a model drug for nociceptive testing. It can be loaded inside nanoparticles [60], or simply be adsorbed onto the surface of the particles [52]. Loperamide-containing particles that are successfully taken up by the brain, can release their drug content in the brain, causing an analgesic effect of loperamide after iv administration [54]. Similar to loperamide, the hexapeptide dalargin has been used for this purpose [67].

To measure nociception, two basic tests have been developed for the use in rats and mice: the tail flick test and the hot plate test. These tests are convenient, because they apply to healthy wild-type animals, requiring no disease induction or transgenic animals. Both tests measure the response to a painful thermal stimulus. In the tail flick test, a light beam is used to apply heat to a small area of the tail. Latency (time) to flick the tail out of the path of the light beam is measured. In the hot plate test, the animal is placed on the surface of a hot plate. Latency to lick the forepaws or to lift one of the hindpaws is recorded. In both tests, latency is usually determined before administration of the drug to determine the background response, and after administration of the drug at one or several time points. To avoid damage if the animal does not respond, a cut off time is predetermined, typically between 10 and 60 seconds [54,60,75]. This time point is regarded as the maximal possible effect (MPE) [76]. The experimental response latencies are usually expressed as percent maximal possible effect (%MPE), which can be calculated using the following formula:

$$\%MPE = \frac{\text{postdrug latency - predrug latency}}{\text{cut off time - predrug latency}} \times 100\%$$

It should be noted that these tests can only be performed with model (analgesic) compounds. The characteristics of other drugs may be different from the tested analgesic. If another drug is used in combination with the nanoparticles, the encapsulation, formulation, and subsequent brain uptake may be different from the model compound.

Motor function and learning & memory tests

Other models that allow for behavioral testing often include induction of disease states in animals, like MPTP-induced Parkinson syndrome. Drugs that treat these syndromes, but normally do not penetrate the BBB in their free form, are candidates for nanoparticle formulation to enhance brain uptake. An example is nerve growth factor (NGF) [47]. NGF has been evaluated for the treatment of neurological diseases such as Alzheimer's disease and Parkinson's disease. However, NGF has a low permeability through the BBB following intravenous administration [40]. Kurakhmaeva *et al*. [69] tested MPTP-treated animals for improvement in symptoms of parkinsonism after iv administration of a NGF nanoparticle formulation. The NGF PBCA nanoparticles lead to a significant reduction in symptoms, including rigidity, tremor, locomotor activity, and orientation-research reaction.

Finally, transgenic mice like the APP/PS1 Alzheimer's disease mice can be used to determine behavioral skills [77]. The Cu/Zn-selective metal chelator clioquinol (CQ), which has a poor BBB penetration, has been encapsulated into PBCA nanoparticles by Kulkarni *et al*. to improve brain uptake [70]. The transgenic mice can be tested with the Y-maze test for improvement in cognitive behavioral skills. Furthermore, brains of Alzheimer's disease mice can be histologically stained for decrease in amyloid plaques.

Quantitative methods

Quantitative methods to study BBB nanoparticle uptake *in vivo*, involve determination of pharmacokinetic (PK) parameters, and biodistribution studies. For both of these studies either the particle itself, or an entrapped compound is labeled. Most commonly, radioisotopes like ^{3}H, ^{14}C or ^{125}I are used. Alternatively, the entrapped compound is quantified by HPLC.

Pharmacokinetic parameters

In most brain targeting studies, the nanoparticles are administered intravenously. The goal of a pharmacokinetic study is to assess the fraction of the administered dose that is distributed to the brain or is excreted from the body [78]. Nanoparticle and/or drug concentrations are measured in the blood(plasma) and in the brain at several time points after administration. From these measurements, the area under the concentration–time curve (AUC) can be obtained for both blood and brain. Pharmacokinetic models quantify the rate and extent of the distribution by mathematically analyzing these data. In this way, a number of PK parameters can be obtained. Commonly, several of these parameters are determined for either blood [51,55], brain or both [49,50]. Other organs can also be included in the PK study [62]. In current brain targeting studies, the most widely determined PK parameters in both blood and brain are:

- C_{max}: peak concentration
- T_{max}: time to reach peak concentration
- AUC: area under the concentration–time curve, from the time of injection (t=0) to a determined time point t ($AUC_{(0 \rightarrow t)}$) or extrapolated to infinity ($AUC_{(0 \rightarrow \infty)}$).
- Half-life ($t_{1/2}$): time it takes for 50% to be eliminated.
- Mean Residence Time (MRT): the average time a compound remains in the blood or brain

Biodistribution studies

For biodistribution studies, the nanoparticles are usually administered intravenously. After administration, the animals are sacrificed at a specific time point, or preferably at several time points. The brain is taken out, along with some of the major organs where the particles are likely to end up, including liver and spleen. If a β-emitting label is used, organs can be dissolved, and radioactivity can be determined by liquid scintillation counting. If a γ-emitting label is used, organs can be directly counted in a γ counter. If the compound itself is to be detected, a tissue extraction can be performed, followed by HPLC determination of the concentration. The amount of drug that was found in the brain and other organs, can be represented as mass/organ or mass/gram. In this way, the increase in brain uptake compared to the control sample is obtained. Along with the experimental samples, the injection sample, as it was administered to the animals, can be assayed for drug content using the same analytical method, so that the amount of drug taken up into the brain can be expressed as a percentage of the injected dose (%ID). For example, Ke *et al*. [56] performed a biodistribution study in mice using dendrimers, which were either unmodified, or modified with an angiopep-2 targeting ligand. They found 0.03 %ID in the brain for the unmodified dendrimers, and 0.25 %ID for the angiopep-2 modified dendrimers. This shows the importance of targeting ligands in enhancing brain uptake of nanoparticles. The absolute increase owing to the targeting ligand (over 8 times more), can be exactly assessed by such a biodistribution study.

Discussion

Each method to determine brain uptake of compounds or nanoparticles has advantages and disadvantages. In this section we discuss the possibilities and limitations of the methods.

Percentage of maximal possible effect

As described above, in nociceptive studies the outcomes are usually represented as time to respond, commonly expressed as the percentage of maximal possible effect (%MPE). This parameter tells whether the encapsulated drug has an effect in the brain, but it provides no information on the amount of drug that was taken up. Therefore, it is difficult to compare different formulations or studies. For example, it cannot be concluded that a formulation resulting in 20% MPE, has a 2 fold higher brain uptake of the drug than a formulation resulting in 10% MPE. Moreover, formulations that are successfully targeted to the brain, will often reach 100% MPE [52,54]. This low dynamic range makes it difficult to distinguish between various formulations. In general, the %MPE will provide an indication whether a formulation works to a higher, moderate, or insignificant extent, rather than provide exact drug uptake values.

Percentage of injected dose

When a biodistribution study has been performed, presenting the mass of drugs or particles in the brain is frequently preferred over presenting the %ID (see table I), although it usually provides less information on the extent of uptake into the brain. The reason for this preference is not always clear. It may lie in the fact that the percentages that are found in the brain are generally low, especially compared to other organs. While targeting to the liver can result in 75 %ID in the liver [79], and targeting to a tumor can produce values around 10% ID/gram tumor [80,81], percentages that are found in the brain are often below 0.5%, and can be as low as 0.01% ID/g brain [43]. Although low, uptake may nonetheless be manifold higher compared to an impermeable control. If a low %ID is found, it raises the question what %ID is actually needed to produce an effect. Although this depends on the drug that is eventually going to be used in combination with the nanoparticle for therapeutic purposes, the percentage needed may not be that high. In general, low concentrations of drugs are sufficient in the brain to result in a therapeutic effect. For example, only about 0.02% of a peripherally administered dose of morphine enters the brain, but that is sufficient to produce analgesia. For most CNS therapeutics on the market, less than 0.2% of the peripheral dose is taken up into brain [82]. When transferrin is used as a targeting ligand, brain uptake *in vivo* is limited due to high endogenous concentrations of transferrin in the blood [9]. Nevertheless, loperamide-

loaded nanoparticles coupled to a transferrin targeting ligand, are able to produce significant analgesia compared to non-targeted nanoparticles [54], demonstrating that low levels of uptake in the brain can be sufficient to produce adequate therapeutic effects.

In general, the percentages of the injected dose found in the brain after targeting of nanoparticles, are highly variable. As shown in table I, the %ID generally ranges from 0.01% to 0.5% in case an intravascular content correction (see below) was applied [42,43,45,47,48]. In case no intravascular content correction was applied, recorded percentages can be over 15 %ID, of which the vascular contribution is unclear [51,64,65,69].

If the %ID is plotted, notion should be taken whether this is %ID/organ or %ID/gram. This also holds for mass/organ or mass/gram. For example, a 20-25 gram Balb/c mouse has an average brain weight of about 0.4 grams. If a brain dose of 1% ID/g is recorded, the actual percentage of the injected dose in the brain is 0.4%. Therefore, it makes little sense to provide the %ID/gram. In the adult rat, however, the average brain weight is above 1 gram, making this expression way more realistic.

Intravascular content

As mentioned before, particles that are still present in the circulation at the time of sacrifice, can contribute to a significant degree to the amount of drug measured in whole brain homogenate. Two methods to correct for intravascular content exist. They are brain perfusion with a buffer, and inclusion of a vascular marker.

If administration of the nanoparticles is performed by *in situ* perfusion, which is usually done under anesthesia, buffer perfusion can be performed directly after infusion of the nanoparticle solution. If the particle administration is performed by iv injection, perfusion can be performed after subsequent anesthesia, or directly after sacrifice. In that case it is recommended to include an anti-coagulant such as heparin in the buffer, to prevent perfusion obstruction by coagulated blood in the microvasculature.

The vascular washout fluid is usually administered either through the jugular vein, or transcardially through the left ventricle of the heart. It should be noted that administration through the heart will result in most of the perfusion fluid to distribute to the rest of the body instead of to the brain, if no vessels are clamped. Therefore, in most cases, the aorta is clamped, causing more of the fluid to reach the carotid arteries. Even so, only 10% of the fluid that reaches a common carotid artery reaches the brain if no additional ligations are placed on the external carotid artery and the pterygopalatine artery [25]. This should be

taken into account when performing a vascular washout, and a sufficient volume should be perfused to ensure that brain vasculature is washed completely. In general, when *in situ* perfusion is performed with external carotid artery and pterygopalatine artery ligated, perfusion of 1 to 5 ml buffer is considered sufficient [22]. When transcardiac perfusion is performed with the descending aorta clamped, 20 ml of buffer is commonly used, as is shown in table II. Outflow of the perfused fluid can be realized by severing the jugular veins [83,84] or cardiac ventricles [22]. Optionally, outflow can be monitored to ensure thorough washout [45,47].

Species	Nanoparticle or drug administration	Washout administration	Clamps or ligations	Washout volume	Washout time	Ref
Rats	common carotid artery	common carotid artery	common carotid & external carotid arteries	1-5 ml	10-15 sec	[22]
Rats	femoral vein	jugular arteries	none	15-20 ml	30 min	[47]
Rats	common carotid artery	common carotid artery	common carotid, external carotid, & occipital arteries	20-30 ml	120-180 sec	[59]
Rats	femoral vein	carotid artery	carotid artery	30-35 ml	60 min	[45]
Rats	tail vein	heart	none	50 ml	10 min	[48]
Mice	common carotid artery	common carotid artery	common carotid artery	1.15 ml	60 sec	[85]
Mice	tail vein	heart	none	2 ml	2 min	[61]
Mice	jugular vein	heart	descending aorta	20 ml	30 sec	[83]
Mice	heart	heart	descending aorta	20 ml	<1 min	[86]
Mice	jugular vein	heart	descending aorta	20 ml	1 min	[87]
Mice	jugular vein	heart	descending aorta	20 ml	1-2 min	[84]
Mice	jugular vein	jugular vein	none	50 ml	-	[53]

Table II. *Vascular washout times and volumes that have been used in mice and rats to clear the brain from intravascular content.*

The second intravascular content correction method is co-administration of a vascular marker. The marker is a substance that does not penetrate the blood-brain barrier, e.g. radiolabeled sucrose. This allows for the determination of the total vascular volume in the brain. As described above (equation 2 and 4), brain vascular blood concentration can be subtracted from the total brain concentration, yielding the amount of particles that is associated with the brain endothelial cells and brain parenchyma. The brain vascular volumes of mice and rats have been determined in many studies, as is shown in table III. Typically, this volume ranges between 11 and 14 µl/gram brain and is on average about 12 µl/gram for both mice and rats.

Species	Method	Vascular volume (µl/gram brain)	Ref
Rats (200-400 g)	femoral vein injection of [^{14}C]sucrose	12.5 ± 0.7 12.9 ± 1.6 12.2 ± 0.8	[88]
Rats (220-330 g)	in situ perfusion of [^{14}C]sucrose	12 ± 1.9	[23]
Rats (220-330 g)	in situ perfusion of [^{14}C]sucrose	13.3 ± 3.4	[89]
Rats	in situ perfusion of [^{14}C]sucrose	12 ± 2	[90]
Mice (20-25 g)	in situ perfusion of [^{3}H]inulin	11.4 ± 0.4	[19]
Mice (20-25 g)	in situ perfusion of [^{14}C]sucrose	11-14	[91]
Mice (8-22 weeks)	in situ perfusion of [^{14}C]sucrose	11.9 ± 2.6 12.8 ± 1.2	[92]

Table III. *Brain vascular volumes that have been found in mice and rats after administration of a vascular marker.*

Correction for vascular content is in many studies not applied. If the concentration of drugs or particles in the blood is sufficiently low, this may not pose a problem. Otherwise, the quantitative amount or %ID found in the brain is likely to be overestimated. To gain insight in the blood background, it is necessary to measure the blood concentration at the time of sacrifice. Due to clearance, the concentration of circulating particles is generally highest at the first time point measured, and will decrease at later time points. If no vascular content correction is applied, the concentration measured in the brain is likely to be highest at the first time point and to decrease as well, due to the blood background. In this case, the brain:blood ratio can be provided in addition to the amount or %ID in the brain [70]. If this ratio remains constant over the measured time points, it cannot be concluded that brain uptake was highest at the earliest time point.

Similarly, this holds for experiments in which comparable types of nanoparticles were included, e.g. targeted and non-targeted particles. The concentration in the brain as well as in the blood can be measured for both particle types. The increase in the brain:blood ratio reflects the increase of brain binding/uptake of the targeted particles compared to the non-targeted particles. In this way, contribution of the targeting ligand to the brain uptake of the particle can be seen, although the quantitative amount found in the brain may be overestimated. In most cases the same type of particle is used for both targeted and non-targeted samples. Therefore, circulation times of both particles are often comparable.

As the brain vascular volume for mice and rats is usually about 12 µl/gram brain, this provides an estimate to subtract the brain vascular concentration from the total brain concentration. Of course, blood concentration at the terminal time point needs to be

measured in order to accomplish this. Although not common, this approach can be used [87,90].

Capillary depletion

If the brain is taken out for analysis, the nanoparticle content that is not present within the blood of the brain microvasculature, may be bound to the endothelium, be present within the endothelial cells or may be transcytosed to the brain parenchyma [39]. A distinction can be made between endothelial-associated particles and particles that have transcytosed into the brain parenchyma, by performing a capillary depletion [93,94]. This technique involves homogenization of the brain, followed by dextran density centrifugation to deplete the homogenate of its vasculature. The nanoparticles can be detected in both the parenchyma and the capillary fraction. It should be noted that particles which are bound to the surface of the capillaries with low affinity, may disassociate from the capillaries during centrifugation, and therefore end up in the parenchyma fraction. This may be prevented when the brain vasculature is flushed before the brain is taken out, to remove the low affinity bound particles. Particles bound with high affinity to the capillaries should remain associated.

Sampling time points

The time points that are chosen to measure brain uptake or drug effect are commonly between 15 minutes and 24 hours. In most cases the earliest time points, between 15 minutes and 2 hours, yield the highest uptake or effect (table I). After that, the amount of particles measured in the brain generally decreases. This may be due to degradation of the particles, followed by elimination of the label or encapsulated drug by degradation, metabolism, efflux, and permeation through the brain capillaries [95]. In many cases, the particle concentration in the brain is highly decreased or undetectable after 24 hours [55,62]. Measurements at later time points are preferably performed with stable compounds. If a metabolizing drug is used for detection, the concentration in the body will be decreased to undetectable levels at later time points [65].

Intravenous administration routes

As mentioned before, nanoparticles are administered intravenously in most studies. The most convenient way to accomplish this is by administration in the tail vein. Other iv administration routes that have been used for brain targeting studies include the femoral vein, the jugular vein, and the carotid artery. Reddy *et al*. [63] demonstrated that the site of iv administration can have significant influence on the uptake of nanoparticles in the brain. They used a rat model, and administered 0.5 ml of a nanoparticle dispersion either through the tail vein, the jugular vein, or the internal carotid artery. After one hour, administration via the internal carotid artery resulted in a 13-fold greater uptake of

nanoparticles in the brain compared to either tail or jugular vein administration. The reason may be decreased exposure of the particles to the reticulo-endothelial system, resulting in an increased concentration of circulating particles available for brain uptake. Although administration via the internal carotid artery is technically more difficult, this finding is worthwhile to take into account in BBB targeting studies.

Conclusion and future prospects

In recent brain targeting studies involving nanoparticles, a wide range of approaches has been used by researchers to determine the extent, rate, and effect of drug and nanoparticle uptake into the brain. Choosing the right method depends on whether you want to obtain quantitative uptake values, visualize the uptake mechanism, or test a drug effect. Each technique has its own advantages and disadvantages, which should be considered before experiments are started. Many parameters like administration route, sampling time points, and the way in which the data are presented should be taken into account. Because contribution of cerebral vascular content can be high, it is recommended to determine the amount of drugs or particles present in the blood at the terminal time point, and to properly correct for this.

Many studies have shown that nanoparticles can reach the brain. Within the brain microenvironment, targeting of nanoparticles starts with binding and uptake of the particles into the endothelial cells. By using techniques such as brain capillary depletion or electron microscopy, it can be shown that particles have crossed the endothelial barrier, and reached the brain parenchyma. However, the intracellular fate of nanoparticles *in vivo* often remains unclear. This is due to limitations of *in vivo* detection methods and techniques. Therefore, intracellular processes such as endocytotic mechanisms currently have to be studied *in vitro* [96,97], in an artificial environment. Progress in the field of *in vivo* detection methods is ongoing [98,99]. In the future, faster and more sensitive detection methods are required to study uptake and trafficking of nanoparticles within the brain.

Acknowledgements

We thank Mike Langeveld for graphic design of Figure 1. This work was performed within the framework of the Dutch Top Institute Pharma project T5-105-1: nanoscience as a tool for improving bioavailability and blood-brain barrier penetration.

References

[1] W.M. Pardridge. Blood-brain barrier delivery, Drug Discovery Today. 12 (2007) 54-61.

[2] A.G. de Boer, I.C. van der Sandt, P.J. Gaillard. The role of drug transporters at the blood-brain barrier, Annu Rev Pharmacol Toxicol. 43 (2003) 629-656.

[3] J.F. Ghersi-Egea, B. Leninger-Muller, G. Suleman, G. Siest, A. Minn. Localization of drug-metabolizing enzyme activities to blood-brain interfaces and circumventricular organs, J.Neurochem. 62 (1994) 1089-1096.

[4] J.F. Ghersi-Egea, B. Leininger-Muller, R. Cecchelli, J.D. Fenstermacher. Blood-brain interfaces: relevance to cerebral drug metabolism, Toxicol.Lett. 82-83 (1995) 645-653.

[5] N.J. Abbott. Prediction of blood-brain barrier permeation in drug discovery from in vivo, in vitro and in silico models, Drug Discov.Today: Technologies. 1 (2004) 337-463.

[6] R. Cecchelli, V. Berezowski, S. Lundquist, M. Culot, M. Renftel, M.P. Dehouck, et al. Modelling of the blood-brain barrier in drug discovery and development, Nat.Rev.Drug Discov. 6 (2007) 650-661.

[7] W.M. Pardridge. Drug targeting to the brain, Pharm.Res. 24 (2007) 1733-1744.

[8] A.B. de Boer, E.L. De Lange, I.C. van der Sandt, D.D. Breimer. Transporters and the blood-brain barrier (BBB), Int.J.Clin.Pharmacol.Ther. 36 (1998) 14-15.

[9] A.G. de Boer, P.J. Gaillard. Drug Targeting to the Brain, Annu Rev Pharmacol Toxicol. 47 (2007) 323-355.

[10] W.M. Pardridge. The blood-brain barrier: bottleneck in brain drug development, NeuroRx. 2 (2005) 3-14.

[11] N.J. Abbott, A.A. Patabendige, D.E. Dolman, S.R. Yusof, D.J. Begley. Structure and function of the blood-brain barrier, Neurobiol.Dis. 37 (2010) 13-25.

[12] N.J. Abbott, L. Ronnback, E. Hansson. Astrocyte-endothelial interactions at the blood-brain barrier, Nat.Rev.Neurosci. 7 (2006) 41-53.

[13] N.J. Abbott, D.E. Dolman, A.K. Patabendige. Assays to predict drug permeation across the blood-brain barrier, and distribution to brain, Curr.Drug Metab. 9 (2008) 901-910.

[14] U. Bickel. How to measure drug transport across the blood-brain barrier, NeuroRx. 2 (2005) 15-26.

[15] W.M. Pardridge. Log(BB), PS products and in silico models of drug brain penetration, Drug Discov.Today. 9 (2004) 392-393.

[16] G.G. Pinter, J.L. Atkins, D.R. Bell. Albumin permeability times surface area (PS) product of peritubular capillaries in kidney, Experientia. 30 (1974) 1045.

[17] Q.R. Smith. A review of blood-brain barrier transport techniques, Methods Mol.Med. 89 (2003) 193-208.

[18] H. Hervonen, O. Steinwall. Endothelial surface sulfhydryl-groups in blood-brain barrier transport of nutrients, Acta Physiol.Scand. 121 (1984) 343-351.

[19] H. Murakami, H. Takanaga, H. Matsuo, H. Ohtani, Y. Sawada. Comparison of blood-brain barrier permeability in mice and rats using in situ brain perfusion technique, Am.J.Physiol.Heart Circ.Physiol. 279 (2000) H1022-8.

[20] B.V. Zlokovic, D.J. Begley, B.M. Djuricic, D.M. Mitrovic. Measurement of solute transport across the blood-brain barrier in the perfused guinea pig brain: method and application to N-methyl-alpha-aminoisobutyric acid, J.Neurochem. 46 (1986) 1444-1451.

[21] Y. Takasato, S.I. Rapoport, Q.R. Smith. An in situ brain perfusion technique to study cerebrovascular transport in the rat, Am.J.Physiol. 247 (1984) H484-93.

[22] Q.R. Smith, D.D. Allen. In situ brain perfusion technique, Methods Mol.Med. 89 (2003) 209-218.

[23] P.R. Lockman, J. Koziara, K.E. Roder, J. Paulson, T.J. Abbruscato, R.J. Mumper, et al. In vivo and in vitro assessment of baseline blood-brain barrier parameters in the presence of novel nanoparticles, Pharm.Res. 20 (2003) 705-713.

[24] S. Lundquist, M. Renftel, J. Brillault, L. Fenart, R. Cecchelli, M.P. Dehouck. Prediction of drug transport through the blood-brain barrier in vivo: a comparison between two in vitro cell models, Pharm.Res. 19 (2002) 976-981.
[25] P.L. Bonate. Animal models for studying transport across the blood-brain barrier, J.Neurosci.Methods. 56 (1995) 1-15.
[26] W.H. Oldendorf. Measurement of brain uptake of radiolabeled substances using a tritiated water internal standard, Brain Res. 24 (1970) 372-376.
[27] P. Riant, S. Urien, E. Albengres, A. Renouard, J.P. Tillement. Effects of the binding of imipramine to erythrocytes and plasma proteins on its transport through the rat blood-brain barrier, J.Neurochem. 51 (1988) 421-425.
[28] W.M. Pardridge, R. Sakiyama, G. Fierer. Transport of propranolol and lidocaine through the rat blood-brain barrier. Primary role of globulin-bound drug, J.Clin.Invest. 71 (1983) 900-908.
[29] R.A. Knight, K. Karki, J.R. Ewing, G.W. Divine, J.D. Fenstermacher, C.S. Patlak, et al. Estimating blood and brain concentrations and blood-to-brain influx by magnetic resonance imaging with step-down infusion of Gd-DTPA in focal transient cerebral ischemia and confirmation by quantitative autoradiography with Gd-[(14)C]DTPA, J.Cereb.Blood Flow Metab. 29 (2009) 1048-1058.
[30] M.C. Ferrier, H. Sarin, S.H. Fung, B. Schatlo, R.M. Pluta, S.N. Gupta, et al. Validation of dynamic contrast-enhanced magnetic resonance imaging-derived vascular permeability measurements using quantitative autoradiography in the RG2 rat brain tumor model, Neoplasia. 9 (2007) 546-555.
[31] M. Lemaire., S. Desrayaud. The priorities/needs of the pharmaceutical industry in drug delivery to the brain, Int.Congr.Ser. 1277 (2005) 32-46.
[32] E.C. de Lange, B.A. de Boer, D.D. Breimer. Microdialysis for pharmacokinetic analysis of drug transport to the brain, Adv.Drug Deliv.Rev. 36 (1999) 211-227.
[33] A. Reichel. Addressing central nervous system (CNS) penetration in drug discovery: basics and implications of the evolving new concept, Chem.Biodivers. 6 (2009) 2030-2049.
[34] A. Doran, R.S. Obach, B.J. Smith, N.A. Hosea, S. Becker, E. Callegari, et al. The impact of P-glycoprotein on the disposition of drugs targeted for indications of the central nervous system: evaluation using the MDR1A/1B knockout mouse model, Drug Metab. Dispos. 33 (2005) 165-174.
[35] N.L. Schlageter, R.E. Carson, S.I. Rapoport. Examination of blood-brain barrier permeability in dementia of the Alzheimer type with [68Ga]EDTA and positron emission tomography, J.Cereb.Blood Flow Metab. 7 (1987) 1-8.
[36] T. Urakami, K. Sakai, T. Asai, D. Fukumoto, H. Tsukada, N. Oku. Evaluation of O-[(18)F]fluoromethyl-D-tyrosine as a radiotracer for tumor imaging with positron emission tomography, Nucl.Med.Biol. 36 (2009) 295-303.
[37] P. Emond, D. Guilloteau, S. Chalon. PE2I: a radiopharmaceutical for in vivo exploration of the dopamine transporter, CNS Neurosci.Ther. 14 (2008) 47-64.
[38] J. Doorduin, H.C. Klein, J.R. de Jong, R.A. Dierckx, E.F. de Vries. Evaluation of [11C]-DAA1106 for imaging and quantification of neuroinflammation in a rat model of herpes encephalitis, Nucl.Med.Biol. 37 (2010) 9-15.
[39] J.A. Nicolazzo, S.A. Charman, W.N. Charman. Methods to assess drug permeability across the blood-brain barrier, J.Pharm.Pharmacol. 58 (2006) 281-293.
[40] J.F. Poduslo, G.L. Curran. Permeability at the blood-brain and blood-nerve barriers of the neurotrophic factors: NGF, CNTF, NT-3, BDNF, Brain Res.Mol.Brain Res. 36 (1996) 280-286.
[41] W.H. Oldendorf. Brain uptake of radiolabeled amino acids, amines, and hexoses after arterial injection, Am.J.Physiol. 221 (1971) 1629-1639.
[42] P.R. Lockman, M.O. Oyewumi, J.M. Koziara, K.E. Roder, R.J. Mumper, D.D. Allen. Brain uptake of thiamine-coated nanoparticles, J.Control.Release. 93 (2003) 271-282.

[43] A. Schnyder, S. Krahenbuhl, J. Drewe, J. Huwyler. Targeting of daunomycin using biotinylated immunoliposomes: pharmacokinetics, tissue distribution and in vitro pharmacological effects, J.Drug Target. 13 (2005) 325-335.

[44] N. Shi, Y. Zhang, C. Zhu, R.J. Boado, W.M. Pardridge. Brain-specific expression of an exogenous gene after i.v. administration, Proc.Natl.Acad.Sci.U.S.A. 98 (2001) 12754-12759.

[45] X. Zhang, Y. Xie, Y. Jin, X. Hou, L. Ye, J. Lou. The effect of RMP-7 and its derivative on transporting Evans blue liposomes into the brain, Drug Deliv. 11 (2004) 301-309.

[46] S. Gosk, C. Vermehren, G. Storm, T. Moos. Targeting anti-transferrin receptor antibody (OX26) and OX26-conjugated liposomes to brain capillary endothelial cells using in situ perfusion, J.Cereb.Blood Flow Metab. 24 (2004) 1193-1204.

[47] Y. Xie, L. Ye, X. Zhang, W. Cui, J. Lou, T. Nagai, et al. Transport of nerve growth factor encapsulated into liposomes across the blood-brain barrier: in vitro and in vivo studies, J.Control.Release. 105 (2005) 106-119.

[48] E. Afergan, H. Epstein, R. Dahan, N. Koroukhov, K. Rohekar, H.D. Danenberg, et al. Delivery of serotonin to the brain by monocytes following phagocytosis of liposomes, J.Control.Release. 132 (2008) 84-90.

[49] H. Chen, L. Tang, Y. Qin, Y. Yin, J. Tang, W. Tang, et al. Lactoferrin-modified procationic liposomes as a novel drug carrier for brain delivery, Eur.J.Pharm.Sci. 40 (2010) 94-102.

[50] J.X. Wang, X. Sun, Z.R. Zhang. Enhanced brain targeting by synthesis of 3',5'-dioctanoyl-5-fluoro-2'-deoxyuridine and incorporation into solid lipid nanoparticles, Eur.J.Pharm.Biopharm. 54 (2002) 285-290.

[51] V. Mishra, S. Mahor, A. Rawat, P.N. Gupta, P. Dubey, K. Khatri, et al. Targeted brain delivery of AZT via transferrin anchored pegylated albumin nanoparticles, J.Drug Target. 14 (2006) 45-53.

[52] K. Michaelis, M.M. Hoffmann, S. Dreis, E. Herbert, R.N. Alyautdin, M. Michaelis, et al. Covalent linkage of apolipoprotein e to albumin nanoparticles strongly enhances drug transport into the brain, J.Pharmacol.Exp.Ther. 317 (2006) 1246-1253.

[53] A. Zensi, D. Begley, C. Pontikis, C. Legros, L. Mihoreanu, S. Wagner, et al. Albumin nanoparticles targeted with Apo E enter the CNS by transcytosis and are delivered to neurones, J.Control.Release. 137 (2009) 78-86.

[54] K. Ulbrich, T. Hekmatara, E. Herbert, J. Kreuter. Transferrin- and transferrin-receptor-antibody-modified nanoparticles enable drug delivery across the blood-brain barrier (BBB), European Journal of Pharmaceutics and Biopharmaceutics. 71 (2009) 251-256.

[55] J. Lode, I. Fichtner, J. Kreuter, A. Berndt, J.E. Diederichs, R. Reszka. Influence of surface-modifying surfactants on the pharmacokinetic behavior of 14C-poly (methylmethacrylate) nanoparticles in experimental tumor models, Pharm.Res. 18 (2001) 1613-1619.

[56] W. Ke, K. Shao, R. Huang, L. Han, Y. Liu, J. Li, et al. Gene delivery targeted to the brain using an Angiopep-conjugated polyethyleneglycol-modified polyamidoamine dendrimer, Biomaterials. 30 (2009) 6976-6985.

[57] R. Huang, W. Ke, L. Han, Y. Liu, K. Shao, C. Jiang, et al. Lactoferrin-modified nanoparticles could mediate efficient gene delivery to the brain in vivo, Brain Res.Bull. 81 (2010) 600-604.

[58] S.V. Vinogradov, E.V. Batrakova, A.V. Kabanov. Nanogels for oligonucleotide delivery to the brain, Bioconjug.Chem. 15 (2004) 50-60.

[59] L. Costantino, F. Gandolfi, G. Tosi, F. Rivasi, M.A. Vandelli, F. Forni. Peptide-derivatized biodegradable nanoparticles able to cross the blood-brain barrier, J.Control.Release. 108 (2005) 84-96.

[60] G. Tosi, L. Costantino, F. Rivasi, B. Ruozi, E. Leo, A.V. Vergoni, et al. Targeting the central nervous system: In vivo experiments with peptide-derivatized nanoparticles loaded with Loperamide and Rhodamine-123, Journal of Controlled Release. 122 (2007) 1-9.

[61] K.S. Rao, M.K. Reddy, J.L. Horning, V. Labhasetwar. TAT-conjugated nanoparticles for the CNS delivery of anti-HIV drugs, Biomaterials. 29 (2008) 4429-4438.

[62] F. Xu, W. Lu, H. Wu, L. Fan, X. Gao, X. Jiang. Brain delivery and systemic effect of cationic albumin conjugated PLGA nanoparticles, J.Drug Target. 17 (2009) 423-434.
[63] M.K. Reddy, V. Labhasetwar. Nanoparticle-mediated delivery of superoxide dismutase to the brain: an effective strategy to reduce ischemia-reperfusion injury, FASEB J. 23 (2009) 1384-1395.
[64] A.V. Vergoni, G. Tosi, R. Tacchi, M.A. Vandelli, A. Bertolini, L. Costantino. Nanoparticles as drug delivery agents specific for CNS: in vivo biodistribution, Nanomedicine. 5 (2009) 369-377.
[65] G. Tosi, A.V. Vergoni, B. Ruozi, L. Bondioli, L. Badiali, F. Rivasi, et al. Sialic acid and glycopeptides conjugated PLGA nanoparticles for central nervous system targeting: In vivo pharmacological evidence and biodistribution, J.Control.Release. 145 (2010) 49-57.
[66] M. Iannone, D. Cosco, F. Cilurzo, C. Celia, D. Paolino, V. Mollace, et al. A novel animal model to evaluate the ability of a drug delivery system to promote the passage through the BBB, Neurosci.Lett. 469 (2010) 93-96.
[67] J. Kreuter, D. Shamenkov, V. Petrov, P. Ramge, K. Cychutek, C. Koch-Brandt, et al. Apolipoprotein-mediated Transport of Nanoparticle-bound Drugs Across the Blood-Brain Barrier, Journal of Drug Targeting. 10 (2002) 317.
[68] C.K. Weiss, M.V. Kohnle, K. Landfester, T. Hauk, D. Fischer, J. Schmitz-Wienke, et al. The first step into the brain: uptake of NIO-PBCA nanoparticles by endothelial cells in vitro and in vivo, and direct evidence for their blood-brain barrier permeation, ChemMedChem. 3 (2008) 1395-1403.
[69] K.B. Kurakhmaeva, I.A. Djindjikhashvili, V.E. Petrov, V.U. Balabanyan, T.A. Voronina, S.S. Trofimov, et al. Brain targeting of nerve growth factor using poly(butyl cyanoacrylate) nanoparticles, J.Drug Target. 17 (2009) 564-574.
[70] P.V. Kulkarni, C.A. Roney, P.P. Antich, F.J. Bonte, A.V. Raghu, T.M. Aminabhavi. Quinoline-n-butylcyanoacrylate-based nanoparticles for brain targeting for the diagnosis of Alzheimer's disease, Wiley Interdiscip.Rev.Nanomed Nanobiotechnol. 2 (2010) 35-47.
[71] J. Rao, A. Dragulescu-Andrasi, H. Yao. Fluorescence imaging in vivo: recent advances, Curr.Opin.Biotechnol. 18 (2007) 17-25.
[72] J.V. Frangioni. In vivo near-infrared fluorescence imaging, Curr.Opin.Chem.Biol. 7 (2003) 626-634.
[73] A. Gaydess, E. Duysen, Y. Li, V. Gilman, A. Kabanov, O. Lockridge, et al. Visualization of exogenous delivery of nanoformulated butyrylcholinesterase to the central nervous system, Chem.Biol.Interact. 187 (2010) 295-298.
[74] A.J. Sadeque, C. Wandel, H. He, S. Shah, A.J. Wood. Increased drug delivery to the brain by P-glycoprotein inhibition, Clin.Pharmacol.Ther. 68 (2000) 231-237.
[75] T. Karl, R. Pabst, S. von Horsten. Behavioral phenotyping of mice in pharmacological and toxicological research, Exp.Toxicol.Pathol. 55 (2003) 69-83.
[76] L.S. Brady, S.G. Holtzman. Analgesic effects of intraventricular morphine and enkephalins in nondependent and morphine-dependent rats, J.Pharmacol.Exp.Ther. 222 (1982) 190-197.
[77] H. Scholtzova, Y.Z. Wadghiri, M. Douadi, E.M. Sigurdsson, Y.S. Li, D. Quartermain, et al. Memantine leads to behavioral improvement and amyloid reduction in Alzheimer's-disease-model transgenic mice shown as by micromagnetic resonance imaging, J.Neurosci.Res. 86 (2008) 2784-2791.
[78] J.E. Riviere. Pharmacokinetics of nanomaterials: an overview of carbon nanotubes, fullerenes and quantum dots, Wiley Interdiscip.Rev.Nanomed Nanobiotechnol. 1 (2009) 26-34.
[79] P. Opanasopit, M. Sakai, M. Nishikawa, S. Kawakami, F. Yamashita, M. Hashida. Inhibition of liver metastasis by targeting of immunomodulators using mannosylated liposome carriers, J.Control.Release. 80 (2002) 283-294.
[80] A. Gabizon, D.C. Price, J. Huberty, R.S. Bresalier, D. Papahadjopoulos. Effect of liposome composition and other factors on the targeting of liposomes to experimental tumors: biodistribution and imaging studies, Cancer Res. 50 (1990) 6371-6378.

[81] J.G. Zheng, T.Z. Tan. Antisense imaging of colon cancer-bearing nude mice with liposome-entrapped 99m-technetium-labeled antisense oligonucleotides of c-myc mRNA, World J.Gastroenterol. 10 (2004) 2563-2566.
[82] W. Banks. Developing drugs that can cross the blood-brain barrier: applications to Alzheimer's disease, BMC Neuroscience. 9 (2008) S2.
[83] A.J. Kastin, V. Akerstrom. Mahogany (1377-1428) enters brain by a saturable transport system, J.Pharmacol.Exp.Ther. 294 (2000) 633-636.
[84] L.B. Jaeger, W.A. Banks, J.L. Varga, A.V. Schally. Antagonists of growth hormone-releasing hormone cross the blood-brain barrier: a potential applicability to treatment of brain tumors, Proc.Natl.Acad.Sci.U.S.A. 102 (2005) 12495-12500.
[85] A. Regina, M. Demeule, C. Che, I. Lavallee, J. Poirier, R. Gabathuler, et al. Antitumour activity of ANG1005, a conjugate between paclitaxel and the new brain delivery vector Angiopep-2, Br J Pharmacol. 155 (2008) 185-197.
[86] W.A. Banks, A.B. Coon, S.M. Robinson, A. Moinuddin, J.M. Shultz, R. Nakaoke, et al. Triglycerides induce leptin resistance at the blood-brain barrier, Diabetes. 53 (2004) 1253-1260.
[87] T.O. Price, S.A. Farr, X. Yi, S. Vinogradov, E. Batrakova, W.A. Banks, et al. Transport across the blood-brain barrier of pluronic leptin, J.Pharmacol.Exp.Ther. 333 (2010) 253-263.
[88] S.R. Ennis, A.L. Betz. Sucrose permeability of the blood-retinal and blood-brain barriers. Effects of diabetes, hypertonicity, and iodate, Invest.Ophthalmol.Vis.Sci. 27 (1986) 1095-1102.
[89] P.R. Lockman, G. McAfee, W.J. Geldenhuys, C.J. Van der Schyf, T.J. Abbruscato, D.D. Allen. Brain uptake kinetics of nicotine and cotinine after chronic nicotine exposure, J.Pharmacol.Exp.Ther. 314 (2005) 636-642.
[90] P.R. Lockman, V.K. Manda, W.J. Geldenhuys, R.K. Mittapalli, F. Thomas, Z.F. Albayati, et al. Carrier-mediated transport of the quaternary ammonium neuronal nicotinic receptor antagonist n,n'-dodecylbispicolinium dibromide at the blood-brain barrier, J.Pharmacol.Exp.Ther. 324 (2008) 244-250.
[91] H. Murakami, N. Sawada, N. Koyabu, H. Ohtani, Y. Sawada. Characteristics of choline transport across the blood-brain barrier in mice: correlation with in vitro data, Pharm.Res. 17 (2000) 1526-1530.
[92] Y.J. Lee, H. Kusuhara, J.W. Jonker, A.H. Schinkel, Y. Sugiyama. Investigation of efflux transport of dehydroepiandrosterone sulfate and mitoxantrone at the mouse blood-brain barrier: a minor role of breast cancer resistance protein, J.Pharmacol.Exp.Ther. 312 (2005) 44-52.
[93] D. Triguero, J. Buciak, W.M. Pardridge. Capillary depletion method for quantification of blood-brain barrier transport of circulating peptides and plasma proteins, J.Neurochem. 54 (1990) 1882-1888.
[94] E.G. Gutierrez, W.A. Banks, A.J. Kastin. Murine tumor necrosis factor alpha is transported from blood to brain in the mouse, J.Neuroimmunol. 47 (1993) 169-176.
[95] A. Misra, S. Ganesh, A. Shahiwala, S.P. Shah. Drug delivery to the central nervous system: a review, J.Pharm.Pharm.Sci. 6 (2003) 252-273.
[96] J. Chang, Y. Jallouli, M. Kroubi, X. Yuan, W. Feng, C. Kang, et al. Characterization of endocytosis of transferrin-coated PLGA nanoparticles by the blood–brain barrier, Int.J.Pharm. 379 (2009) 285-292.
[97] Y. Jallouli, A. Paillard, J. Chang, E. Sevin, D. Betbeder. Influence of surface charge and inner composition of porous nanoparticles to cross blood-brain barrier in vitro, Int.J.Pharm. 344 (2007) 103-109.
[98] R.A. de Kemp, F.H. Epstein, C. Catana, B.M. Tsui, E.L. Ritman. Small-animal molecular imaging methods, J.Nucl.Med. 51 Suppl 1 (2010) 18S-32S.
[99] D.M. Chudakov, M.V. Matz, S. Lukyanov, K.A. Lukyanov. Fluorescent proteins and their applications in imaging living cells and tissues, Physiol.Rev. 90 (2010) 1103-1163.

Chapter 3

Comparison of five different targeting ligands to enhance accumulation of liposomes into the brain

Inge van Rooy
Enrico Mastrobattista
Gert Storm
Wim E Hennink
Raymond M Schiffelers

Journal of Controlled Release 150 (1):30-36 (2011)

Abstract

In many different studies nanoparticles modified with targeting ligands have been used to target to the brain. Many ligands have been successful, but it is difficult to compare results from different studies to determine which targeting ligand is the best. Therefore, we selected five targeting ligands (transferrin, RI7217, COG133, angiopep-2, and CRM197) and compared their ability to target liposomes to the brain in vitro and in vivo. In vitro, only CRM197-modified liposomes were able to bind to murine endothelial cells (bEnd.3). Both CRM197 and RI7217-modified liposomes associated with human endothelial cells (hCMEC/D3). In vivo, uptake of targeted liposomes was tested at 12 hours after iv injection. For some of the ligands, additional time points of 1 and 6 hours were tested. Only the RI7217 was able to significantly enhance brain uptake in vivo at all time points. Uptake in the brain capillaries was up to 10 times higher compared to untargeted liposomes, and uptake in the brain parenchyma was up to 4.3 times higher. Additionally, these results show that many targeting ligands that have been described for brain targeting, do not target to the brain in vivo when coupled to a liposomal delivery vehicle.

Introduction

Blood-brain barrier targeting

Drug transport to the brain is limited by the presence of the blood-brain barrier (BBB). To overcome this barrier, many delivery strategies have been attempted, such as local injection, induction of enhanced permeability, and targeted delivery [1]. Receptor mediated-targeting can be achieved by directly coupling of a targeting ligand to a drug molecule or by encapsulating drugs into nanoparticles. These are then actively targeted to receptors on the BBB. Some of the most widely used receptors for this purpose include the transferrin receptor, the insulin receptor, the low-density lipoprotein receptor family, and the diphtheria toxin receptor [2]. When ligands bind to these receptors, they are taken up into the brain endothelial cells by endocytosis. Large molecules or nanoparticles attached to these ligands can be taken up along, enabling intrinsically BBB-impermeable compounds to enter the BBB [3]. Subsequent transcytosis to the abluminal (brain) side is required for entry into the brain. For many nanoparticles it has been shown that they could be recovered from the brain parenchyma [4-7].

Ligands that have been used to target nanoparticles to the BBB receptors include endogenous and foreign proteins, antibodies, and peptides derived from protein binding domains. Many ligands have shown good targeting properties in many different studies, but it is difficult to compare results of different studies and therefore to decide which ligand has the best capacity to target a nanoparticle to the brain. In this study, we compare five ligands that have been described in literature for their brain targeting potential, and investigate their ability to target liposomes to the brain *in vitro* and *in vivo*. Liposomes were chosen as a delivery vehicle because they have been widely used for brain delivery *in vivo* [8-11]. The five selected targeting ligands are described below.

Holo-transferrin

The transferrin receptor (TfR) is the most widely studied receptor for BBB targeting. TfR is a transmembrane glycoprotein, consisting of two linked 90-kDa subunits, that each can bind a transferrin molecule. The receptor is highly expressed on immature erythroid cells, placental tissue, and rapidly dividing cells, both normal and malignant [12]. Furthermore it is expressed on hepatocytes and endothelial cells of the blood–brain barrier. The role of the receptor is the regulation of cellular uptake of iron from transferrin, a plasma protein which transports iron in the circulation. Cellular iron uptake from transferrin is initiated by the binding of holo-transferrin to the transferrin receptor, followed by endocytosis [13]. Iron-bound transferrin has a high affinity for the TfR, therefore it has been used as a ligand for targeting to brain endothelial cells [14,15]. However, this application is limited *in vivo*, because endogenous levels of transferrin are high, resulting in nearly saturated transferrin

receptors [1]. Nevertheless, successful brain targeting using transferrin as a targeting ligand has been accomplished *in vivo* [16,17].

RI7217

Because of the limitations of using transferrin as a targeting ligand *in vivo*, antibodies directed against the TfR have been used instead. The most well known is OX26. This anti-rat TfR monoclonal antibody binds to an epitope of the TfR that is different from the transferrin binding site. Therefore, it does not compete with the natural ligand [18]. OX26 has been successfully used in many brain targeting studies *in vivo* [19]. As OX26 is directed against the rat TfR, other monoclonal antibodies have been used to target the mouse TfR, including 8D3 [20] and RI7217 [21]. When directly compared, brain uptake of 8D3 is higher (3.1 %ID/g) than uptake of RI7217 (1.6 % ID/g) at 60 minutes [22]. However, RI7217 is more selective for the brain, as it is poorly taken up by the liver and kidney, in contrast to 8D3 [22]. It has been shown that RI7217 covalently coupled to human serum albumin nanoparticles is able to transport loperamide across the BBB [17].

COG133

Apolipoprotein E (apoE) is a 34-kDa protein that transports cholesterol and other lipids in the plasma and in the CNS [23]. ApoE is a constituent of both very-low-density lipoprotein (VLDL) and high-density lipoprotein (HDL) [24]. These complexes can be taken up in the brain through recognition of apoE by specific receptors at the BBB, including the low-density lipoprotein receptor (LDLR) and the LDLR-related protein (LRP). It has been shown that nanoparticles covalently linked to apoE can be targeted to the brain *in vivo* [5,25-27]. Previous experience with the protein taught us that apoE is a delicate protein that is difficult to work with [28]. The region of apoE that is critical for interaction with the LDL receptor resides between amino acid residues 140 and 160. Laskowitz et al. [24] derived an apoE-mimetic peptide from amino acids 133-149, named COG133 (LRVRLASHLRKLRKRLL), which retains its biological activity *in vitro* and *in vivo* [29]. COG133 is an attractive alternative for the whole apoE protein. Therefore, COG133 was used in this study.

Angiopep-2

The β-amyloid precursor protein (APP) can bind to the LRP present on brain endothelial cells. APP contains a sequence called the Kunitz protease inhibitor (KPI) domain. It has been suggested that this domain is important for recognition and internalization of APP by the LRP [30,31]. Several other proteins, including aprotinin, bikunin, and Kunitz-inhibitor precursor, contain a similar KPI domain. Demeule *et al*. [31] aligned these proteins, and from this alignment a family of peptides named angiopeps was designed and tested for brain uptake using an *in vitro* BBB model and *in situ* brain perfusion. In

particular, a peptide named angiopep-2 (TFFYGGSRGKRNNFKTEEY) showed a high transcytosis capacity and parenchymal accumulation. When angiopep-2 was conjugated to paclitaxel, it was shown that the conjugate enters the brain to a greater extent than paclitaxel alone and bypasses the P-gp [32]. Angiopep-2 has recently been used as a BBB targeting ligand for dendrimers [33] and micelles [34,35].

CRM197

Heparin-binding epidermal growth factor (EGF)-like growth factor (HB–EGF) is a member of the EGF family of growth factors that stimulate growth and differentiation [36]. Like all EGF family members, HB-EGF is synthesized as transmembrane precursor, and is then proteolytically processed to release the soluble mature protein from the cell surface. Uniquely, transmembrane HB–EGF, which has no known endogenous ligand, has been identified as the diphtheria toxin receptor (DTR). Diphtheria toxin (DT) binds to this receptor and enters the cell via endocytosis [37]. Enzymatic activity of the toxin blocks protein synthesis, resulting in cell death. Cross reacting material (CRM) 197 is a mutated form of DT which contains a single point mutation at position 52 (Gly→Glu), resulting in loss of enzymatic activity. Therefore CRM197 is non-toxic, but it retains the ability to bind to HB-EGF [38]. HB-EGF is expressed in various regions of the brain. Brain targeting of CRM197 conjugated to horseradish peroxidase has been shown *in vitro* and *in vivo* [39], and targeting of liposomal CRM197 has been shown *in vitro* [40].

Materials and Methods

Materials

Holo-transferrin, CRM197, and cholesterol were obtained from Sigma (St. Louis, MO). Purified rat anti-mouse CD71 (transferrin receptor) clone RI7217 isotype lgG2a,κ was obtained from Biolegend (San Diego, CA). COG133 peptide and angiopep-2 were synthesized by Caslo Laboratory ApS (Lyngby, Denmark) with a purity of 92% and 99%, respectively. Terminal ends were acetylated and amidated, and the peptides contained a C-terminal cysteine, resulting in Ac-LRVRLASHLRKLRKRLLC-NH_2 (COG133) and Ac-TFFYGGSRGKRNNFKTEEYC-NH_2 (angiopep-2). [^{3}H]cholesteryl hexadecyl ether, Soluene350, and Hionic-Fluor were obtained from PerkinElmer (Groningen, The Netherlands). Egg phosphatidylcholine (EPC) and egg phosphotidylglycerol (EPG) were obtained from Lipoid GmbH (Ludwigshafen, Germany). Maleimidophenyl butyryl phosphatidylethanolamine (MPB-PE) was obtained from Avanti Polar Lipids, Inc (Alabaster, AL).

Preparation of liposomes

Liposomes were composed of EPC, cholesterol, EPG, and MPB-PE, in a 6.5:2.6:0.8:0.1 molar ratio. A conventional liposome composition was chosen to ensure that the majority of liposomes was cleared from the blood at the 12-hour time point, as vascular content can greatly contribute to the concentration measured in the brain [41]. Liposomes were labeled with trace amounts of [^{3}H]cholesteryl hexadecyl ether (5 Ci/mol total lipid). This non-exchangeable and metabolically inert label is reliable to monitor the fate of liposomes *in vivo* [42]. Lipids were dissolved in chloroform, and a lipid film was made by rotary evaporation. The lipid film was hydrated in HBS (10 mM HEPES, 146 mM NaCl, pH 7.4) to a final concentration of 10 µmol/ml of total lipid. Liposomes were sized by repeated extrusion through polycarbonate membranes with a final pore size of 100 nm, using a high-pressure extruder. One batch of liposomes was prepared and divided into aliquots before coupling of ligands to each aliquot, so that each sample contained the same amount of lipids and ^{3}H. After coupling of proteins or peptides overnight, liposomes were incubated with 2-mercaptoethanol in a 1:1 thiol:maleimide molar ratio, to inactivate unreacted maleimide groups.

Coupling of proteins to liposomes

Transferrin, CRM197, and RI7217 were diluted to a concentration of ~60 µM in HBS buffer, and were incubated with *N*-Succinimidyl-S-acetylthioacetate, (SATA, Pierce, Rockford, IL) in a 1:8 (transferrin and RI7217) or 1:16 (CRM197) protein:SATA molar ratio, for 40 min at room temperature. Free SATA was removed by filter centrifugation (3 kDa MWCO). Upon use, SATA groups were deacetylated in HBS containing 0.5 M hydroxylamine.HCl and 0.02 mM TCEP, pH 7.4, for 90 minutes at room temperature, to generate sulfhydryl groups. This resulted in a SH/protein (mol/mol) ratio of 2.6, 3.3, and 3.0 for transferrin, CRM197, and RI7217 respectively, as determined by Ellman's reagent assay (Pierce). Directly after deacetylation, proteins were incubated with liposomes in a ratio of 0.4 nmol protein/µmol total lipid overnight at 4°C.

Coupling of peptides to liposomes

COG133 peptide and angiopep-2 were incubated with TCEP Gel slurry (Pierce) for 1 hour at room temperature to reduce the C-terminal cysteine thiol groups. Peptides were separated from TCEP Gel slurry by centrifugation in paper filter spin cups (Pierce), and immediately afterwards incubated with liposomes in a ratio of 0.4 nmol peptide/µmol total lipid overnight at 4°C.

Characterization of liposomes

To determine ligand coupling efficiency, samples of liposomes without ^{3}H label and free peptides were applied to a Waters Acquity UPLC system (Waters corporation, Milford, MA)

using a BEH300 C18 1.7µm column, at a flow rate of 0.25 ml/min. Gradient mobile phase was changed during 10 minutes from 100% solvent A (acetonitrile:H_2O 5:95) to 100% solvent B (acetonitrile), and ran additionally for 2 minutes at 100% solvent B. Both solvents contained 0.1% trifluoroacetic acid. UV detection was performed at 210 nm to detect uncoupled peptide, according to the method described by Koning *et al.* [43] Coupling efficiency was >90% for each ligand. This was estimated to result in 22 to 25 protein molecules per liposome, assuming that 80,000 phospholipid molecules form one unilamellar liposome of 100 nm [44].
The mean particle size distribution and the polydispersity index of the liposomes were determined by dynamic light scattering (DLS) in a Malvern ALV CGS-3 goniometer (Malvern Instruments, Malvern, UK) containing a He-Ne laser source (λ=632.8 nm, 22 mW output power) under an angle of 90°.The zeta-potential of the liposomes was determined using a Malvern zetasizer Nano-Z (Malvern Instruments). Measurements were performed in HBS (10 mM HEPES, 146 mM NaCl, pH 7.4).

Cells

Murine brain endothelial cells (bEnd.3) were obtained from ATCC (Manassas, VA) Cells were cultured at 37°C, 5% CO_2, in DMEM containing L-glutamine and 4.5 g/L glucose, supplemented with 10% FBS and antibiotics (penicillin and streptomycin).
Human brain endothelial cells (hCMEC/D3) [45] were obtained from Institut National de la Santé et de la Recherche Médicale (INSERM, Paris, France). Cells were cultured at 37°C, 5% CO_2, in EBM-2 basal medium supplemented with EGM-2 MV BulletKit (Lonza, Basel, Switzerland), containing growth factors and 2.5% FBS. Additionally, 10 mM HEPES, 1 ng/ml bFGF (Invitrogen), and antibiotics (penicillin and streptomycin) were added. hCMEC/D3 cells were grown on surfaces coated with 100 µg/ml Rat tail collagen type 1 (BD Biosciences). Prior to use, cell culture medium was replaced by cell differentiation medium, consisting of EBM-2 basal medium supplemented with 2.5% FBS, 1.4 µM hydrocortisone, 1 ng/ml bFGF, 10 mM HEPES, and antibiotics. Cells were grown to a monolayer in differentiation medium for one week. Medium was replaced every 2-3 days.

Incubation of liposomes with cells

bEnd.3 and hCMEC/D3 cells were seeded and grown confluent in 12-wells plates. Liposomes were diluted to 460 nmol/ml of total lipid in culture medium containing 0.5% fetal calf serum. Liposome dispersion (480 µl) was added to the cells, and incubated for 1 hour at 4°C or 37°C. The liposome dispersion was aspired and cells were washed 1x with 1 ml culture medium containing 0.5% serum and 2x with 1 ml PBS. Cells were trypsinized in 450 µl trypsin/EDTA and transferred to liquid scintillation vials. Twenty µl of the added liposome doses were also pipetted into liquid scintillation vials.

Liquid scintillation analysis of cells

One ml of Soluene350 was added to the cell lysates and to the input doses. The samples were incubated for 2 hours at 50°C, and additionally for 3 days at room temperature in the dark. Next, 10 ml of Hionic-Fluor was added. After vortexing, samples were temperature and light adapted by storing them in the dark for 2 to 5 hours. Samples were analyzed in a Tri-Carb 2200 CA Liquid Scintillation Analyzer (Packard).

Biodistribution studies

Male 22-30 g Balb/c mice (Harlan, Horst, The Netherlands) were used. Food and water were supplied *ad libitum*. Animal studies were performed according to national regulations and were approved by the local animal experiments ethical committee. Liposomes were injected intravenously into the tail vein at a dose of 2 µmol total lipid per mouse, corresponding to a ^{3}H dose of 10 µCi per mouse.

For the 12-hour time point, animals were sacrificed by CO_2 asphyxiation 12 hours after injection. Thorax was opened and blood was withdrawn from the heart. For the 1 and 6 hour time point, blood was withdrawn by cheek puncture 5 minutes before sacrifice. At 1 or 6 hours, animals were sacrificed by CO_2 asphyxiation. Subsequently, thorax was opened and a bulldog clamp with 8 x 1.2 mm serrated jaws (WPI, Berlin, Germany) was placed on the descending aorta. Right atrium of the heart was severed, and 25 ml of Hank's Balanced Salt Solution (HBSS, Invitrogen), containing 50 U/ml of heparin, was perfused through the left ventricle of the heart within 1-2 minutes.

For all time points the following organs were collected: brain cerebrum, brain cerebellum, liver, spleen, skin, muscle, kidney, lung, and heart. Brain cerebrum was further subjected to capillary depletion. For each organ, a 100-200 mg sample was transferred to a glass vial and weighed. For blood samples, a 30-50 mg sample was transferred to a glass vial and weighed. To each sample 2 ml of Soluene350 was added. Samples were incubated for 4 hours at 50°C, and additionally for 5-7 days at room temperature in the dark. Next, 10 ml of Hionic-Fluor was added. After vortexing, samples were temperature and light adapted by storing them in the dark for 2 to 5 hours. Samples were analyzed in a Tri-Carb 2200 CA Liquid Scintillation Analyzer. Organ uptake is represented as the percentage of the injected dose per whole organ. Blood volume of mice was assumed to be 7.2 ml per 100 g of body weight [46].

Brain capillary depletion

The capillary depletion method, as modified for mice [47,48] was performed to separate the cerebral capillaries from the parenchymal tissue. Mouse cerebrum was placed in a glass homogenizer on ice and 0.8 ml of ice cold depletion buffer was added (10 mM HEPES in HBSS, pH 7.4). Brain was homogenized with 10 strokes of the pestle in the homogenizer, and 1.6 ml of depletion buffer containing 26% dextran (MW 64-76 kDa,

Sigma) was added to the homogenate. Brain was homogenized a second time with 3 strokes of the pestle. A sample of this homogenate was taken, and the remainder was centrifuged at 5400xg for 15 minutes. The supernatant containing the brain parenchyma was separated from the pellet containing the brain microvasculature. The pellet was carefully washed with depletion buffer. Supernatant and pellet were transferred to glass vials and prepared for liquid scintillation counting as described above.

Statistical analysis

Data were analyzed using Graphpad Prism 4 for Windows software (Graphpad Software, San Diego, CA)

Results

Preparation and characterization of liposomes

Five brain-targeting ligands (holo-transferrin, RI7217, COG133, angiopep-2, and CRM197) were selected, and their ability to target liposomes to the brain was investigated. ^{3}H-labeled liposomes, composed of EPC, cholesterol, and EPG were prepared by lipid film hydration and extrusion. These liposomes contained 1% of a maleimide-linked PE, which was used to couple the ligands via their thiol groups to the liposomes. The peptides COG133 and angiopep-2 contained an intrinsic thiol group (C-terminal cysteine) and thiol groups of proteins RI7217, CRM197 and transferrin were introduced by SATA modification. The amount of ligand per liposomal lipid (mol/mol) was kept at the same ratio for all ligands, so that liposomal samples with the same number of targeting ligands per liposome were obtained. Final liposome characteristics are shown in Table I.

Ligands		**Final liposome characteristics**			
Name	*Molecular weight (kDa)*	*Estimated no. of ligands per liposome*	*Size (nm)*	*ζ potential (mV)*	*PDI*
no ligand	-	-	101 ±7	-22.1 ±0.6	0.08 ±0.01
COG133	2.27	22-25	103 ±9	-19.0 ±0.9	0.09 ±0.02
angiopep-2	2.45	22-25	102 ±8	-17.7 ±0.5	0.10 ±0.01
CRM197	63	22-25	109 ±3	-15.9 ±1.5	0.10 ±0.05
transferrin	76-81	22-25	120 ±2	-15.2 ±1.3	0.11 ±0.01
RI7217	150	22-25	116 ±17	-14.8 ±3.5	0.11 ±0.01

Table I. *Characteristics of ligands and ligand-coupled liposomes. Particle size z-average (nm), zeta (ζ) potential (mV), and polydispersity index (PDI) are shown as mean ±s.d. (n=2).*

Liposomal association with brain endothelial cells *in vitro*

Association of the targeted (ligand coupled) and untargeted ("no ligand") liposomes with murine brain endothelial cells (bEnd.3) was tested in vitro. 3H-labeled liposomes were incubated for 1 hour at 4°C or 37°C [49] with a monolayer of bEnd.3 cells in culture medium containing 0.5% serum. After incubation, the monolayer was washed and cells were detached and transferred to glass vials for liquid scintillation analysis (Figure 1 A, B). Of the 5 selected ligands, only CRM197 showed a significantly higher binding to the endothelial cells compared to the untargeted liposomes. The associated percentage of CRM197-targeted liposomes was comparable at 4°C and 37°C, indicating binding but not uptake after 1 hour. Liposome association with human brain endothelial cells (hCMEC/D3) was tested in the same way as for bEnd.3 cells at 37°C (Figure 1C). For hCMEC/D3 cells, the bound percentage of CRM197-targeted liposomes was comparable to the percentage bound to bEnd.3 cells. Interestingly, RI7217, which is an anti-mouse antibody, showed significant binding to these human endothelial cells but not to the murine endothelial cells.

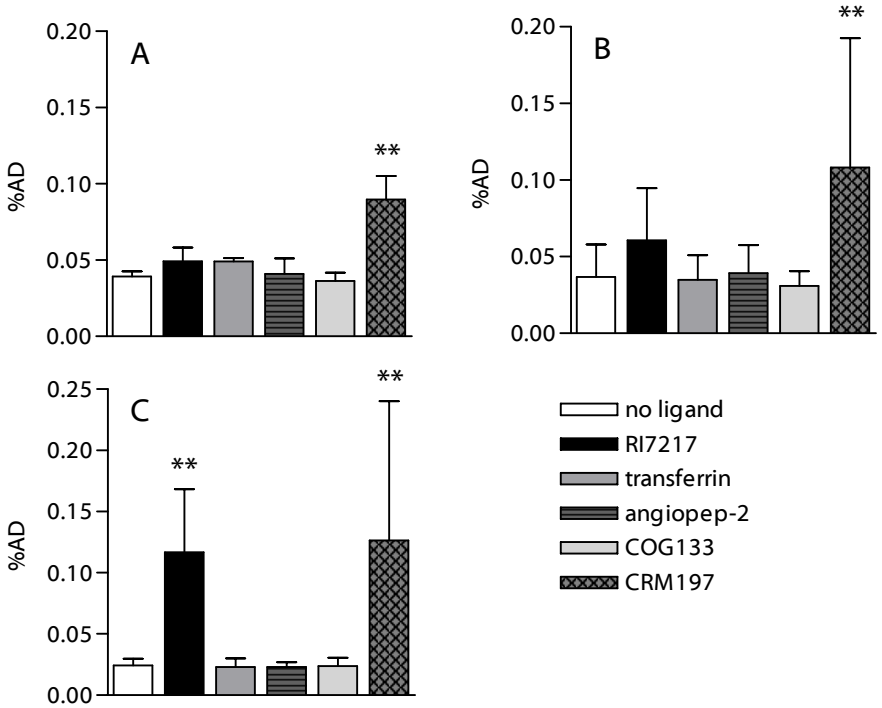

Figure 1. *Liposome association with brain endothelial cells in vitro, expressed as percentage of added dose (%AD). (**A**) association with bEnd.3 cells (murine origin) at 4°C. (**B**) association with bEnd.3 cells at 37°C. (**C**) association with hCMEC/D3 cells (human origin) at 37°C. Mean±s.d, n=4. One way ANOVA after log transformation to correct for non-Gaussian distributions. Dunnett's multiple comparison test vs no ligand **p<0.01.*

Liposome biodistribution after 12 hours

Mice were intravenously injected with the ^{3}H-labeled targeted liposomes. Twelve hours after injection, animals were sacrificed and blood, brain, and major organs were collected. The percentage of the injected dose (%ID) for the whole organs or the total blood volume is shown in Figure 2. As shown in Figure 2A, the amount of liposomes still present in the circulation after 12 hours was on average 12%.There was no significant increase or decrease in the uptake of the targeted liposomes in any of the organs, compared to the untargeted liposomes.

After the brain was taken out, it was divided into the cerebellum and the cerebrum. As the percentage of liposomes still circulating after 12 hours was reasonably low, no washout of the brain vasculature was performed. Estimates on the blood content of brain tissue are 12 µl/g brain tissue [50-52], which would (with 12% of the dose still circulating) put the maximum contribution of the vascular compartment to 0.04% of the total brain accumulation. The cerebrum was homogenized, and a sample of this homogenate was taken. The technique of brain capillary depletion was used to further divide the cerebrum into 2 fractions. Capillary depletion involves dextran density centrifugation, and results in a pellet which contains the brain vasculature, together with capillary red blood cells and some brain cell nuclei [47,48]. The supernatant contains the brain parenchyma and cerebral blood plasma. Liposomal radioactivity was counted in each of these brain fractions separately (Figure 2B).

For 4 of the 5 tested ligands, the %ID found in the different brain regions was not significantly different from the untargeted liposomes. Only liposomes modified with the RI7217 antibody showed a significantly higher dose in the brain fractions. The dose of the untargeted liposomes in the cerebrum (homogenate) was comparable to the dose in the parenchyma. However, as no vascular washout was performed and the untargeted liposomes are not expected to transcytose into the parenchyma to a great extent, the parenchymal dose is most likely to originate from liposomes present in cerebral plasma (or loosely adhering to the capillaries). In the brain capillary fraction, the dose of RI7217 liposomes was 10 times higher compared to the untargeted liposomes. This indicates uptake of these liposomes into the brain endothelial cells. The RI7217 liposome dose found in the parenchyma fraction was 2.6 times higher compared to the untargeted liposomes, suggesting that at least a fraction of these RI7217 liposomes was able to transcytose from the endothelial cells into the brain parenchyma.

Uptake measured in total homogenized brain (cerebrum + cerebellum) was 0.08%ID for untargeted liposomes and 0.22%ID for RI7217 liposomes (Figure 2B). If the dose originating from liposomes present in the circulation (0.04%) is subtracted, the dose in the brain results in 0.04%ID for untargeted liposomes and 0.18%ID for RI7217 liposomes, a 4.5 times increase.

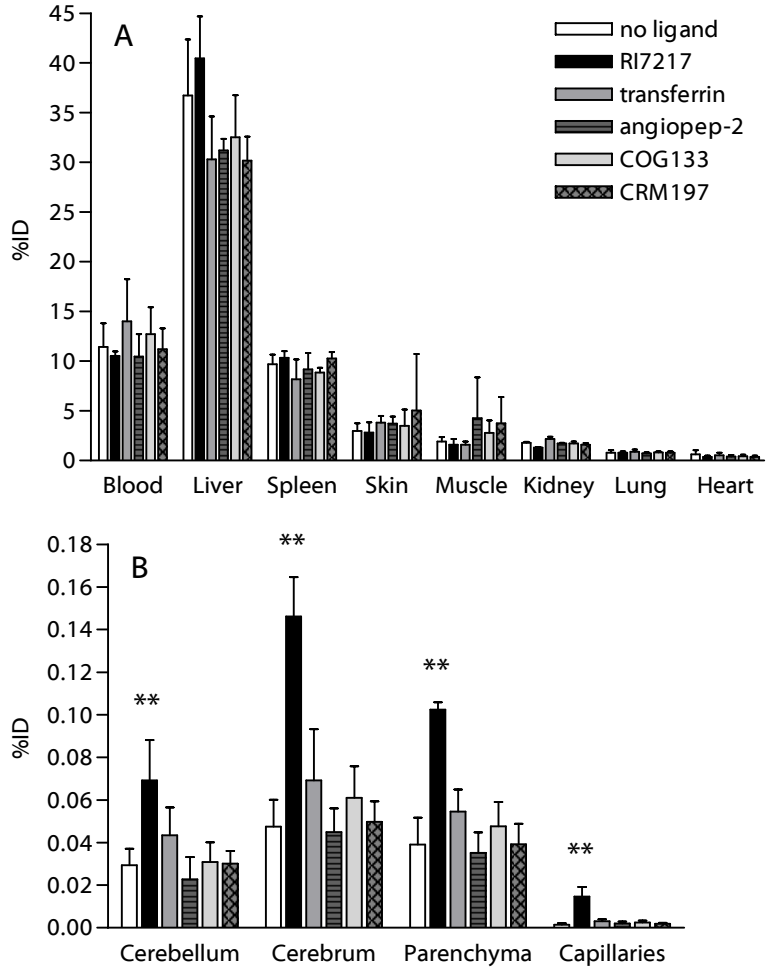

Figure 2. *Biodistribution of liposomes in mice, 12 hours after injection, expressed as percentage of injected dose (%ID). (**A**) Distribution in blood and major organs. (**B**) Distribution in the brain: total cerebellum, total cerebrum, cerebral parenchyma, and cerebral capillaries. Mean±s.d (n=5). One way ANOVA after log transformation to correct for non-Gaussian distributions. Dunnett's multiple comparison test vs no ligand **p<0.01.*

Liposome biodistribution after 1 and 6 hours

In this study, most of the targeted liposomes did not show any brain targeting after 12 hours. In many studies, brain targeting is shown at earlier time points [53-55]. Therefore, distribution of two of the ligands that did not show targeting at 12 hours (transferrin and angiopep-2) was studied after 1 hour. Also RI7217 was included as this ligand showed best targeting potential. In addition to the 1 hour time point, RI7217 liposome distribution was also studied at 6 hours after injection. Because the amount of liposomes in the circulation is higher at earlier time points, a vascular washout of the brain capillaries [56-58] was performed prior to excision of the brain and organs.

Similar to the 12-hour time point, the amount of liposomes still present in the circulation was comparable for all formulations at the 1 and 6 hour time points. About 56% of the liposomes was present in the circulation after 1 hour (Figure 3A). This percentage dropped to about 27% after 6 hours. After 1 hour, significantly more RI7217 liposomes had accumulated in the liver compared to the untargeted liposomes. After 6 hours, this difference was not observed anymore.

As shown in Figure 3B, transferrin and angiopep-2 were not able to target the liposomes to the brain 1 hour after injection, while RI7217 again significantly enhanced brain uptake in the cerebrum, parenchyma and capillaries.
At the 1 hour time point, most of the untargeted liposomes in the cerebrum were found in the parenchyma fraction. As transcytosis of untargeted liposomes is unlikely, this fraction may represent liposomes that were not properly washed out from the brain vasculature. The percentage of untargeted liposomes in the parenchyma fraction decreased after 6 hours, presumably because the percentage of liposomes in the circulation (background) decreased. For the RI7217-liposomes, the %ID did not decrease with the decreasing circulation percentages, indicating uptake of RI7217 liposomes into the brain parenchyma.
At 6 hours after injection, the difference between untargeted and RI7217-targeted liposomes was highest; 4.3 times more RI7217 liposomes were found in the brain parenchyma compared to the untargeted liposomes.

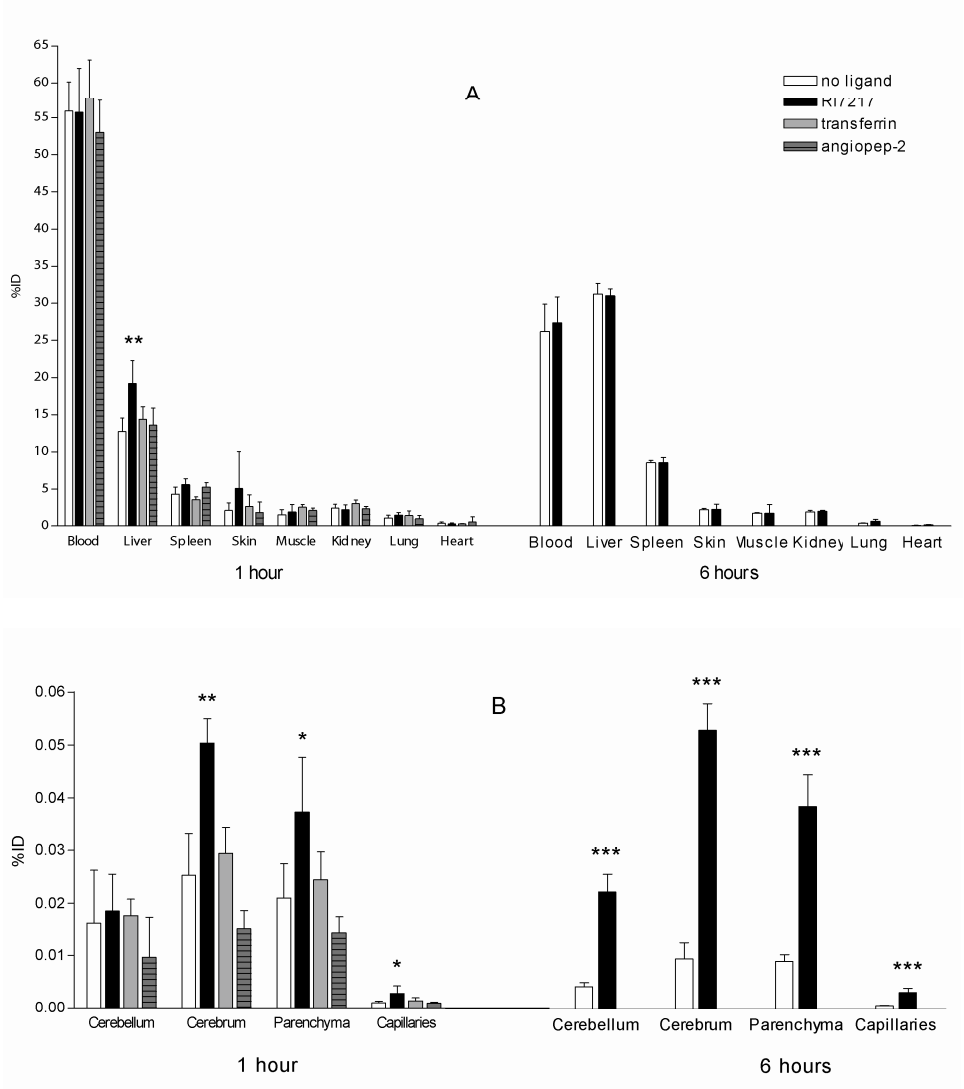

Figure 3. *Biodistribution of liposomes in mice, 1 and 6 hours after injection, expressed as percentage of injected dose (%ID). (**A**) Distribution in blood and major organs. (**B**) Distribution in the brain: total cerebellum, total cerebrum, cerebral parenchyma, and cerebral capillaries. Mean±s.d. One hour time point (n=4): one way ANOVA after log transformation to correct for non-Gaussian distributions. Dunnett's multiple comparison test vs no ligand. Six hour time point (n=3): students t-test after log transformation. *p<0.05 **p<0.01 ***p<0.005.*

Discussion

In vitro experiments showed that RI7217, which is an anti-mouse antibody, induced significant binding to human (hCMEC/D3) endothelial cells. Reactivity of this antibody with the human TfR has not been documented, but is plausible to occur, since the mouse and human transferrin receptor show 86% homology at the amino acid level [59]. Moreover, the anti-rat TfR antibody OX26 was also shown to bind to the hCMEC/D3 cells [60], indicating the likeliness of cross-species reactivity of anti-TfR antibodies towards the TfR expressed on these cells. Binding of RI7217 liposomes to murine (bEnd.3) cells was not significantly elevated, which may indicate a lower level of TfR expression on bEnd.3 cells compared to hCMEC/D3 cells.
Interestingly, RI7217 but not holo-transferrin was able to bind to hCMEC/D3 cells. Holo-transferrin has a high affinity for the transferrin receptor. This affinity strongly decreases when iron disassociates from transferrin (apo-transferrin) [12]. If disassociation occurred during the incubation, this could explain why transferrin-coupled liposomes did not bind to the endothelial cells *in vitro*.

CRM197-conjugated liposomes did not show increased uptake at 37°C compared to 4°C after 1 hour in murine bEnd.3 cells. Mice are known to be less sensitive to diphtheria toxin compared to humans, rabbits and guinea pigs. Although similar numbers of HB-EGF are expressed in the mouse to which diphtheria toxin can specifically bind, toxin entry into murine cells is blocked, resulting in the absence of toxic effects [61,62]. This could explain why CRM197 uptake was not observed in bEnd.3 cells.
Because CRM197 was the best binding ligand to murine brain endothelial cells *in vitro*, it was interesting to investigate brain binding also *in vivo*. However, CRM197 was not able to target the liposomes to the murine brain *in vivo*. This could be due to the mentioned lack of cell entry of CRM197 in the mouse. Additionally, it has been shown that within the brain endothelium, HB-EGF is especially upregulated in hypoxic and ischemic areas after brain infarction [63]. Therefore, it is possible that the DTR is not expressed to a sufficient level in healthy mice to mediate the targeting of particles to the brain.

The COG133 peptide was unable to target the liposomes to the BBB *in vitro* and *in vivo*. COG133 is derived from the receptor binding region of apoE, and does not include the polymorphic residues that define the E2, E3, and E4 isoforms of ApoE in humans [64]. Although mice have only one isoform of apoE, it was shown that human apoE3 mediates transport of nanoparticles to the murine brain, whereas human apoE2 does not [25]. Human apoE2 and apoE3 differ by only one amino acid outside of the receptor binding region, however, this mutation apparently has great impact on binding to the LDLR on

brain endothelial cells. Therefore, the receptor-binding region only (COG133) may not possess the right properties to mediate uptake of particles at the BBB.

The *in vivo* experiments showed that of the 5 targeting ligands that were tested, only the RI7217 antibody was able to significantly target liposomes to the brain. Brain targeting of unconjugated and albumin nanoparticle-conjugated RI7217 has been shown before *in vivo* [17,22], but this is the first report that shows targeting of liposome-conjugated RI7217 to the brain. The RI7217 liposome dose that reached the brain was about 0.18% after 12 hours. Although this may seem low, it is comparable to the %ID that others have found using targeted nanoparticles [9,10,33,53], and low brain uptake percentages can be sufficient for a drug to exert an effect in the brain. For example, only about 0.02% of a peripherally administered dose of morphine enters the brain, but that is sufficient to produce analgesia [65]. The stronger brain targeting of RI7217 compared to the other ligands may be due to the size of the antibody. RI7217 has the highest molecular weight of the ligands tested, and may therefore stick out the most from the negatively charged surface of the liposomes, enhancing receptor interaction. Furthermore, the high affinity of the RI7217 antibody for its receptor compared to the other ligands may result in stronger binding of the liposomes.

Although the conjugated ligand is the main parameter that induces uptake of the particle into the brain, the type of nanoparticle may also influence uptake, due to different size, shape, or surface properties [66-68]. Ligands that did not enhance brain uptake of liposomes, may do so when attached to a different type of nanoparticle, e.g. an albumin nanoparticle, polymeric nanoparticle, solid lipid nanoparticle, or directly conjugated to a drug.

Next to the particle type and formulation parameters, the ligand density also plays an important role in targeting efficacy [43,69]. In the present study, ligand coupling was performed using the same ligand per lipid ratio for each of the targeting ligands, resulting in an estimated number of 22 to 25 ligands per liposome. We considered keeping the same number of ligands per liposome to be the fairest comparison between the ligands. However, optimal ligand density can be different for each ligand, and changing the density could yield a different outcome.

In conclusion, we showed that for liposomes composed of EPC, cholesterol, EPG, and MPB-PE, the RI7217 anti-TfR antibody is a suitable ligand for targeting to the brain *in vivo*. Uptake in the brain capillaries was up to 10 times higher compared to untargeted liposomes, and uptake in the brain parenchyma was up to 4.3 times higher. These results show the importance of liposomes and the transferrin receptor for targeting to the brain

in vivo. Potential CNS drugs with poor BBB penetration can be encapsulated inside the liposomes. In this way, RI7217-coupled liposomes could increase uptake of CNS drugs into the brain.

Acknowledgements

We thank Pierre-Olivier Couraud, Ignacio Romero, and Babette Weksler for providing the hCMEC/D3 cells. This work was performed within the framework of the Dutch Top Institute Pharma, project T5-105-1: nanoscience as a tool for improving bioavailability and blood-brain barrier penetration.

References

[1] A.G. de Boer, P.J. Gaillard. Drug Targeting to the Brain, Annu Rev Pharmacol Toxicol. 47 (2007) 323-355.

[2] A.G. de Boer, I.C. van der Sandt, P.J. Gaillard. The role of drug transporters at the blood-brain barrier, Annu Rev Pharmacol Toxicol. 43 (2003) 629-656.

[3] W.M. Pardridge. The blood-brain barrier: bottleneck in brain drug development, NeuroRx. 2 (2005) 3-14.

[4] K.S. Rao, M.K. Reddy, J.L. Horning, V. Labhasetwar. TAT-conjugated nanoparticles for the CNS delivery of anti-HIV drugs, Biomaterials. 29 (2008) 4429-4438.

[5] A. Zensi, D. Begley, C. Pontikis, C. Legros, L. Mihoreanu, S. Wagner, et al. Albumin nanoparticles targeted with Apo E enter the CNS by transcytosis and are delivered to neurones, J.Control.Release. 137 (2009) 78-86.

[6] A. Cerletti, J. Drewe, G. Fricker, A.N. Eberle, J. Huwyler. Endocytosis and transcytosis of an immunoliposome-based brain drug delivery system, J.Drug Target. 8 (2000) 435-446.

[7] G. Tosi, A.V. Vergoni, B. Ruozi, L. Bondioli, L. Badiali, F. Rivasi, et al. Sialic acid and glycopeptides conjugated PLGA nanoparticles for central nervous system targeting: In vivo pharmacological evidence and biodistribution, J.Control.Release. 145 (2010) 49-57.

[8] N. Shi, Y. Zhang, C. Zhu, R.J. Boado, W.M. Pardridge. Brain-specific expression of an exogenous gene after i.v. administration, Proc.Natl.Acad.Sci.U.S.A. 98 (2001) 12754-12759.

[9] Y. Xie, L. Ye, X. Zhang, W. Cui, J. Lou, T. Nagai, et al. Transport of nerve growth factor encapsulated into liposomes across the blood-brain barrier: in vitro and in vivo studies, J.Control.Release. 105 (2005) 106-119.

[10] A. Schnyder, S. Krahenbuhl, J. Drewe, J. Huwyler. Targeting of daunomycin using biotinylated immunoliposomes: pharmacokinetics, tissue distribution and in vitro pharmacological effects, J.Drug Target. 13 (2005) 325-335.

[11] E. Afergan, H. Epstein, R. Dahan, N. Koroukhov, K. Rohekar, H.D. Danenberg, et al. Delivery of serotonin to the brain by monocytes following phagocytosis of liposomes, J.Control.Release. 132 (2008) 84-90.

[12] P. Ponka, C.N. Lok. The transferrin receptor: role in health and disease, Int.J.Biochem.Cell Biol. 31 (1999) 1111-1137.

[13] T. Moos, T. Rosengren Nielsen, T. Skjorringe, E.H. Morgan. Iron trafficking inside the brain, J.Neurochem. 103 (2007) 1730-1740.

[14] C.C. Visser, S. Stevanovic, L.H. Voorwinden, L.v. Bloois, P.J. Gaillard, M. Danhof, et al. Targeting liposomes with protein drugs to the blood-brain barrier in vitro, European Journal of Pharmaceutical Sciences. 25 (2005) 299-305.
[15] J. Chang, Y. Jallouli, M. Kroubi, X. Yuan, W. Feng, C. Kang, et al. Characterization of endocytosis of transferrin-coated PLGA nanoparticles by the blood–brain barrier, Int.J.Pharm. 379 (2009) 285-292.
[16] V. Mishra, S. Mahor, A. Rawat, P.N. Gupta, P. Dubey, K. Khatri, et al. Targeted brain delivery of AZT via transferrin anchored pegylated albumin nanoparticles, J.Drug Target. 14 (2006) 45-53.
[17] K. Ulbrich, T. Hekmatara, E. Herbert, J. Kreuter. Transferrin- and transferrin-receptor-antibody-modified nanoparticles enable drug delivery across the blood-brain barrier (BBB), European Journal of Pharmaceutics and Biopharmaceutics. 71 (2009) 251-256.
[18] A. Jones, E. Shusta. Blood–Brain Barrier Transport of Therapeutics via Receptor-Mediation, Pharmaceutical Research. 24 (2007) 1759-1771.
[19] J. Huwyler, D. Wu, W.M. Pardridge. Brain drug delivery of small molecules using immunoliposomes, Proc.Natl.Acad.Sci.U.S.A. 93 (1996) 14164-14169.
[20] K. Kissel, S. Hamm, M. Schulz, A. Vecchi, C. Garlanda, B. Engelhardt. Immunohistochemical localization of the murine transferrin receptor (TfR) on blood-tissue barriers using a novel anti-TfR monoclonal antibody, Histochem.Cell Biol. 110 (1998) 63-72.
[21] J. Lesley, R. Hyman, R. Schulte, J. Trotter. Expression of transferrin receptor on murine hematopoietic progenitors, Cell.Immunol. 83 (1984) 14-25.
[22] H.J. Lee, B. Engelhardt, J. Lesley, U. Bickel, W.M. Pardridge. Targeting Rat Anti-Mouse Transferrin Receptor Monoclonal Antibodies through Blood-Brain Barrier in Mouse, J Pharmacol Exp Ther. 292 (2000) 1048-1052.
[23] G. Bu. Apolipoprotein E and its receptors in Alzheimer's disease: pathways, pathogenesis and therapy, Nat.Rev.Neurosci. 10 (2009) 333-344.
[24] D.T. Laskowitz, A.D. Thekdi, S.D. Thekdi, S.K. Han, J.K. Myers, S.V. Pizzo, et al. Downregulation of microglial activation by apolipoprotein E and apoE-mimetic peptides, Exp.Neurol. 167 (2001) 74-85.
[25] K. Michaelis, M.M. Hoffmann, S. Dreis, E. Herbert, R.N. Alyautdin, M. Michaelis, et al. Covalent linkage of apolipoprotein e to albumin nanoparticles strongly enhances drug transport into the brain, J.Pharmacol.Exp.Ther. 317 (2006) 1246-1253.
[26] U. Hulsermann, M.M. Hoffmann, U. Massing, G. Fricker. Uptake of apolipoprotein E fragment coupled liposomes by cultured brain microvessel endothelial cells and intact brain capillaries, J.Drug Target. 17 (2009) 610-618.
[27] J. Kreuter, D. Shamenkov, V. Petrov, P. Ramge, K. Cychutek, C. Koch-Brandt, et al. Apolipoprotein-mediated Transport of Nanoparticle-bound Drugs Across the Blood-Brain Barrier, Journal of Drug Targeting. 10 (2002) 317.
[28] P.C. Rensen, R.M. Schiffelers, A.J. Versluis, M.K. Bijsterbosch, M.E. Van Kuijk-Meuwissen, T.J. Van Berkel. Human recombinant apolipoprotein E-enriched liposomes can mimic low-density lipoproteins as carriers for the site-specific delivery of antitumor agents, Mol.Pharmacol. 52 (1997) 445-455.
[29] F.Q. Li, G.D. Sempowski, S.E. McKenna, D.T. Laskowitz, C.A. Colton, M.P. Vitek. Apolipoprotein E-derived peptides ameliorate clinical disability and inflammatory infiltrates into the spinal cord in a murine model of multiple sclerosis, J.Pharmacol.Exp.Ther. 318 (2006) 956-965.
[30] M.Z. Kounnas, R.D. Moir, G.W. Rebeck, A.I. Bush, W.S. Argraves, R.E. Tanzi, et al. LDL receptor-related protein, a multifunctional ApoE receptor, binds secreted β-amyloid precursor protein and mediates its degradation, Cell. 82 (1995) 331-340.
[31] M. Demeule, A. Regina, C. Che, J. Poirier, T. Nguyen, R. Gabathuler, et al. Identification and design of peptides as a new drug delivery system for the brain, J Pharmacol Exp Ther. 324 (2008) 1064-1072.
[32] A. Regina, M. Demeule, C. Che, I. Lavallee, J. Poirier, R. Gabathuler, et al. Antitumour activity of ANG1005, a conjugate between paclitaxel and the new brain delivery vector Angiopep-2, Br J Pharmacol. 155 (2008) 185-197.

[33] W. Ke, K. Shao, R. Huang, L. Han, Y. Liu, J. Li, et al. Gene delivery targeted to the brain using an Angiopep-conjugated polyethyleneglycol-modified polyamidoamine dendrimer, Biomaterials. 30 (2009) 6976-6985.
[34] J. Shen, C. Zhan, C. Xie, Q. Meng, B. Gu, C. Li, et al. Poly(ethylene glycol)-block-poly(d,l-lactide acid) micelles anchored with angiopep-2 for brain-targeting delivery, J.Drug Target. In Press (2010).
[35] K. Shao, R. Huang, J. Li, L. Han, L. Ye, J. Lou, et al. Angiopep-2 modified PE-PEG based polymeric micelles for amphotericin B delivery targeted to the brain, J.Controlled Release. In Press.
[36] G. Raab, M. Klagsbrun. Heparin-binding EGF-like growth factor, Biochimica et Biophysica Acta (BBA) - Reviews on Cancer. 1333 (1997) F179-F199.
[37] G. Giannini, R. Rappuoli, G. Ratti. The amino-acid sequence of two non-toxic mutants of diphtheria toxin: CRM45 and CRM197, Nucleic Acids Res. 12 (1984) 4063-4069.
[38] M. Kaefer, S. Vemulapalli, M.R. Freeman. A nontoxic diphtheria toxin analogue inhibits neonatal bladder smooth muscle cell proliferation, J.Urol. 163 (2000) 580-584.
[39] P.J. Gaillard, A. Brink, A.G. de Boer. Diphtheria toxin receptor-targeted brain drug delivery, Int.Congr.Ser. 1277 (2005) 185-198.
[40] P.J. Gaillard, A.G. de Boer. A novel opportunity for targeted drug delivery to the brain, J.Control.Release. 116 (2006) e60-2.
[41] I. van Rooy, S. Cakir-Tascioglu, W.E. Hennink, G. Storm, R.M. Schiffelers, E. Mastrobattista. In Vivo Methods to Study Uptake of Nanoparticles into the Brain, Pharm.Res. 28 (2011) 456-471.
[42] G.L. Pool, M.E. French, R.A. Edwards, L. Huang, R.H. Lumb. Use of radiolabeled hexadecyl cholesteryl ether as a liposome marker, Lipids. 17 (1982) 448-452.
[43] G.A. Koning, R.M. Schiffelers, M.H.M. Wauben, R.J. Kok, E. Mastrobattista, G. Molema, et al. Targeting of angiogenic endothelial cells at sites of inflammation by dexamethasone phosphate-containing RGD peptide liposomes inhibits experimental arthritis, Arthritis & Rheumatism. 54 (2006) 1198-1208.
[44] D. Kirpotin, J.W. Park, K. Hong, S. Zalipsky, W.L. Li, P. Carter, et al. Sterically stabilized anti-HER2 immunoliposomes: design and targeting to human breast cancer cells in vitro, Biochemistry. 36 (1997) 66-75.
[45] B.B. Weksler, E.A. Subileau, N. Perriere, P. Charneau, K. Holloway, M. Leveque, et al. Blood-brain barrier-specific properties of a human adult brain endothelial cell line, FASEB J. 19 (2005) 1872.
[46] K.H. Diehl, R. Hull, D. Morton, R. Pfister, Y. Rabemampianina, D. Smith, et al. A good practice guide to the administration of substances and removal of blood, including routes and volumes, J.Appl.Toxicol. 21 (2001) 15-23.
[47] D. Triguero, J. Buciak, W.M. Pardridge. Capillary depletion method for quantification of blood-brain barrier transport of circulating peptides and plasma proteins, J.Neurochem. 54 (1990) 1882-1888.
[48] E.G. Gutierrez, W.A. Banks, A.J. Kastin. Murine tumor necrosis factor alpha is transported from blood to brain in the mouse, J.Neuroimmunol. 47 (1993) 169-176.
[49] J.A.A.M. Kamps, G.L. Scherphof, Binding, uptake, and processing of liposome components and liposome contents, in: Torchilin VP, Weissig V (Eds.), Liposomes: a practical approach, 2nd ed., Oxford University Press, Oxford, 2003, pp. 271-272.
[50] H. Murakami, H. Takanaga, H. Matsuo, H. Ohtani, Y. Sawada. Comparison of blood-brain barrier permeability in mice and rats using in situ brain perfusion technique, Am.J.Physiol.Heart Circ.Physiol. 279 (2000) H1022-8.
[51] Y.J. Lee, H. Kusuhara, J.W. Jonker, A.H. Schinkel, Y. Sugiyama. Investigation of efflux transport of dehydroepiandrosterone sulfate and mitoxantrone at the mouse blood-brain barrier: a minor role of breast cancer resistance protein, J.Pharmacol.Exp.Ther. 312 (2005) 44-52.
[52] H. Murakami, N. Sawada, N. Koyabu, H. Ohtani, Y. Sawada. Characteristics of choline transport across the blood-brain barrier in mice: correlation with in vitro data, Pharm.Res. 17 (2000) 1526-1530.

[53] J. Lode, I. Fichtner, J. Kreuter, A. Berndt, J.E. Diederichs, R. Reszka. Influence of surface-modifying surfactants on the pharmacokinetic behavior of 14C-poly (methylmethacrylate) nanoparticles in experimental tumor models, Pharm.Res. 18 (2001) 1613-1619.
[54] X. Zhang, Y. Xie, Y. Jin, X. Hou, L. Ye, J. Lou. The effect of RMP-7 and its derivative on transporting Evans blue liposomes into the brain, Drug Deliv. 11 (2004) 301-309.
[55] H. Chen, L. Tang, Y. Qin, Y. Yin, J. Tang, W. Tang, et al. Lactoferrin-modified procationic liposomes as a novel drug carrier for brain delivery, Eur.J.Pharm.Sci. 40 (2010) 94-102.
[56] A.J. Kastin, V. Akerstrom. Mahogany (1377-1428) enters brain by a saturable transport system, J.Pharmacol.Exp.Ther. 294 (2000) 633-636.
[57] L.B. Jaeger, W.A. Banks, J.L. Varga, A.V. Schally. Antagonists of growth hormone-releasing hormone cross the blood-brain barrier: a potential applicability to treatment of brain tumors, Proc.Natl.Acad.Sci.U.S.A. 102 (2005) 12495-12500.
[58] T.O. Price, S.A. Farr, X. Yi, S. Vinogradov, E. Batrakova, W.A. Banks, et al. Transport across the blood-brain barrier of pluronic leptin, J.Pharmacol.Exp.Ther. 333 (2010) 253-263.
[59] E. Wang, N. Obeng-Adjei, Q. Ying, L. Meertens, T. Dragic, R.A. Davey, et al. Mouse mammary tumor virus uses mouse but not human transferrin receptor 1 to reach a low pH compartment and infect cells, Virology. 381 (2008) 230-240.
[60] B. Poller, H. Gutmann, S. Krähenbühl, B. Weksler, I. Romero, P. Couraud, et al. The human brain endothelial cell line hCMEC/D3 as a human blood-brain barrier model for drug transport studies, J Neurochem. 107 (2008) 1358-1368.
[61] T. Chang, D.M. Neville Jr. Demonstration of diphtheria toxin receptors on surface membranes from both toxin-sensitive and toxin-resistant species, J.Biol.Chem. 253 (1978) 6866-6871.
[62] J.R. Didsbury, J.M. Moehring, T.J. Moehring. Binding and uptake of diphtheria toxin by toxin-resistant Chinese hamster ovary and mouse cells, Mol.Cell.Biol. 3 (1983) 1283-1294.
[63] N. Tanaka, M. Sasahara, M. Ohno, S. Higashiyama, Y. Hayase, M. Shimada. Heparin-binding epidermal growth factor-like growth factor mRNA expression in neonatal rat brain with hypoxic/ischemic injury, Brain Res. 827 (1999) 130-138.
[64] D.T. Laskowitz, S.E. McKenna, P. Song, H. Wang, L. Durham, N. Yeung, et al. COG1410, a novel apolipoprotein E-based peptide, improves functional recovery in a murine model of traumatic brain injury, J.Neurotrauma. 24 (2007) 1093-1107.
[65] W. Banks. Developing drugs that can cross the blood-brain barrier: applications to Alzheimer's disease, BMC Neuroscience. 9 (2008) S2.
[66] K. Zhang, H. Fang, Z. Chen, J.S. Taylor, K.L. Wooley. Shape effects of nanoparticles conjugated with cell-penetrating peptides (HIV Tat PTD) on CHO cell uptake, Bioconjug.Chem. 19 (2008) 1880-1887.
[67] P. Chaudhuri, R. Harfouche, S. Soni, D.M. Hentschel, S. Sengupta. Shape effect of carbon nanovectors on angiogenesis, ACS Nano. 4 (2010) 574-582.
[68] S. Gelperina, O. Maksimenko, A. Khalansky, L. Vanchugova, E. Shipulo, K. Abbasova, et al. Drug delivery to the brain using surfactant-coated poly(lactide-co-glycolide) nanoparticles: influence of the formulation parameters, Eur.J.Pharm.Biopharm. 74 (2010) 157-163.
[69] J.W. Park, D.B. Kirpotin, K. Hong, R. Shalaby, Y. Shao, U.B. Nielsen, et al. Tumor targeting using anti-her2 immunoliposomes, J.Controlled Release. 74 (2001) 95-113.

Chapter 4

Identification of peptide ligands for targeting to the blood-brain barrier

Inge van Rooy
Serpil Cakir-Tascioglu
Pierre-Olivier Couraud
Ignacio A Romero
Babette Weksler
Gert Storm
Wim E Hennink
Raymond M Schiffelers
Enrico Mastrobattista

Pharmaceutical Research 27(4):673-82 (2010)

Abstract

Purpose. Transport of drugs to the brain is limited by the blood-brain barrier. New, specific, brain endothelium ligands can facilitate brain-specific delivery of drugs.
Methods. We used phage display in an *in situ* brain perfusion model, to screen for new brain endothelium peptide ligands.
Results. Two phage clones, displaying 15-amino acid peptides (GLA and GYR) that were selected for brain binding in the mouse model, showed significant binding to human brain endothelium (hCMEC/D3), compared to a random control phage. This binding was not seen for other human endothelial cells (HUVEC). Binding to hCMEC/D3 cells was dose dependent. When phage GLA and GYR were individually perfused through the murine brain, their ability to bind to the brain was 6-fold (GLA) and 5-fold (GYR) higher than the control phage. When compared to lung perfusion, phage showed a 8.5-fold (GYR) and 48-fold (GLA) preference for brain over lung compared to the control.
Conclusions. These results indicate that two new peptide ligands have been identified that may be used for specific targeting of drugs to the blood-brain barrier.

Introduction

Transport of drugs to the brain is limited by the presence of the blood-brain barrier (BBB). This barrier is formed by specialized endothelial cells and supported by other cell types such as astrocytes and pericytes [1]. The BBB regulates homeostasis of the brain and is selectively permeable for the uptake and efflux of ions, nutrients and metabolites [2]. Drug transport via the paracellular route is prevented by tight junctions between the endothelial cells. Free diffusion via the transcellular route is accessible only to lipophilic compounds smaller than approximately 400 Da [3]. This limits the treatment of many brain diseases, such as Alzheimer's disease and Parkinson's disease. Even in certain pathological situations where the BBB is partly disrupted, drug transport remains limited [4].

To overcome this limitation carrier systems such as nanoparticles have been used to deliver drugs to the brain. Antibody ligands have been successfully coupled to the nanoparticles to target the brain endothelial cell receptors [5,6]. The main receptors that have been targeted are the transferrin receptor [7] and the insulin receptor [8]. However, these receptors are not brain specific. They are widely expressed in peripheral organs [9], limiting their selectivity and applicability as brain targeting receptors. Therefore, identification of new brain targets is needed to deliver drugs more selectively into the brain. The objective of this study was to identify new targeting ligands that can be used for active targeting of drug delivery systems to the brain, aiming for selectivity for brain endothelium.

Peptides are highly suitable for ligand screening, when expressed on a phage display system, and they have been widely used as targeting ligands [10]. Phage display is a powerful technology for ligand identification [11-14]. Large libraries, expressing peptides or proteins can be screened for target affinity [15]. We used a random 15-mer peptide library to identify brain-targeting peptide ligands. *In vivo*, blood-brain barrier endothelial cells get stimulated by their surrounding cells [16,17] and intraluminal blood flow [18]. This contributes to the complexity of the blood-brain barrier and regulates the expression of specific receptors at the cell surface in a polarized fashion. For this reason, ligand screening should preferably be performed *in vivo*. However, as *in vivo* phage screening in humans was impossible for ethical reasons, we choose to pre-select phage in a mouse perfusion model, to enrich for peptides recognizing brain endothelial cells in their natural environment. Because the brain remains intact, the endothelial cells keep their polarity and their contact with the surrounding cells, maintaining expression of relevant receptors. After the pre-selection for *in vivo* relevant receptors, identified ligands were tested for

cross-reactivity with human cell-surface receptors expressed by human endothelial cells *in vitro*. In this way, the complexity of the *in vivo* BBB and the significance of the human BBB were combined.

Materials and Methods

Phage library and bacteria

Filamentous phage fd-tet, which confers tetracycline resistance on the host [19], was used for this study. Random peptide library f3-15mer [20], containing 2.5 x 10^8 primary clones (GenBank Accession AF246445) with foreign 15-mer peptide displayed on pIII was provided by George P. Smith (Columbia, MO). Kanamycin resistant *E. coli* K91BluKan (K91BK) host bacteria were also provided by George P. Smith. The K91BK sex is Hfr Cavalli, resulting in deployment of the F pilus: the attachment site for filamentous phage infection.

Animals

In situ phage display screening was performed in male 6-8 weeks old C57Bl/6 mice (Charles River, The Netherlands). Perfusion of single clones was done in male 28-32 g Balb/c mice (Harlan, Horst, The Netherlands). Food and water were supplied *ad libitum*. Animal studies were performed according to national regulations and were approved by the local animal experiments ethical committee.

In situ brain perfusion of phage

40 units of heparin (Sigma) were injected i.v. into the tail vein to prevent coagulation of blood inside the microvessels [21]. Five minutes after injection mice were sacrificed by CO_2 asphyxiation. Next, thorax was opened and bulldog clamps with 8 x 1.2 mm serrated jaws (WPI, Berlin, Germany) were placed on descending aorta (left from the carotid arteries) and pulmonary veins and arteries. Inferior caval vein was cut to allow outflow of perfused fluids. A 26G needle, connected to a peristaltic pump, was inserted into the left ventricle of the heart [22]. Mice were initially perfused with 1.5 ml Hanks' Balanced Salt Solution (HBSS, pH 7.0-7.4, Invitrogen, Carlsbad, CA) in all experiments. Directly afterwards, mice were perfused with phage. Upon the three selection rounds, 1 ml of phage library in HBSS (8.9 x 10^{11} TU, 3.1 x 10^{11} TU, and 4.8 x 10^{10} TU for the first, second and third selection rounds, respectively) were perfused (input). To wash away non-binders, 3.5 ml HBSS was perfused directly afterwards. For the third selection round, HBSS + 1% FBS was used instead of HBSS. For perfusions of selected phage (single clones), 750 µl of phage (~10^{10} TU) in HBSS + 1% FBS was perfused, directly followed by 2 ml of HBSS + 1% serum to

wash. Peristaltic pump speed was 200 µl/min. Directly after perfusion, brains were taken out. For the phage display screening, phage were isolated from the brain (see below).

Phage isolation from brain

After phage display selection rounds, brain cerebrum was ground in 600 µl 100 mM triethanolamine (Fluka, Munich, Germany) and centrifuged for 10 min at 3300 xg. Supernatant was transferred to a new tube, neutralized with 300 µl 1 M Tris pH 7.4, and centrifuged for 5 min at 3300 xg. Late log phase K91BK were obtained by inoculation of 10 ml of terrific broth with 100 µl of an overnight culture, and incubation for 4 hours in a shaker incubator (250 rpm, 37 °C). When late log phase was reached (when the OD_{600} of a 10 x dilution reached 0.2 on a spectrophotometer), shaking was slowed down to 75 rpm for 5 minutes to allow sheared F pili to regenerate. Brain supernatant was incubated with late log phase K91BK for 10 min to allow phage to infect the bacteria. The infected bacteria were added to 40 ml LB Broth (Sigma), containing 0.2 µg/ml tetracycline and amplified for 30 min in a shaker incubator (250 rpm, 37 °C). Two hundred µl of the infected K91BK were spread on LB agar plates for titration. Tetracycline concentration was then brought to 20 µg/ml, and phage were amplified overnight in the shaker incubator. Cultures were cleared of bacteria by two 10 min centrifugations at 3000 and 8000 xg. To the cleared culture 0.15 volume PEG/NaCl (16.7% /3.3 M stock) was added (PEG 8000, Promega, Breda, The Netherlands). Phage were precipitated overnight at 4 °C. Precipitated phage were collected by centrifugation for 15 min at 17500 xg at 4 °C. Pellets were dissolved in 1 ml TBS and precipitated again with 0.15 volume PEG/NaCl for at least 1 hour at 4 °C. Phage were collected by centrifugation for 5 min at 16000 xg. Pellets were dissolved in 400 µl TBS and stored at 4 °C. Two hundred µl of purified phage + 800 µl HBSS were used for the next selection round. Three successive selection rounds were done in total. After the third selection round, brain cerebrum was separated into anterior and posterior part. Phage were separately isolated from both parts. Titration of input phage was performed as described below. After perfusion of single phage clones, whole brains were ground in 1000 µl triethanolamine and centrifuged for 10 min at 3300 xg. Two hundred µl supernatant was transferred to a new tube, and neutralized with 100 µl 1 M Tris pH 7.4. Titration of both input and output phage was performed as described below.

Titration of phage

Transducing units (TU) were determined by titration. Phage were serially diluted in 0.1% (w/v) gelatin in TBS. Ten µl of phage dilution were incubated with 10 µl of late log phase K91BK for 10 min at room temperature. 1 ml LB, containing 0.2 µg/ml tetracycline was added. This was incubated for 40 min in a shaker incubator (250 rpm, 37 °C). Two hundred µl of the infected K91BK were spread on LB agar plates containing 40 µg/ml tetracycline and 100 µg/ml kanamycin. Plates were incubated overnight at 37 °C. Next day, the

number of colonies was counted and the number of transducing units was calculated. Input phage were titrated as well at the same time for recovery percentage calculations.

Immunohistochemistry brain cryosections

Frozen untreated brains were coated with OCT embedding matrix (Cellpath, Newtown, UK). Sections were cut along the sagittal plane using low profile microtome blades (Leica, Heidelberg, Germany) on a CM3050 cryostat (Leica). Sections were transferred onto Superfrost Plus glass slides (Menzel, Germany). Section thickness was 5 µm. They were dried overnight at room temp and stored at -80 °C. Upon use, sections were allowed to thaw for 20 min, fixed in acetone for 10 min, and air dried for 30 min. Separate sections were encircled with a liquid-repellent marker. All incubations were done in a moist environment, and incubation volumes were 90 µl/section. Non-specific binding sites and endogenous biotin were blocked simultaneously with avidin/biotin blocking solution in PBS + 5% FCS (Vector Laboratories, Inc., Burlingame, USA), according to manufacturer. Brain sections were incubated with either the enriched library, or the unselected library (both 2.37 x 10^{13} V/ml), for 1 hour at room temperature. Sections were incubated with 0.8 µg/ml biotinylated anti-phage antibody (Abcam, Cambridge, UK) for 1 hour. Thereafter, sections were incubated with 5 µg/ml alexa568-conjugated streptavidin (Invitrogen) for 35 min. Sections were mounted in FluorSave (Calbiochem, San Diego, CA) and viewed under a Nikon Eclipse TE2000-U epi-fluorescence microscope (Nikon, Tokyo, Japan) at a 20x magnification.

Sequence alignment

Peptide sequences were aligned to check for peptides consensus sequences along the 15 amino acids. Software used was Vector NTI Advance 10 AlignX (Invitrogen).

Cells

Human brain endothelial cells (hCMEC/D3) were obtained from Institut National de la Santé et de la Recherche Médicale (INSERM, Paris, France). Cells were cultured at 37°C, 5% CO_2, in EBM-2 basal medium supplemented with EGM-2 MV BulletKit (Lonza, Basel, Switzerland), containing growth factors and 2.5% FBS. Additionally, 10 mM HEPES, 1 ng/ml bFGF (Invitrogen), and antibiotics (Penicillin and Streptomycin) were added. hCMEC/D3 cells were grown on surfaces coated with 100 µg/ml Rat tail collagen type 1 (BD Biosciences). Prior to use, cell culture medium was replaced by cell differentiation medium, consisting of EBM-2 basal medium supplemented with 2.5% FBS, 1.4 µM hydrocortisone, 1 ng/ml bFGF, 10 mM HEPES, and antibiotics. Cells were grown to a monolayer in differentiation medium for one week. Medium was replaced every 2-3 days.

Human umbilical vein endothelial cells (HUVEC) were cultured at 37°C, 5% CO_2, in EBM-2 basal medium supplemented with antibiotics and EGM-2 BulletKit (Lonza), containing growth factors and 2% FBS.

In vitro binding of single phage clones

Cells were seeded at $3.4 \cdot 10^5$ cells/well in 12-well plates. Single phage clones were diluted to ~10^{10} TU/ml in 25mM HEPES in HBSS, and 1 ml phage solution was incubated with either hCMEC/D3 or HUVEC cells for 1 hour at 37°C. The buffer containing unbound phage was removed and cells were washed 3 times with PBS. Cells were washed 3 times with 1 ml of 0.2 M glycine (pH 2.2) to elute surface-bound phage [23,24]. Three ml wash eluate was collected and neutralized with 0.45 ml 1 M tris (pH 9.1). Cells were washed again with 1 ml of PBS and were subsequently lysed with 0.25 ml 100 mM triethanolamine for 10 min [25,26]. Cell lysates were collected and neutralized with 0.0625 ml 1 M tris (pH 7.4). The neutralized wash eluates (binding fraction) and cell lysates (strong binding/uptake fraction) were titrated as described above. Input phage were titrated as well at the same time for recovery percentage calculations.

Immunohistochemistry hCMEC/D3 cells

hCMEC/D3 cells were grown to a monolayer on Rat tail collagen coated Lab-Tek chamber slides (Nunc, Rochester, NY). Single phage clones were diluted to $5 \cdot 10^{12}$ V/ml in HBSS, and 100 µl phage solution or 100 µl HBSS only was incubated with the cells for 1 hour at 37°C. The buffer containing unbound phage was removed and cells were washed 3 times with PBS. Cells were fixed in 4% formaldehyde for 30 min. Cells were washed 2 times with PBS and incubated with 0.8 µg/ml biotinylated anti-phage antibody for 1 hour. Thereafter, cells were incubated with 5 µg/ml alexa568-conjugated streptavidin for 35 min, and washed 3 times. Cells were incubated with 300 nM DAPI (Invitrogen) for 2 minutes and washed 3 times with demi water. Cells were mounted in FluorSave and viewed under a Nikon Eclipse TE2000-U epi-fluorescence microscope at a 20x magnification.

In situ lung perfusion of phage

In situ lung perfusion was performed in the same way as was done for brain perfusions of single clones, with the only modification being the placement of the bulldog clamps. The ascending aorta was clamped and phage were perfused through the left ventricle of the heart. Inferior caval vein was cut to allow outflow of perfused fluids. Phage isolation and titration were also performed in the same was as was done for the brain perfusions.

Statistical analysis

Data were analyzed using Graphpad Prism 4 for Windows software (Graphpad Software, San Diego, CA)

Results

In situ phage display screening was used as a tool to search for new blood-brain barrier-binding peptides. Screening was performed by perfusion of a 15 amino acid random peptide phage display library through the murine brain *in situ*. Phage perfusion [27,28] was chosen over intravenous injection, because clearance of phage occurs rapidly via the major organs of the reticuloendothelial system (mainly liver and spleen), resulting in a half-life of fd-tet of only 12 minutes [29]. Therefore, phage were directly perfused via the heart through the brain, preventing loss to other organs, and ensuring a high fraction of individual peptide-displaying phage to reach the target tissue.

Various *in situ* brain perfusion methods have been developed [30]. Most models have been established in rats, but murine models have been used as well [22,31,32]. Most perfusion models have been used to study brain uptake of substrates and were performed under anesthesia. Since filamentous phage are approximately 1 µm in size [33], they are not likely to be taken up into the brain, and the perfusion allows screening for binding rather than for internalizing peptides. Therefore, body temperature maintenance was not required, and perfusion was performed at room temperature, postmortem. The large majority of brain proteins are stable during a postmortem interval of up to 4 hours at 25 °C [34]. As perfusions were completed within 30 min after sacrifice, the postmortem state was not expected to cause significant changes in brain microvessel morphology.

Phage were infused via the heart. The major advantage compared to direct infusion into the brain is that the phage have to travel some distance before they reach the brain. On their way, they already encounter endothelial cells: the endothelium of the aorta and carotid arteries. Phage with affinity to ubiquitous endothelial receptors are given the opportunity to bind to these cells and will not reach the brain. This negative selection filters out unspecific binders, and allows for the identification of peptides that bind more specifically to brain endothelium [35,36].

Phage display screening was performed by perfusion of a mouse brain with 8.9×10^{11} Transducing Units (TU) in Hanks' Balanced Salt Solution (HBSS), containing 1 g/L glucose, to keep the brain in a viable state. Phage were perfused for 5 minutes. Phage incubation times of 5-15 minutes are common and have been successful *in vivo* [11,37-40]. Non-binders were washed away by perfusion of HBSS. The brain was taken out and phage were isolated from the cerebrum, and submitted to the next selection round. During the third selection round, 1% FBS was added to the HBSS, to limit unspecific interactions. Because the infused fluid was not evenly perfused throughout the brain (see supporting

A. Clones isolated from anterior cerebrum

Clone	*Name*	*Sequence*	*Frequency*	*pI*	*charge at pH 7*	*Tested in vitro*
A1	RFL	RFLEFPRFFPAIILP	1	9.60	+0.76	
A2	PGR	PGRLLPGVIQRHFFI	1	12.50	+1.85	
A3	GAF	GAFSSPRSLTVPLRR	1	12.80	+2.76	
A4	PFA	PFARAPVEHHDVVGL	2	5.99	-1.06	y
A5	CGG	CGGLFAGCAALIDVF	1	3.80	-1.26	y
A6	EFP	EFPTFSWSYINDSLL	1	3.67	-2.24	
A7	ADW	ADWPHARGKFALGNA	1	8.75	+0.85	y
A8	GFT	GFTDVHLHLPGNSHR	1	7.02	+0.02	y
A9	GLD	GLDLLGDVRIPVVRR	2	9.51	+0.76	y
A10	PVA	PVAGMPLFPTAWFAH	1	6.74	-0.15	
A11	SAY	SAYAATVRGPLSSAS	1	8.75	+0.76	y
A12	RYA	RYASQLSDQILFTLP	1	5.84	-0.24	y
A13	RDG	RDGAFSPPVRWWSFS	1	9.60	+0.76	
A14	TGA	TGAQAGLHEWRPWGV	1	6.75	-0.15	
A15	EDW	EDWFSASIRRVPTFA	1	6.07	-0.24	y
A16	GTW	GTWSSTCPLCSATAV	1	5.51	-0.26	y
A17	PWL	PWLPSNLGSRPGLMR	1	12.50	+1.76	

B. Clones isolated from posterior cerebrum

Clone	*Name*	*Sequence*	*Frequency*	*pI*	*charge at pH 7*	*Tested in vitro*
P1	GVV	GVVNYARAFNVGAAV	1	8.75	+0.76	y
P2	GLD	GLDLLGDVRIPVVRR	2	9.51	+0.76	y
P3	HAA	HAAFEPRGDVRHTLL	1	6.92	-0.06	y
P4	GDG	GDGRFHFLRGFFDSD	1	5.30	-1.15	y
P5	VRS	VRSIALFPPEWSATS	1	6.00	-0.24	y
P6	GLA	GLAHSFSDFARDFVA	1	5.21	-1.15	y
P7	VTG	VTGTQIRLPAYLRFD	1	8.75	+0.76	
P8	GYR	GYRPVHNIRGHWAPG	1	10.84	+1.93	y
P9	ITR	ITRGGYVIYHDALLA	1	6.74	-0.15	
P10	GAY	GAYFLSNHAVVRGVG	1	8.75	+0.85	
P11	PFA	PFARAPVEHHDVVGL	2	5.99	-1.06	y
P12	VGR	VGRPGGLVGGFASSL	1	9.75	+0.76	
P13	LGR	LGRAGQSYPSFARGL	1	10.83	+1.76	y
P14	VVS	VVSSRSVLSSQYRGH	1	10.84	+1.85	y
P15	ALP	ALPCNGAGCSRVTAR	1	9.02	+1.74	y
P16	VPM	VPMGLGFLGRGLAPL	1	9.75	+0.76	
P17	RSS	RSSHHPSFAVSLEPL	1	6.92	-0.06	y

C. Random control clones

Clone	*Name*	*Sequence*	*Frequency*	*pI*	*charge at pH 7*	*Tested in vitro*
C1	SVE	SVEVALVPGRQSRHF	-	9.61	+0.85	y
C2	YLR	YLRWAALCSIGSSCW	-	8.06	+0.74	y
C3	RVR	RVREPYPGMLERYRA	-	9.97	+1.76	y

Table I. *Sequenced phage clones. Clones after 3 selection rounds, isolated from anterior (**A**) and posterior (**B**) cerebrum. (**C**) Control clones, randomly taken from naive library. Isoelectric point (pI) and charge at pH 7 were calculated by Vector NTI Advance 10 software. Clones tested in vitro (y = yes) are shown in Figure 2.*

information paragraph), cerebrum was divided into its anterior (weakly perfused) and posterior (strongly perfused) side after the third selection round, to investigate whether different ligands could be identified in the different brain parts.

After three successive selection rounds, 17 clones isolated from the anterior part, and 17 clones isolated from the posterior part of the brain were sequenced (table I). Two of the sequences were found twice, once in the anterior part and once in the posterior part. However, most of the sequences were found only once. There was no clear discrimination in amino acid sequence between clones isolated from the different brain parts. Alignment analysis revealed no consensus sequences. This is not surprising, considering the complexity of the brain endothelium surface, and the many possible targets it may contain.

After selection, the enriched library was tested for its ability to bind to the brain by immunohistochemistry. Frozen untreated murine brains were sectioned and both the unselected (naive) and enriched library were incubated on the brain sections. Bound phage were stained with a labeled anti-phage antibody. Fluorescence microscopy revealed that the enriched library showed enhanced binding to the brain sections, compared to the naive library (Figure 1). The staining was comparable in the anterior and posterior side.

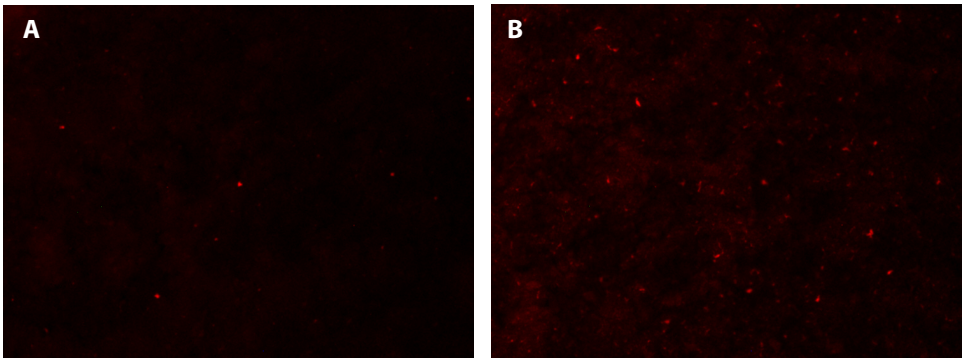

Figure 1. *Naive library (**A**) and selected (**B**) phage incubated on murine brain cryosections. A view on the posterior side of the cerebrum is shown. Phage were labeled with alexa-568. Magnification 20x.*

The peptides were selected for affinity to the *in vivo* relevant murine brain. However, for clinical applications, affinity for human endothelium is desired. Cross-reactivity between mouse and human has been shown for phage display selected peptides [39]. Therefore, a number of selected and sequenced phage clones were tested for their ability to bind human brain endothelial cells (picked at random from table I A, B). Additionally, three

clones were randomly chosen from the naive library as a negative control (table I, C). The hCMEC/D3 cell line was used to represent the human blood-brain barrier. hCMEC/D3 is a stable, fully characterized, well-differentiated human brain endothelial cell line [41,42]. Phage were added to the cells and incubated for 1 hour at 37°C [23,25,43]. Cell-associated phage were recovered in two steps [25,26]. First, by washing the cell surface with a low pH glycine buffer (stripping surface-bound phage), and subsequently by lysing the cells (collecting strongly bound and internalized phage). The percentages of recovered phage (percentage from input) are shown in Figure 2. Figure 2A shows that only seven out of nineteen selected clones showed higher binding to the cells compared to the highest random control clone (SVE). This may be due to non-specific electrostatic interactions of the peptides with the cell membranes, limiting discrimination between specific and non-specific binders. However, when looking at strong binding/internalization, these non-specific interactions are at background level. As shown in Figure 2B, seventeen out of nineteen selected clones showed a higher cell association as compared to the highest random control clone (YLR), indicating that peptides were identified that can specifically associate with brain endothelial cells. When the anterior and posterior sides of the cerebrum are compared, phage isolated from the posterior side showed significantly higher cell association (Figure 2B) than phage isolated from the anterior side. This can be correlated to the perfusion pattern seen upon Evans blue perfusion, which showed better perfusion through the posterior side of the brain (see supporting information paragraph). Likely, more individual phage reached the posterior side, increasing the selection strength, and resulting in stronger binding phage. Of all clones tested *in vitro*, phage GLA and GYR showed the best brain endothelium binding. Therefore GLA and GYR were chosen for further testing.

In order to investigate dose dependency, binding of phage GLA, GYR, and negative control YLR to the hCMEC/D3 cells was determined for different concentrations of input phage. Figure 3 shows that the phage bound to the cells in a dose dependent manner. Significantly more GLA and GYR were bound to the cells compared to control phage YLR.

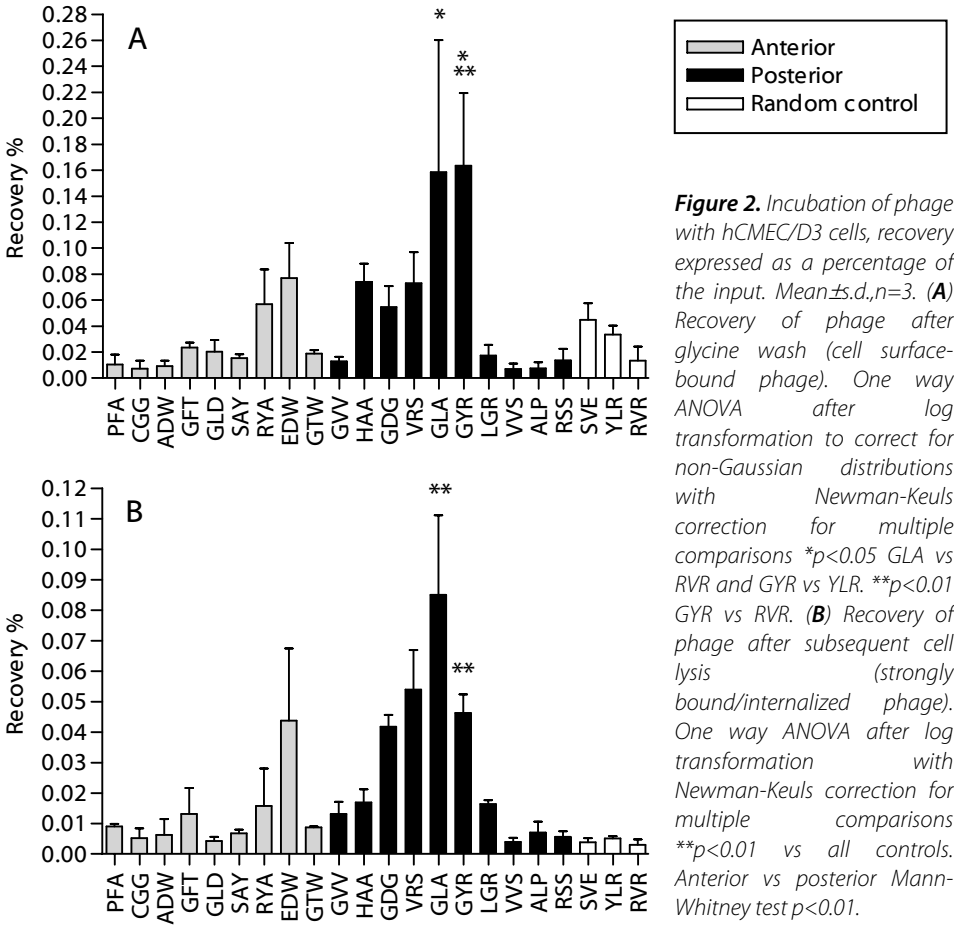

Figure 2. *Incubation of phage with hCMEC/D3 cells, recovery expressed as a percentage of the input. Mean±s.d.,n=3. (**A**) Recovery of phage after glycine wash (cell surface-bound phage). One way ANOVA after log transformation to correct for non-Gaussian distributions with Newman-Keuls correction for multiple comparisons *p<0.05 GLA vs RVR and GYR vs YLR. **p<0.01 GYR vs RVR. (**B**) Recovery of phage after subsequent cell lysis (strongly bound/internalized phage). One way ANOVA after log transformation with Newman-Keuls correction for multiple comparisons **p<0.01 vs all controls. Anterior vs posterior Mann-Whitney test p<0.01.*

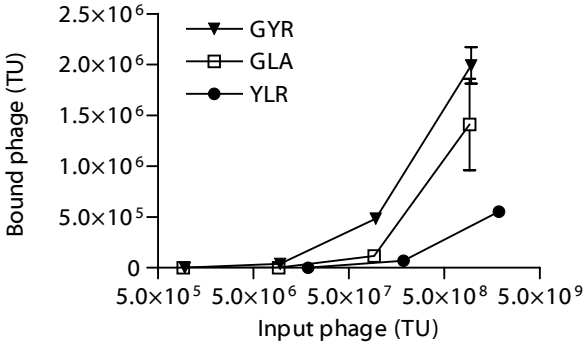

Figure 3*. Dose-response curve of phage GLA, GYR and control phage YLR. Mean±s.d., n=2. One way ANOVA after log transformation to correct for non-Gaussian distributions with Dunnet's correction for multiple comparisons against control. GLA and GYR vs YLR p<0.01. AUC is 14x and 26x higher for GLA and GYR, respectively.*

The results indicate that phage GLA and GYR show affinity for the hCMEC/D3 brain endothelium. We tested *in vitro* whether this affinity was brain-specific, or whether these phage have affinity for other endothelial cells as well. Therefore, phage association was tested on non-brain endothelium: human umbilical vein endothelial cells (HUVEC). Best hCMEC/D3 binding phage GLA and GYR were tested, as well as poor hCMEC/D3 binding phage GTW, and random control phage YLR. Phage GLA and GYR show significantly less affinity to HUVECs compared to hCMECs (Figure 4), indicating that these phage do not have affinity to all endothelial cells, and seem to be brain endothelium specific.

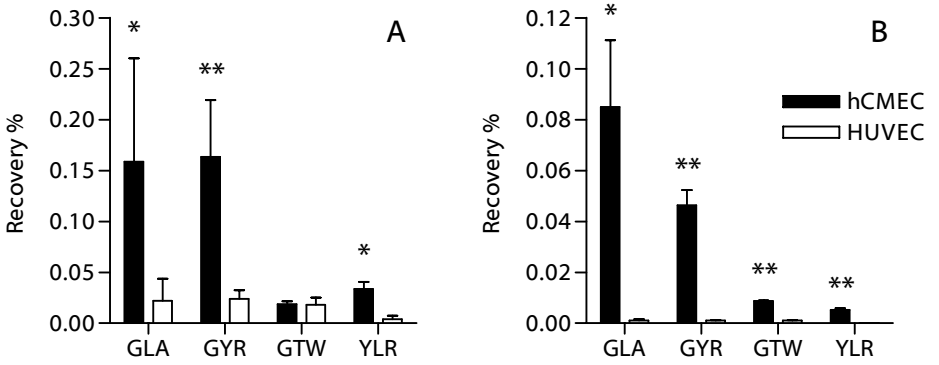

Figure 4. *Incubation of selected phage GLA, GYR, GTW and control phage YLR with hCMEC/D3 and HUVEC cells, recovery expressed as a percentage of the input. Mean±s.d., n=3. (**A**) Recovery of phage after glycine wash (cell surface-bound phage). (**B**) Recovery of phage after subsequent cell lysis (strongly bound/internalized phage).Students t-test after log transformation to correct for non-Gaussian distributions. *p<0.05, **p<0.01 hCMEC/D3 vs HUVEC.*

To confirm their ability to bind to brain endothelium *in situ*, GLA, GYR, and random control phage RVR were individually perfused through the brain again in the *in situ* perfusion model. After perfusion and washing, phage were recovered from the brain, and the percentages of the input were determined (Figure 5). Phage GYR showed a 5.0 times higher affinity to the brain than random control phage RVR. Phage GLA showed a 5.9 times higher affinity. This confirms that brain binding phage were identified. Although the recovery percentages seem low, they are comparable to *in vivo* phage recovery percentages found by others [39].

After establishment of brain specificity in vitro, specificity was investigated in situ as well. The lung was considered a suitable control perfusion organ. Just like brain, lung comprises microvascular endothelium, and affinity of the phage for this endothelium was tested. Phage GLA, GYR, and control phage RVR were perfused through murine lungs, and were processed in exactly the same way as was done for the brain perfusion. As is shown in

Figure 6, GLA binds significantly less to the lungs compared to control phage RVR. Binding of GYR is comparable to RVR. The negative charge of GLA is likely to be the cause of lower affinity to the lungs.

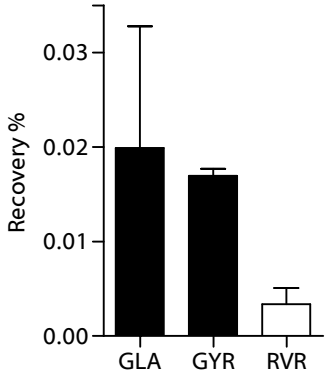

Figure 5. *Recovery of phage GLA, GYR, and control phage RVR from whole murine brains after phage perfusion and washing. Recovery is expressed as a percentage of the input. Mean±s.d., n=3. One way ANOVA after log transformation to correct for non-Gaussian distributions with Dunnet's correction for multiple comparisons against control. GLA and GYR vs RVR p<0.01.*

From both brain and lung recovery percentages, the preference ratio for brain over lung compared to RVR was calculated. Phage GYR showed a 8.5-fold preference and phage GLA showed a 48-fold preference for brain over lung compared to the control, implying specific affinity of these phage-displayed peptides to brain endothelium.

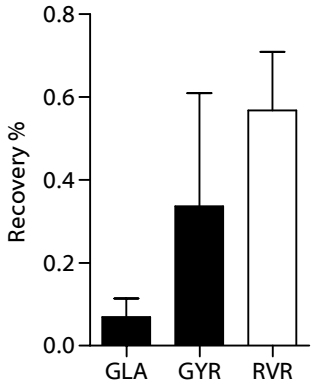

Figure 6. *Recovery of phage GLA, GYR, and control phage RVR from whole murine lungs after phage perfusion and washing. Recovery is expressed as a percentage of the input. Mean±s.d., n=3. One way ANOVA after log transformation to correct for non-Gaussian distributions with Dunnet's correction for multiple comparisons against control. GLA vs RVR p<0.05.*

To visualize the binding of phage GLA and GYR to human brain endothelial cells, hCMEC/D3 cells were incubated with single phage clones for 1 hour at 37°C. After washing, bound phage were stained with a labeled anti-phage antibody. Fluorescence microscopy showed phage staining throughout the cell monolayer. The pictures clearly show enhanced binding of selected phage GLA and GYR compared to the control phage RVR (Figure 7). This is in agreement with the previous *in vitro* and *in vivo* experiments, and confirms the BBB-targeting properties of these selected phage-displayed peptides.

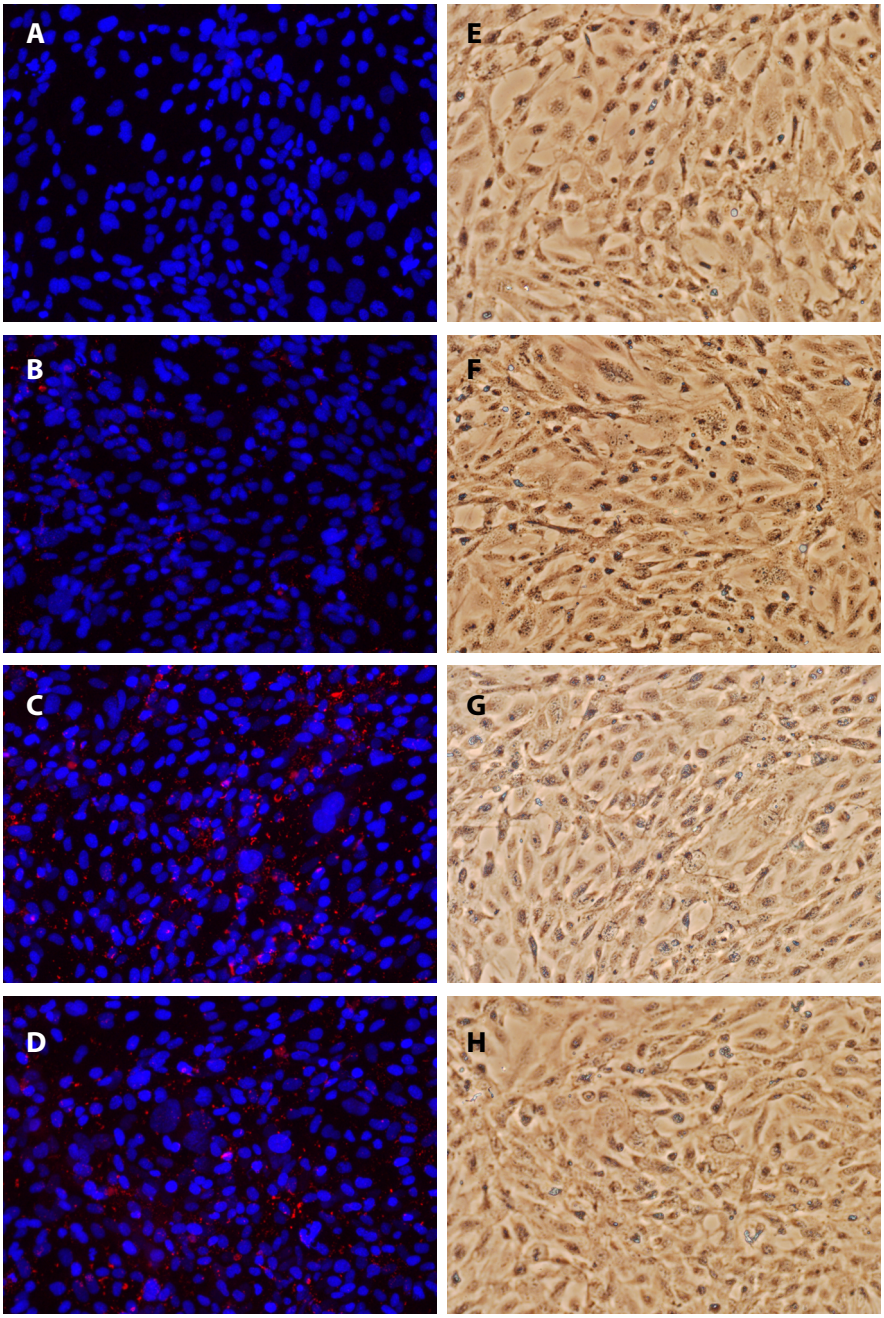

***Figure 7**. Microscopic images of hCMEC/D3 cells. (**A-D**) Fluorescence microscopy image of phage labeled with alexa-568 (red) and DAPI-stained cell nuclei (blue). (**A**) No phage. (**B**) Control phage RVR. (**C**) Selected phage GLA. (**D**) Selected phage GYR. (**E-H**) Light microscopy images of the same view on the cell monolayer as the fluorescence image to the left.*

Discussion

Using the powerful technique of phage display we identified two peptides that show significant binding to the brain compared to a control peptide. It is interesting to see that two peptides with opposite net charges both bind to the blood-brain barrier. Cell membranes are negatively charged [44]. Therefore, positively charged molecules may bind to the cell surface non-specifically by electrostatic interactions [45]. Selected peptide GYR and control peptide RVR are both positively charged (table 1), yet GYR shows a significantly higher binding to the brain than RVR. Furthermore, also the negatively charged GLA shows significant binding to the brain. These results indicate that the binding of the selected peptides is dependent on more than electrostatic interactions with the endothelium.

When looking at the recovery from brain and lung, a notable difference in recovery percentages was evident. The base level of phage recovery from lung was higher than from brain. This can be explained by mainly two factors. First, traveling from heart to brain, the perfused fluid passes a longer distance compared to perfusion through the lung. Lungs are directly connected to the heart, allowing all of the perfused fluid to reach the lungs. For reaching the brain, fluids have to cover some distance, of which not all branching vessels (i.e. subclavian arteries) could be clamped. This may have resulted in increased loss of phage. Secondly, the total surface area of the lung vasculature is larger than the total brain surface area.

Identification of the peptide binding site can be an important step in the ligand discovery process. This can give insight into the ligand-target interaction and the uptake mechanism. The binding site should preferably be a receptor, which can specifically internalize a ligand, and the attached drug delivery vehicle, into the cells. Alternatively, nanocarriers such as liposomes can be delivered to transfer their drug load to the target cells without the need for internalization. Lipophilic drugs can be transferred from liposomes to cell membranes when they are brought in close proximity by a targeting ligand [46]. This can result in higher uptake of drugs with a low but not absent brain penetration capacity.
The GLA and GYR binding sites and potential uptake mechanisms are as yet unknown.
Because of the negative selection that was performed by perfusion through the heart, the binding site is likely to be brain endothelium specific. Therefore it could be a new, yet unidentified receptor, suitable for specific targeting to the blood-brain barrier.

A literature search showed that 4 out of the 34 selected peptides (PFA [47], GLD [48], SAY [49], and HAA [50]) had been selected before by other groups, for very diverse purposes. Two possible explanations could account for this observation. These phage may have been selected in diverse settings because they contain biologically relevant motifs, suitable for multiple *in vitro* and *in vivo* applications. Alternatively, these motifs may also just enhance phage amplification rates, making them typical background phage that do not offer a specific target interaction.

Our selected peptides, as they have been tested here, are expressed on a phage, displaying 5 peptides each. Attached to a nanoparticle (e.g. liposome), the number of peptides per particle can be greatly increased. This multivalency may result in a stronger binding of the targeted nanoparticle (i.e. avidity), compared to the phage tested here.

Conclusion

Two new peptides have been identified that may be used for specific targeting to the blood-brain barrier. In the future, these peptides could act as targeting ligands on nanoparticles to enhance uptake of CNS drugs into the brain.

Acknowledgements

We thank George P. Smith for providing the phage display library and the host bacteria. This work was performed within the framework of the Dutch Top Institute Pharma project T5-105-1: nanoscience as a tool for improving bioavailability and blood-brain barrier penetration.

References

[1] A.G. de Boer, P.J. Gaillard. Drug Targeting to the Brain, Annu Rev Pharmacol Toxicol. 47 (2007) 323-355.

[2] A.R. Calabria, E.V. Shusta. Blood-brain barrier genomics and proteomics: elucidating phenotype, identifying disease targets and enabling brain drug delivery, Drug Discovery Today. 11 (2006) 792-799.

[3] W.M. Pardridge. Blood-brain barrier delivery, Drug Discovery Today. 12 (2007) 54-61.

[4] E. Garcia-Garcia, K. Andrieux, S. Gil, P. Couvreur. Colloidal carriers and blood-brain barrier (BBB) translocation: A way to deliver drugs to the brain? International Journal of Pharmaceutics. 298 (2005) 274-292.

[5] W.M. Pardridge. Blood-brain barrier delivery of protein and non-viral gene therapeutics with molecular Trojan horses, Journal of Controlled Release. 122 (2007) 345-348.

[6] Jones, E. Shusta. Blood–Brain Barrier Transport of Therapeutics via Receptor-Mediation, Pharmaceutical Research. 24 (2007) 1759-1771.

[7] H.J. Lee, B. Engelhardt, J. Lesley, U. Bickel, W.M. Pardridge. Targeting Rat Anti-Mouse Transferrin Receptor Monoclonal Antibodies through Blood-Brain Barrier in Mouse, J Pharmacol Exp Ther. 292 (2000) 1048-1052.

[8] R.J. Boado, Y. Zhang, Y. Zhang, W.M. Pardridge. Humanization of anti-human insulin receptor antibody for drug targeting across the human blood-brain barrier, Biotechnology and Bioengineering. 96 (2007) 381-391.

[9] A.G. de Boer, I.C. van der Sandt, P.J. Gaillard. The role of drug transporters at the blood-brain barrier, Annu Rev Pharmacol Toxicol. 43 (2003) 629-656.

[10] M. Teixidó, E. Giralt. The role of peptides in blood-brain barrier nanotechnology, Journal of Peptide Science. 14 (2008) 163-173.

[11] W. Arap, W. Haedicke, M. Bernasconi, R. Kain, D. Rajotte, S. Krajewski, et al. Targeting the prostate for destruction through a vascular address, Proc Natl Acad Sci USA. 99 (2002) 1527-1531.

[12] B. Zhang, Y. Zhang, J. Wang, Y. Zhang, J. Chen, Y. Pan, et al. Screening and identification of a targeting peptide to hepatocarcinoma from a phage display peptide library. Mol Med. 13 (2007) 246-254.

[13] T. Lee, C. Lin, S. Kuo, D. Chang, H. Wu. Peptide-Mediated Targeting to Tumor Blood Vessels of Lung Cancer for Drug Delivery, Cancer Res. 67 (2007) 10958-10965.

[14] Y.H. Chen, M. Chang, B.L. Davidson. Molecular signatures of disease brain endothelia provide new sites for CNS-directed enzyme therapy, Nat Med. 15 (2009) 1215-1218.

[15] G.P. Smith, V.A. Petrenko. Phage Display, Chem. Rev. 97 (1997) 391-410.

[16] R.C. Janzer, M.C. Raff. Astrocytes induce blood-brain barrier properties in endothelial cells, Nature. 325 (1987) 253-257.

[17] P.J. Gaillard, d.S. van I, L.H. Voorwinden, D. Vu, J.L. Nielsen, A.G. de Boer, et al. Astrocytes increase the functional expression of P-glycoprotein in an in vitro model of the blood-brain barrier, Pharm.Res. 17 (2000) 1198-1205.

[18] W. Neuhaus, R. Lauer, S. Oelzant, U.P. Fringeli, G.F. Ecker, C.R. Noe. A novel flow based hollow-fiber blood-brain barrier in vitro model with immortalised cell line PBMEC/C1-2, Journal of Biotechnology. 125 (2006) 127-141.

[19] A.N. Zacher, C.A. Stock, J.W. Golden, G.P. Smith. A new filamentous phage cloning vector: fd-tet, Gene. 9 (1980) 127-140.

[20] T. Nishi, R.J.A. Budde, J.S. McMurray, N.U. Obeyesekere, N. Safdar, V.A. Levin, et al. Tight-binding inhibitory sequences against pp60c-src identified using a random 15-amino-acid peptide library, FEBS Letters. 399 (1996) 237-240.

[21] X. Gao, P. Kouklis, N. Xu, R.D. Minshall, R. Sandoval, S.M. Vogel, et al. Reversibility of increased microvessel permeability in response to VE-cadherin disassembly, Am J Physiol Lung Cell Mol Physiol. 279 (2000) L1218-1225.

[22] M. Shayo, R.N. McLay, A.J. Kastin, W.A. Banks. The putative blood-brain barrier transporter for the [beta]-amyloid binding protein apolipoprotein j is saturated at physiological concentrations, Life Sciences. 60 (1997) PL115.

[23] M.J. McGuire, K.N. Samli, S.A. Johnston, K.C. Brown. In vitro Selection of a Peptide with High Selectivity for Cardiomyocytes In vivo, Journal of Molecular Biology. 342 (2004) 171-182.

[24] S. Liang, T. Lin, J. Ding, Y. Pan, D. Dang, C. Guo, et al. Screening and identification of vascular-endothelial-cell-specific binding peptide in gastric cancer, Journal of Molecular Medicine. 84 (2006) 764-773.

[25] D. Lu, J. Shen, M.D. Vil, H. Zhang, X. Jimenez, P. Bohlen, et al. Tailoring in Vitro Selection for a Picomolar Affinity Human Antibody Directed against Vascular Endothelial Growth Factor Receptor 2 for Enhanced Neutralizing Activity, J. Biol. Chem. 278 (2003) 43496-43507.

[26] Y. Kim, A.M. Lillo, S.C.J. Steiniger, Y. Liu, C. Ballatore, A. Anichini, et al. Targeting Heat Shock Proteins on Cancer Cells: Selection, Characterization, and Cell-Penetrating Properties of a Peptidic GRP78 Ligand, Biochemistry. 45 (2006) 9434-9444.

[27] F. Maruta, A.L. Parker, K.D. Fisher, P.G. Murray, D.J. Kerr, L.W. Seymour. Use of a Phage Display Library to Identify Oligopeptides Binding to the Lumenal Surface of Polarized Endothelium by Ex Vivo Perfusion of Human Umbilical Veins, Journal of Drug Targeting. 11 (2003) 53-59.

[28] C. Laumonier, J. Segers, S. Laurent, A. Michel, F. Coppee, A. Belayew, et al. A New Peptidic Vector for Molecular Imaging of Apoptosis, Identified by Phage Display Technology, J Biomol Screen. 11 (2006) 537-545.

[29] J. Zou, M.T. Dickerson, N.K. Owen, L.A. Landon, S.L. Deutscher. Biodistribution of filamentous phage peptide libraries in mice, Molecular Biology Reports. 31 (2004) 121-129.

[30] C. Dagenais, C. Rousselle, G.M. Pollack, J. Scherrmann. Development of an In Situ Mouse Brain Perfusion Model and Its Application to mdr1a P-Glycoprotein-Deficient Mice, J Cereb Blood Flow Metab. 20 (2000) 381-386.

[31] C. Rousselle, M. Smirnova, P. Clair, J. Lefauconnier, A. Chavanieu, B. Calas, et al. Enhanced Delivery of Doxorubicin into the Brain via a Peptide-Vector-Mediated Strategy: Saturation Kinetics and Specificity, J Pharmacol Exp Ther. 296 (2001) 124-131.

[32] S. Bihorel, G. Camenisch, G. Gross, M. Lemaire, J. Scherrmann. Influence of Hydroxyurea On Imatinib Mesylate (Gleevec) Transport at the Mouse Blood-Brain Barrier, Drug Metab Dispos. 34 (2006) 1945-1949.

[33] W.G.T. Willats. Phage display: practicalities and prospects, Plant Molecular Biology. 50 (2002) 837-854.

[34] S.W. Hunsucker, B. Solomon, J. Gawryluk, J.D. Geiger, G.N. Vacano, M.W. Duncan, et al. Assessment of post-mortem-induced changes to the mouse brain proteome, Journal of Neurochemistry. 105 (2008) 725-737.

[35] D. Rajotte, W. Arap, M. Hagedorn, E. Koivunen, R. Pasqualini, E. Ruoslahti. Molecular heterogeneity of the vascular endothelium revealed by in vivo phage display, The Journal of Clinical Investigation. 102 (1998) 430-437.

[36] Muruganandam, J. Tanha, S. Narang, D. Stanimirovic. Selection of phage-displayed llama single-domain antibodies that transmigrate across human blood-brain barrier endothelium, FASEB J. 16 (2002) 240-242.

[37] R. Pasqualini, E. Ruoslahti. Organ targeting In vivo using phage display peptide libraries, Nature. 380 (1996) 364-366.

[38] R. Pasqualini, E. Koivunen, E. Ruoslahti. alpha v Integrins as receptors for tumor targeting by circulating ligands, Nat Biotech. 15 (1997) 542-546.

[39] W. Arap, R. Pasqualini, E. Ruoslahti. Cancer Treatment by Targeted Drug Delivery to Tumor Vasculature in a Mouse Model, Science. 279 (1998) 377-380.

[40] M. Böckmann, M. Drosten, B.M. Pützer. Discovery of targeting peptides for selective therapy of medullary thyroid carcinoma, The Journal of Gene Medicine. 7 (2005) 179-188.

[41] B.B. Weksler, E.A. Subileau, N. Perriere, P. Charneau, K. Holloway, M. Leveque, et al. Blood-brain barrier-specific properties of a human adult brain endothelial cell line, FASEB J. 19 (2005) 1872.

[42] B. Poller, H. Gutmann, S. Krähenbühl, B. Weksler, I. Romero, P. Couraud, et al. The human brain endothelial cell line hCMEC/D3 as a human blood-brain barrier model for drug transport studies, J Neurochem. 107 (2008) 1358-1368.

[43] S.C. Meyer, T. Gaj, I. Ghosh. Highly Selective Cyclic Peptide Ligands for NeutrAvidin and Avidin Identified by Phage Display, Chemical Biology & Drug Design. 68 (2006) 3-10.

[44] I.S. Zuhorn, D. Hoekstra. On the Mechanism of Cationic Amphiphile-mediated Transfection. To Fuse or not to Fuse: Is that the Question? Journal of Membrane Biology. 189 (2002) 167-179.

[45] J. He, R.M. Haney, M. Vora, V.V. Verkhusha, R.V. Stahelin, T.G. Kutateladze. Molecular mechanism of membrane targeting by the GRP1 PH domain, J. Lipid Res. 49 (2008) 1807-1815.
[46] G.A. Koning, H.W.M. Morselt, M.J. Velinova, J. Donga, A. Gorter, T.M. Allen, et al. Selective transfer of a lipophilic prodrug of 5-fluorodeoxyuridine from immunoliposomes to colon cancer cells, Biochimica et Biophysica Acta (BBA) - Biomembranes. 1420 (1999) 153-167.
[47] F. Li, A. Dluzewski, A.M. Coley, A. Thomas, L. Tilley, R.F. Anders, et al. Phage-displayed Peptides Bind to the Malarial Protein Apical Membrane Antigen-1 and Inhibit the Merozoite Invasion of Host Erythrocytes, J. Biol. Chem. 277 (2002) 50303-50310.
[48] N. Oku, T. Asai, K. Watanabe, K. Kuromi, M. Nagatsuka, K. Kurohane, et al. Anti-neovascular therapy using novel peptides homing to angiogenic vessels, Oncogene. 21 (2002) 2662-2669.
[49] C.D. Pond, K.M. Marshall, L.R. Barrows. Identification of a small topoisomerase I-binding peptide that has synergistic antitumor activity with 9-aminocamptothecin, Mol Cancer Ther. 5 (2006) 739-745.
[50] Roos, A.J. Nauta, D. Broers, M.C. Faber-Krol, L.A. Trouw, J.W. Drijfhout, et al. Specific Inhibition of the Classical Complement Pathway by C1q-Binding Peptides, J Immunol. 167 (2001) 7052-7059.

Supplementary information to chapter 4

Introduction

A murine *in situ* perfusion model was created, based on existing models [1-3]. To verify whether the perfusion procedure was able to get the perfused fluids into the brain, an Evans Blue solution was perfused, and blue staining in the brain was assessed.

Materials and Methods

In this model, 40 units of heparin (Sigma) were injected i.v. into the tail vein to prevent coagulation of blood inside the microvessels [4]. Five minutes after injection mice were sacrificed by CO_2 asphyxiation. Directly after asphyxiation, thorax was opened and bulldog clamps with 8 x 1.2 mm serrated jaws (WPI, Berlin, Germany) were placed on aorta (left from the carotid arteries) and pulmonary veins and arteries. Inferior caval vein was cut to allow outflow of perfused fluids. A 26G needle, connected to a peristaltic pump, was inserted into the left ventricle of the heart [5]. Pump speed was 200 µl/min. To test whether this perfusion setup was suited for getting solutes to the brain, athymic nude mice (Harlan) were sacrificed by CO_2 asphyxiation and 0.8 ml of 0.1% Evans Blue (Sigma) was injected into the left ventricle of the heart of mice with or without aortic and pulmonary clamps applied.

Results and Discussion

Without clamping, Evans Blue was able to spread to the lungs (Figure 1), and evenly throughout the whole body of the mouse (Figure 2). In the brain however, no blue staining could be seen. Upon clamping, Evans Blue was not able to disperse to the lungs, and the major quantity of the dye remained in the upper part of the body. In the brain, blue staining was clearly visible, mainly located in the posterior side of the cerebrum (Figure 3). The cerebellum remained colorless, indicating that this particular perfusion setup was mainly suitable for perfusion through the cerebrum.

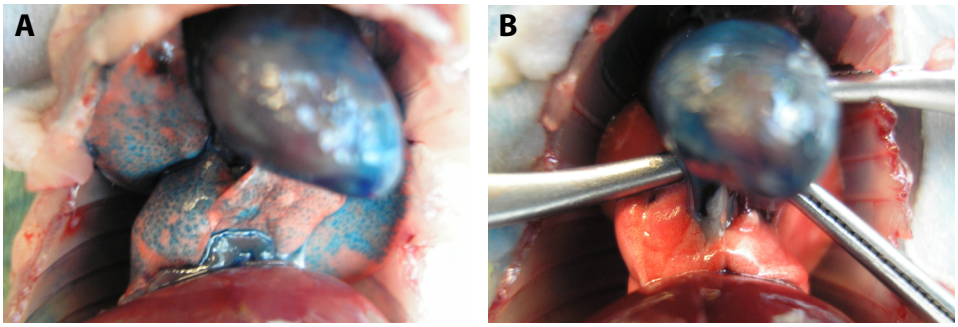

Figure 1. *Mouse heart and lungs after in situ perfusion of Evans Blue. (**A**) Unclamped. (**B**) Clamped.*

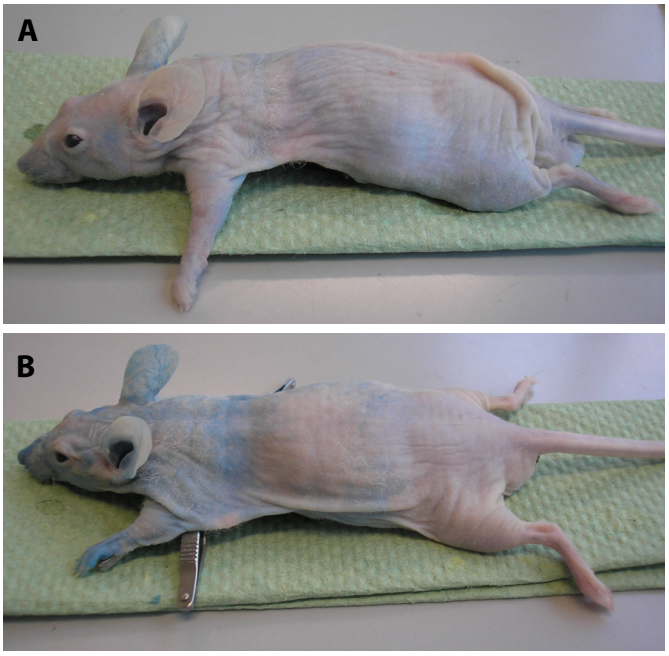

Figure 2. *Mice after in situ perfusion of Evans Blue. (**A**) Unclamped. (**B**) Clamped.*

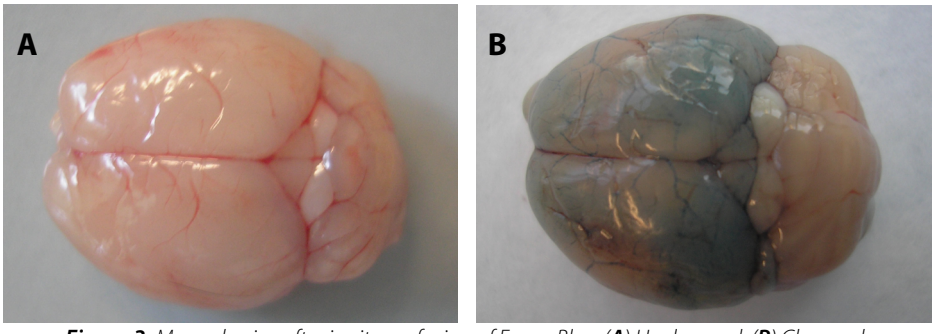

Figure 3. *Mouse brains after in situ perfusion of Evans Blue. (**A**) Unclamped. (**B**) Clamped.*

References

[1] C. Dagenais, C. Rousselle, G.M. Pollack, J. Scherrmann. Development of an In Situ Mouse Brain Perfusion Model and Its Application to mdr1a P-Glycoprotein-Deficient Mice, J Cereb Blood Flow Metab. 20 (2000) 381-386.

[2] C. Rousselle, M. Smirnova, P. Clair, J. Lefauconnier, A. Chavanieu, B. Calas, et al. Enhanced Delivery of Doxorubicin into the Brain via a Peptide-Vector-Mediated Strategy: Saturation Kinetics and Specificity, J Pharmacol Exp Ther. 296 (2001) 124-131.

[3] S. Bihorel, G. Camenisch, G. Gross, M. Lemaire, J. Scherrmann. Influence of Hydroxyurea On Imatinib Mesylate (Gleevec) Transport at the Mouse Blood-Brain Barrier, Drug Metab Dispos. 34 (2006) 1945-1949.

[4] X. Gao, P. Kouklis, N. Xu, R.D. Minshall, R. Sandoval, S.M. Vogel, et al. Reversibility of increased microvessel permeability in response to VE-cadherin disassembly, Am J Physiol Lung Cell Mol Physiol. 279 (2000) L1218-1225.

[5] M. Shayo, R.N. McLay, A.J. Kastin, W.A. Banks. The putative blood-brain barrier transporter for the [beta]-amyloid binding protein apolipoprotein j is saturated at physiological concentrations, Life Sciences. 60 (1997) PL115.

Chapter 5

Attaching the phage display-selected GLA peptide to liposomes: factors influencing target binding

Inge van Rooy
Wim E Hennink
Gert Storm
Raymond M Schiffelers
Enrico Mastrobattista

Submitted for publication

Abstract

In chapter 4 of this thesis, phage display selections were performed by *in situ* perfusion of a random peptide library through a mouse brain. This yielded two phage-displayed peptides (GLA and GYR) that showed a 5 to 6 times higher brain binding capacity after perfusion compared to a random control phage. These phage-displayed peptides also showed significant binding to human brain endothelial cells (hCMEC/D3), but not to human umbilical vein endothelial cells (HUVEC). In the current chapter, these peptides were produced synthetically and coupled to liposomes to study the capacity of the peptides to act as ligands for targeting to hCMEC/D3 cells. Flow cytometry studies showed that these peptides when coupled to liposomes showed weak binding to the target brain endothelial cells. We hypothesized that the weak endothelial cell binding of the selected peptides when coupled to liposomes as compared to the binding of the peptides displayed on phage particles may be ascribed to: change of vehicle shape, change of peptide density, or change of peptide conformation. Peptide density on the liposomes influenced binding of the liposomes to the cells, however, this effect was minor. To study the influence of the peptide conformation, the GLA peptide was recombinantly produced fused to the N1-N2 domains of the phage p3 minor coat protein (p3-GLA) to mimic its conformation when displayed on phage particles. Binding of liposomes modified with either the GLA peptide or the p3-GLA protein to hCMEC/D3 cells was studied, and the p3-GLA-liposomes showed a higher binding to the cells compared to the GLA-liposomes. The experiments demonstrate that bringing the GLA peptide into the original phage protein environment restores and improves the peptide binding capacity and suggest that the GLA peptide, with some modifications, may be used as a brain-targeting ligand in the future.

Introduction

Many drugs or drug candidates cannot enter the brain in sufficient amounts because of the low permeability of blood-brain barrier (BBB) [1]. One strategy to cross this barrier is by encapsulating the drugs into nanoparticles, and target the particles to the endothelial cells of the BBB. Binding of drug delivery systems to the brain endothelial cells can subsequently result in uptake and transcytosis of the particles into the brain [2]. Several types of nanoparticles have been used for this purpose, including liposomes, solid lipid nanoparticles, albumin nanoparticles, and polymeric particles such as poly(lactic-co-glycolic acid) (PLGA) and poly(butyl cyanoacrylate) (PBCA) nanoparticles [3]. In order to promote an interaction of the particles with the brain endothelium, BBB targeting ligands should be coupled to the surface of the particles. Some of the ligands that have been used include transferrin, antibodies against the transferrin and insulin receptors, CRM197, and apolipoprotein E. Although brain uptake of nanoparticles using these ligands has been demonstrated, none of these ligands are specific for the endothelium of the brain, and they are also taken up at other sites of the body [4]. Therefore, it is of great importance to find new targeting ligands, preferably ligands which are more specific for the brain.

In the previous chapter of this thesis, the technique of phage display was used to identify new brain-targeting ligands. By perfusing a phage library through a mouse brain *in situ*, phage-displayed peptide ligands were preselected for brain endothelium affinity. From this preselection, two phage clones, displaying 15-amino acid peptides GLAHSFSDFARDFVA and GYRPVHNIRGHWAPG, additionally showed significant binding to human brain endothelial cells *in vitro* (hCMEC/D3). Binding to non-brain human endothelial cells (HUVEC) was not seen, implying brain specificity. When these phage were individually perfused through a mouse brain *in situ*, their ability to bind to the brain was 5 to 6 fold higher compared to a random control phage.

During these binding studies, the selected peptides were fused to the minor coat proteins of an fd phage. The aim of the present study was to investigate the potential of these peptides to act as brain-targeting ligands on liposomes. Liposomes were chosen as a delivery vehicle because they have been widely used for brain delivery [5-8]. Binding of the peptide-coupled liposomes to human brain endothelial cells *in vitro* was investigated by flow cytometry, and brain targeting *in vivo* was determined by *in situ* perfusion and intravenous (iv) injection.

Materials and Methods

Materials

Holo-transferrin and cholesterol were obtained from Sigma (St. Louis, MO). GLA, GYR, and RVR peptides was synthesized by Caslo Laboratory ApS (Lyngby, Denmark) at a purity of >90%. Terminal ends were acetylated and amidated, and the peptides contained a C-terminal cysteine, resulting in the sequences Ac-GLAHSFSDFARDFVAGC-NH_2 (GLA), Ac-GYRPVHNIRGHWAPGGC-NH_2 (GYR), and Ac-RVREPYPGMLERYRAGC-NH_2 (RVR). The cyclic 5mer RGD (c(RGDf(ε-S-acetylthioacetyl)K) was synthesized at a purity of 95% by Ansynth Service (Roosendaal, The Netherlands), equipped with a thioacetyl group at the lysine residue for linking to the liposomes [9]. P3-GLA was expressed and purified by GenScript Corp. (Piscataway, NJ) at a purity of 70%. The protein (highlighted in Figure 4) contained an N-terminal methionine and a C-terminal His-tag. [^{3}H]cholesteryl hexadecyl ether, Soluene350, and Hionic-Fluor were obtained from PerkinElmer (Groningen, The Netherlands). Dipalmitoyl phosphatidylcholine (DPPC), distearoyl phosphatidylethanolamine-polyethyleneglycol$_{2000}$ (DSPE-PEG$_{2000}$), Egg phosphatidylcholine (EPC) and egg phosphotidylglycerol (EPG) were obtained from Lipoid GmbH (Ludwigshafen, Germany). DSPE-PEG$_{2000}$-maleimide and maleimidophenyl butyryl phosphatidylethanolamine (MPB-PE) were obtained from Avanti Polar Lipids, Inc (Alabaster, AL). N-(7-nitrobenz-2-oxa-1,3-diazol-4-yl)-1,2-dihexadecanoyl-sn-glycero-3-phosphoethanolamine, triethylammonium salt (NBD-PE) was obtained from Invitrogen (Carlsbad, CA).

Preparation of liposomes

For flow cytometry and *in situ* perfusion experiments, liposomes were composed of DPPC, cholesterol, DSPE-PEG$_{2000}$, and DSPE-PEG$_{2000}$-maleimide, in a 1.85:1:0.12:0.03 molar ratio. For *in situ* perfusion experiments, liposomes were labeled with trace amounts of the metabolically inert [^{3}H]cholesteryl hexadecyl ether (0.9 Ci/mol total lipid). For flow cytometry studies, liposomes were labeled with NBD-PE, 1% (mol/mol) of total lipid. Lipids were dissolved in chloroform, and a lipid film was made by rotary evaporation. The lipid film was hydrated in HBS (10 mM HEPES, 146 mM NaCl, pH 7.4) to a final lipid concentration of 40 µmol/ml. Liposomes were sized by repeated extrusion through polycarbonate membranes with a final pore size of 200 nm, using a high-pressure extruder. One batch of liposomes was prepared and divided into aliquots before coupling of ligands to each aliquot, so that each sample contained the same amount of lipids and label. After coupling of proteins or peptides overnight (see below), liposomes were incubated with 2-mercaptoethanol in a 1:1 thiol:maleimide molar ratio, to block unreacted maleimide groups. Uncoupled ligands and 2-mercaptoethanol were removed from

liposomes by gel permeation chromatography over a sephadex G-25 M column (GE healthcare, Buckinghamshire, UK).
For biodistribution studies, liposomes were prepared as described above, with following modifications: liposomes were composed of EPC, cholesterol, EPG, and MPB-PE, in a 6.5:2.6:0.8:0.1 molar ratio. Liposomes were labeled with 5 Ci/mol total lipid of [^{3}H]cholesteryl hexadecyl ether. The lipid film was hydrated to a final concentration of 10 µmol/ml of total lipid. Final extrusion pore size was 100 nm.

Coupling of ligands to liposomes

Holo-transferrin and p3-GLA were incubated with *N*-succinimidyl-S-acetylthioacetate, (SATA, Pierce, Rockford, IL) in a 1:8 and 1:17 protein:SATA molar ratio, respectively, for 40 min at room temperature. Free SATA was removed by filter centrifugation (30 and 10 kDa MWCO, respectively). Upon use, SATA groups were deacetylated in HBS containing 0.5 M hydroxylamine.HCl and 0.02 mM TCEP, pH 7.4, for 90 minutes at room temperature, to generate sulfhydryl groups. This resulted in a SH/protein (mol/mol) ratio of 3 and 5.5 for holo-transferrin and p3-GLA, respectively, as determined by Ellman's reagent assay (Pierce). The activated proteins were incubated overnight at 4 °C with the liposomes at various concentrations (see specifications per figure) to form a thioether bond with the DSPE-PEG_{2000}-maleimide incorporated in the bilayer. Peptides GLA, GYR, and RVR were incubated with TCEP Gel slurry (Pierce) for 1 hour at room temperature to reduce the C-terminal cysteine thiol group. Peptides were separated from TCEP Gel slurry by centrifugation in paper filter spin cups (Pierce), and immediately incubated with liposomes.

Characterization of liposomes

Ligand coupling efficiency was determined by UPLC, according to the method described by Koning *et al*. [10] (see supporting information). Coupling efficiency was >90% for each ligand. Estimations on the number of ligands per liposome were based on the amount of ligand added to the liposome and the assumption that 80,000 phospholipid molecules form one unilamellar liposome of 100 nm [11].
The mean particle size distribution and the polydispersity index of the liposomes were determined by dynamic light scattering (DLS) in a Malvern ALV CGS-3 (Malvern Instruments, Malvern, UK) containing a He-Ne laser source (λ=632.8 nm, 22 mW output power) under an angle of 90°.The zeta-potential of the liposomes was determined using a Malvern zetasizer Nano-Z (Malvern Instruments). Measurements were performed in HBS (10 mM HEPES, 146 mM NaCl, pH 7.4). The phospholipid content of the liposomal dispersions was determined colorimetrically according to Rouser *et al*. [12]. After the phosphate determination, the liposomes were diluted to the desired concentration for each experiment.

Cells

Human brain endothelial cells (hCMEC/D3) were kindly provided by Institut National de la Santé et de la Recherche Médicale (INSERM, Paris, France). Cells were cultured at 37°C, 5% CO_2, in EBM-2 basal medium supplemented with EGM-2 MV BulletKit (Lonza, Basel, Switzerland), containing growth factors and 2.5% FBS. Additionally, 10 mM HEPES, 1 ng/ml bFGF (Invitrogen), and antibiotics (Penicillin and Streptomycin) were added. hCMEC/D3 cells were grown on surfaces coated with 100 µg/ml Rat tail collagen type 1 (BD Biosciences). Prior to use, cell culture medium was replaced by cell differentiation medium, consisting of EBM-2 basal medium supplemented with 2.5% FBS, 1.4 µM hydrocortisone, 1 ng/ml bFGF, 10 mM HEPES, and antibiotics. Cells were grown to a monolayer in differentiation medium for one week. Medium was replaced every 2-3 days.
Human epithelial ovarian carcinoma cells (HeLa) were a kindly provided by the Institute of Biomembranes (Utrecht University, The Netherlands). Cells were cultured at 37°C, 5% CO_2, in DMEM supplemented with 10% FBS and antibiotics (Penicillin and Streptomycin). Cells were split twice weekly.

Flow cytometry analysis of binding

hCMEC/D3 cells were grown to a monolayer and then brought into suspension by trypsinization (trypsin/EDTA 0.05%/0.02% (w/v) for 5 min at 37°C). HeLa cells were grown to 80-90% confluency and then brought into suspension by trypsinization. Cells were centrifuged for 5 min at 250 xg at 4ºC, and washed in Hanks' Balanced Salt Solution (HBSS, pH 7.4, Invitrogen) containing 0.5% bovine serum albumin (BSA). Cells were transferred into round-bottom 96-well plates ($2{\cdot}10^5$ cells per well) and centrifuged again, followed by removal of buffer. Cells were incubated with 250 µl targeted NBD-PE labeled liposomes for 1 hour at 4°C. Liposome concentrations were either 100, 500, or 1500 nmol lipid per ml. After washing, liposome binding was investigated by flow cytometry on a FACSCantoII (BD Biosciences, Mountain View, CA) equipped with a 488 nm 20 mW solid state diode laser and a 633 nm 20 mW He-Ne laser. 10,000 cells were counted per sample in the FITC channel. For each sample, the mean fluorescence intensity (MFI) of the whole alive cell population was used. Dead cell population was determined by propidium iodine staining and counting in the PE channel. Also liposomes only were counted in the FITC channel, and gated out of the cell plots when necessary.

Animals

Male 25-30 g Balb/c mice (Harlan, Horst, The Netherlands) were used. Food and water were supplied *ad libitum*. Animal studies were performed according to national regulations and were approved by the local animal experiments ethical committee.

In situ brain perfusion of liposomes

^{3}H labeled liposomes were diluted to a concentration of 3.75 µmol/ml total lipid in HBS (10 mM HEPES, 146 mM NaCl, pH 7.4). Mice were injected with 40 units of heparin (Sigma) iv into the tail vein to prevent coagulation of blood inside the microvessels [13]. Five minutes after injection mice were sacrificed by CO_2 asphyxiation. Next, thorax was opened and bulldog clamps with 8 x 1.2 mm serrated jaws (WPI, Berlin, Germany) were placed on descending aorta and pulmonary veins and arteries. Caval vein was cut to allow outflow of perfused fluids. A 26G needle, connected to a peristaltic pump, was inserted into the left ventricle of the heart [14]. Mice were perfused with 1.5 ml Hanks' Balanced Salt Solution (HBSS, pH 7.4, Invitrogen) containing 1% serum. Next, mice were perfused with 750 µl liposomes in HBS, directly followed by 2.5 ml of HBSS to wash. Peristaltic pump speed was 200 µl/min. Directly after perfusion, brains were taken out and placed in a glass vial. Two ml of Soluene350 was added to each brain. Samples were incubated for 5-7 days at room temperature in the dark. Next, 10 ml of Hionic-Fluor was added. After vortexing, samples were temperature and light adapted by storing them in the dark for 2 to 5 hours. Samples were analyzed in a Tri-Carb 2200 CA Liquid Scintillation Analyzer (Packard).

Biodistribution of liposomes

Targeted radioactive liposomes were injected iv into the tail vein of mice (n=5). After 12 hours, mice were sacrificed and organs were collected and counted for radioactivity. Brains were submitted to capillary depletion to discriminate between liposomes that had bound to brain capillaries and liposomes that had transcytosed into the brain parenchyma. Capillary depletion was performed by the method described by Triguero and Gutierrez [15,16].

Liposomes were injected intravenously into the tail vein at a dose of 2 µmol total lipid per mouse. Animals were sacrificed by CO_2 asphyxiation 12 hours after injection. Thorax was opened and blood was withdrawn from the heart. The following organs were collected: brain cerebrum, brain cerebellum, liver, spleen, skin, muscle, and kidney. Brain cerebrum was further subjected to capillary depletion. For each organ, a 100-200 mg sample was transferred into a glass vial and weighed. For blood samples, a 30-50 mg sample was transferred into a glass vial and weighed. To each sample 2 ml of Soluene350 was added. Samples were incubated for 4 hours at 50°C, and additionally for 5-7 days at room temperature in the dark. Next, 10 ml of Hionic-Fluor was added. After vortexing, samples were temperature and light adapted by storing them in the dark for 2 to 5 hours before analysis. The percentage of the injected dose was represented per total organ. Blood volume of mice was assumed to be 7.2 ml per 100 g of body weight [17].

Software

Statistical analysis was performed using Graphpad Prism 4 for Windows software (Graphpad Software, San Diego, CA). Peptide Isoelectric point and charge at pH 7 were calculated by Vector NTI Advance 10 AlignX software (Invitrogen).

Results and Discussion

Peptide-coupled liposomes

Peptides GLA and GYR that had been selected by phage display, as well as a peptide that was randomly selected from a naive phage library as a negative control (RVR), were obtained by solid phase synthesis. The sequences of both selected and control peptides are shown in table I. These linear peptides were synthesized with a C-terminal cysteine to enable coupling to liposomal maleimide integrated in the lipid bilayer. The liposomes were prepared by lipid film hydration and extrusion, and labeled with NBD-PE for fluorescent detection. Next to the selected and negative control peptides, the endothelium-binding peptide RGD (SATA modified) was included as a positive control.

Peptide	Name	Displayed sequence	pI	charge at pH 7	Synthesized sequence
selected	GLA	GLAHSFSDFARDFVA	5.21	-1.15	Ac-GLAHSFSDFARDFVAGC-NH_2
selected	GYR	GYRPVHNIRGHWAPG	10.84	+1.93	Ac-GYRPVHNIRGHWAPGGC-NH_2
control	RVR	RVREPYPGMLERYRA	9.97	+1.76	Ac-RVREPYPGMLERYRAGC-NH_2

Table I. *Peptides previously selected by phage display [18]. Isoelectric point (pI) and charge at pH 7 were calculated by Vector NTI Advance 10 AlignX software.*

After preparation, liposomes were obtained with an average diameter of 190 nm, and an average polydispersity index of 0.2. Based on the liposome size and the finding that >90% of the peptides were coupled to the liposomes (UPLC analysis, see supporting information), it was estimated that 1250 peptides were coupled per liposome [11].

Liposome binding to hCMEC/D3 cells in vitro

To investigate the binding of the peptide-coupled liposomes to human brain endothelial cells (hCMEC/D3), 3 concentrations of liposome dispersions were incubated with the cells for 1 hour at 4 °C. After washing, binding was determined by flow cytometry. As shown in Figure 1, the selected peptides GLA and GYR did not significantly enhance binding of the liposomes to the cells compared to liposomes without peptide ligands. The positive control liposomes, containing the cyclic RGD peptides, showed a concentration-dependent level of cell binding.

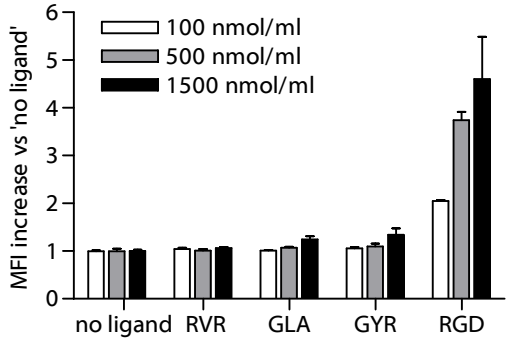

Figure 1. *Flow cytometry analysis of liposome binding to hCMEC/D3 cells. Three different concentrations of liposomes were used (100, 500, and 1500 nmol lipid per ml). On the y-axis, the mean fluorescence intensity (MFI) increase compared to the liposomes without ligand is shown. Mean±s.d, n=3.*

Liposome binding to brain endothelium *in vivo*

In chapter 4 of this thesis, phage-displayed peptides GLA and GYR had been selected because of their affinity to the hCMEC/D3 cells. Before this selection step, they had been preselected for affinity to mouse brain endothelium in an *in situ* perfusion model. Therefore, in the current study, binding of the peptide-coupled liposomes was investigated by *in situ* perfusion of the liposomes through the mouse brain. Liposomes were ^{3}H-labeled, and perfused through the brain by infusion via the heart while the descending aorta and pulmonary veins and arteries were clamped. After perfusion of the liposomes, non-binders were washed out of the brain vasculature by perfusion of buffer, and the brain was taken out. The radioactivity of the liposomes that were bound inside the brain vasculature was measured. As shown in Figure 2A, there was no increase in binding of the GLA and GYR-targeted liposomes to the brain endothelium compared to the controls. Additionally, no significant increase in brain uptake was seen when GLA liposomes were injected intravenously (Figure 2 B,C).

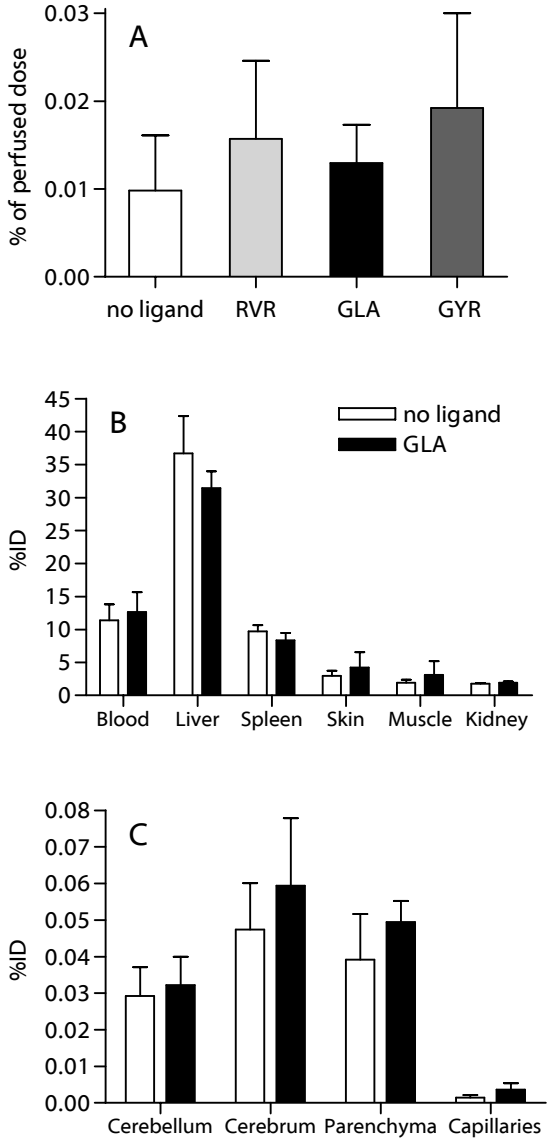

Figure 2. *Binding of peptide-coupled liposomes to the mouse brain in vivo. (**A**) Liposomes were perfused through the brain in situ, followed by perfusion (washing) with buffer. Shown is the percentage of the perfused dose that was found in the whole brain. Mean±s.d, n=4. (**B, C**) Biodistribution of liposomes in mice, 12 hours after iv injection, expressed as percentage of injected dose (%ID). In this experiment, the average liposome size was 101 nm, the average polydispersity index was 0.08. GLA liposomes were estimated to contain 25 GLA peptides per liposome. The GLA peptide was chosen for in vivo biodistribution studies. (**B**) Distribution in blood and major organs. (**C**) Distribution in the brain: total cerebellum, total cerebrum, cerebral parenchyma, and cerebral capillaries. Mean±s.d, n=5.*

Factors influencing phage versus synthetic peptide binding

Although phage display selections had yielded two phage that showed significant binding to brain endothelium both *in vitro* and *in* vivo (see previous chapter), surprisingly, this level of binding was not observed when the peptides responsible for binding were attached to a different vehicle (i.e. liposome). In order to explain this, we hypothesized that three main factors could be responsible for the observed weak binding when peptides were attached to liposomes. They are: change of vehicle shape, change of peptide density, and change of peptide conformation. These 3 factors are discussed in detail below.

1. Change of vehicle shape

The phage used in this study was an fd phage, which is part of the Ff family of filamentous phage. A filamentous phage has a rod-like shape, with an average length of 1 µm, and a width of 6 nm [19,20]. The used liposomes were spherical vesicles, with a diameter of 100-200 nm. Transferring the peptide from the phage to the liposome therefore considerably changes the vehicle that carries the peptide. It has been shown in literature for nanoparticles and nanotubes that the shape of the particle can be of influence on many particle properties, including binding properties and the rate of cell entry [21-23]. Therefore, changing the vehicle from phage to liposome may have had an influence on the binding properties of these peptides combined with their vehicle.

2. Change of peptide density

On the tip of the fd phage, five copies of the p3 minor coat protein are expressed. Therefore, up to five copies of the library peptide can be displayed on each phage [19]. On a liposome, the number of peptides per particle can be varied, and therefore much more peptides can be attached to a liposome compared to a phage. This could enhance binding of the particle to the target through avidity effects. On the other hand, too many peptides can cause steric hindrance, and therefore one particular peptide density could be optimal for binding [24]. To test whether the peptide density was of influence on the binding of GLA liposomes to the hCMEC/D3 cells, liposomes were prepared with either 0, 100, 200, 1000, or 1250 peptides coupled to the surface. The liposomes were incubated with hCMEC/D3 cells for 1 hour at 4 °C, and binding was determined. Figure 3 shows that increasing the number of peptides per liposome was of influence on the binding of the liposomes to the cells. Interestingly, coupling of 100 ligands per liposome decreased cell binding compared to liposomes without any ligand. Coupling of 1000 or 1250 ligands significantly increased binding compared to 100 ligands, however, compared to the untargeted liposomes binding was not significantly increased. Therefore, although of influence, peptide density could not be the only explanation for the lack of binding compared to the control.

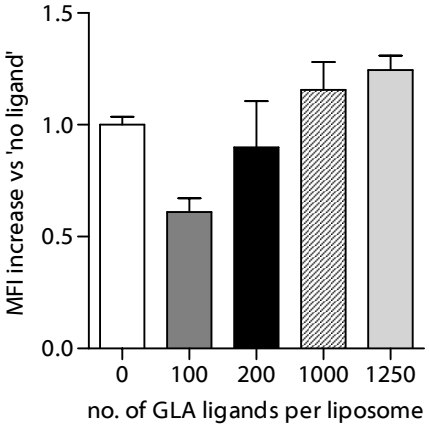

Figure 3. *Flow cytometry analysis of liposome binding to hCMEC/D3 cells. On the y-axis, the mean fluorescence intensity (MFI) increase compared to the liposomes without ligand is shown. Peptide densities were varied from 100-1250 peptides per liposome. Liposome concentration was 1500 nmol lipid per ml. In this experiment, the average liposome size was 180 nm, the average polydispersity index was 0.18. Mean±s.d, n=3. One way ANOVA after log transformation to correct for non-Gaussian distributions, Bonferroni's multiple comparison test: 0 vs 100 p<0.05. 100 vs 1000 p<0.01. 100 vs 1250 p<0.01.*

3. Change of peptide conformation

The final factor that may have an influence on the binding properties of the peptide, is the conformation of the peptide itself. As explained, the library peptide is fused to the minor coat protein (p3) when it is displayed on the phage. The whole p3 protein (406 amino acids) is much larger than the library peptide (15 amino acids) and therefore this likely has an influence on the peptide conformation. The amino acid sequence of the mature fd phage p3 protein is shown in Figure 4, in which the 15-amino acid library peptide (GLA) is indicated in bold. The p3 protein contains eight cysteines, which are at positions 30, 59, 69, 76, 211, 224, 377, and 394. It has been shown for the wild-type phage, that each of the cysteines of mature p3 is involved in a disulfide bond with a neighboring cysteine [25]. The disulfide sites are Cys30-Cys59, Cys69-Cys76, Cys211-Cys224, and Cys377-Cys394. As a result, the p3 protein is thought to have a folded structure [25]. How p3 precisely influences the peptide conformation on the phage is difficult to predict, as it may be different for each individual peptide. The peptides that were produced synthetically were in a linear conformation. However, it is unknown which conformation the peptides had in the phage environment. It has been shown for the tripeptide RGD that the cyclic form is 10 times more efficient in receptor binding than the linear form [26,27]. This shows that besides the amino acid sequence, the conformation can be of influence on the binding properties of a peptide. Next to providing conformation support, the p3 protein also flanks the library peptide with amino acids. Whether these amino acids may support the interaction of the library peptide with the target is unknown.

```
1     ADGAGLAHSF SDFARDFVAG AAGAETVESC LAKPHTENSF TNVWKDDKTL
51    DRYANYEGCL WNATGVVVCT GDETQCYGTW VPIGLAIPEN EGGGSEGGGS
101   EGGGSEGGGT KPPEYGDTPI PGYTYINPLD GTYPPGTEQN PANPNPSLEE
151   SQPLNTFMFQ NNRFRNRQGA LTVYTGTVTQ GTDPVKTYYQ YTPVSSKAMY
201   DAYWNGKFRD CAFHSGFNED PFVCEYQGQS SDLPQPPVNA GGGSGGGSGG
251   GSEGGGSEGG GSEGGGSEGG GSGGGSGSGD FDYEKMANAN KGAMTENADE
301   NALQSDAKGK LDSVATDYGA AIDGFIGDVS GLANGNGATG DFAGSNSQMA
351   QVGDGDNSPL MNNFRQYLPS LPQSVECRPY VFGAGKPYEF SIDCDKINLF
401   RGVFAFLLYV ATFMYVFSTF ANILRNKES
```

Figure 4. *Amino acid sequence of the mature p3 minor coat protein of the fd filamentous phage, including the sequence of the fused GLA peptide (p3-GLA). The protein consists of the GLA peptide (residues 5-19, bold), the N1 domain (residues 24-90), the N2 domain (residues 110-240), the CT domain (residues 280-429), the G1 linker (residues 91-109), the G2 linker (residues 241-279), and two primer-incorporated cloning sequences (residues 1-4 and 20-23) Cysteines are highlighted in dark grey and the recombinantly produced protein is highlighted in light grey. The function of the p3 protein is bacterial attachment and penetration: the N2 domain initiates bacterial attachment by binding to the bacterial F-pilus, and the N1 domain induces the penetration into the bacterial membrane. The CT domain caps the phage particle.*

To investigate the role of the p3 protein on the interaction of the GLA peptide with hCMEC/D3 cells, part of the p3 protein, with the GLA peptide fused to it (p3-GLA), was recombinantly produced. The p3 protein consists of 3 domains, named N1, N2, and CT, connected by glycine-rich linkers G1 and G2 (see Figure 4). It has been shown that the N1-N2 domain, including the G1 linker, could be successfully cloned, expressed in bacteria, and purified [28]. Therefore, only this domain of p3 was chosen for production, fused to the GLA peptide. The produced 240-amino acid sequence is highlighted in Figure 4. The recombinant p3-GLA protein was SATA-modified, and subsequently coupled to the liposomes. The obtained p3-GLA-modified liposome is schematically represented in Figure 5, next to the original GLA-modified liposome.

To investigate binding of p3-GLA compared to GLA only, liposomes modified with these ligands were prepared, and several ligand densities were used. Also liposomes with holo-transferrin and no ligand were prepared. The final liposome characteristics are presented in table II. The liposomes were incubated with hCMEC/D3 cells for 1 hour at 4 °C and binding was determined. As shown in Figure 6A, more p3-GLA liposomes were bound to the hCMEC/D3 cells compared to GLA liposomes, especially when a higher ligand density of p3-GLA was used. To check whether this binding was specific for hCMEC/D3 cells, and not a-specifically caused by the p3 protein, the liposomes were also incubated with an unrelated cell line (HeLa). As shown in Figure 6B, binding of p3-GLA liposomes to HeLa cells was much lower compared to hCMEC/D3 cells. This shows that p3-GLA does not just nonspecifically bind to any cell membrane, and that the p3 protein influences the binding capacity of the GLA peptide.

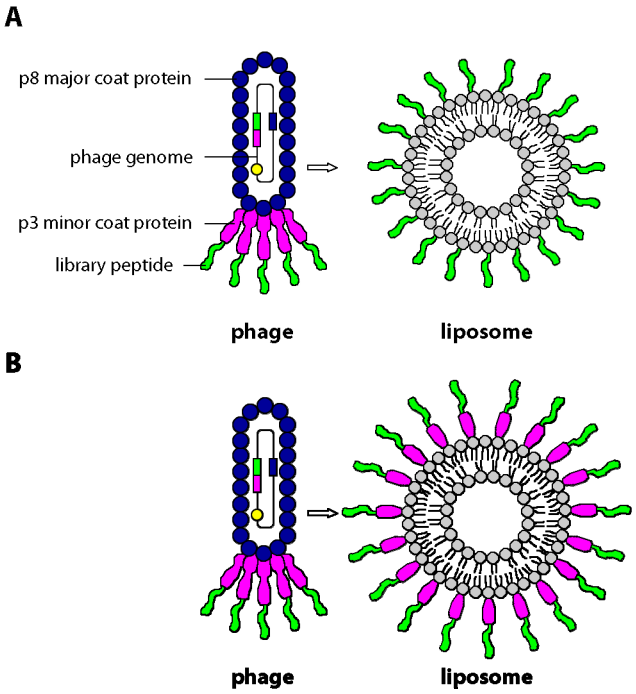

Figure 5. *Schematic representation of an fd phage, and the modified liposomes as used in this study. (**A**) The phage library peptide (GLA) is coupled to the liposome. (**B**) The phage library peptide and part of the p3 minor coat protein (p3-GLA) is coupled to the liposome. Size is not to scale.*

Ligands		**Final liposome characteristics**			
Name	*Molecular weight (kDa)*	*Estimated no. of ligands per liposome*	*Size (nm)*	*ζ potential (mV)*	*PDI*
no ligand	-	-	177	-7.4	0.16
GLA	1.84	100	176	-8.0	0.15
		200	176	-7.6	0.16
		1000	182	-7.6	0.21
p3-GLA	36	50	187	-9.2	0.18
		100	209	-11.0	0.19
		200	217	-13.7	0.20
transferrin	76-81	50	187	-7.9	0.19
		100	202	-8.2	0.22
		200	226	-9.3	0.17

Table II. *Characteristics of ligands and ligand-coupled liposomes. Particle size z-average (nm), zeta (ζ) potential (mV), and polydispersity index (PDI) are shown.*

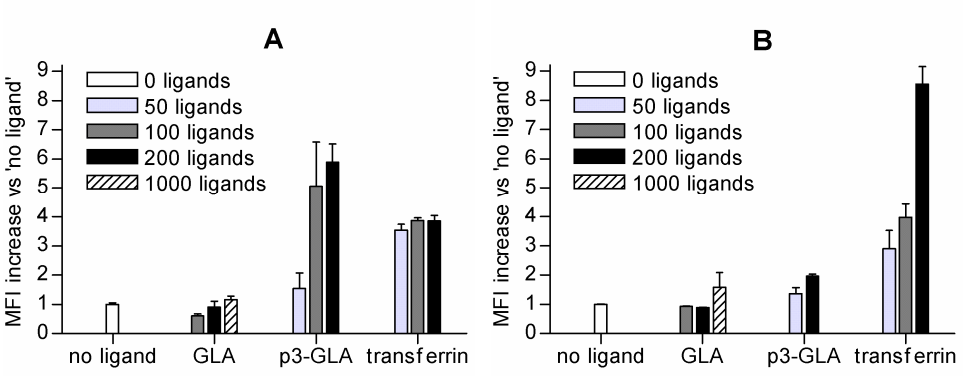

Figure 6. *Flow cytometry analysis of liposome binding to hCMEC/D3 cells (**A**) and HeLa cells (**B**). On the y-axis, the mean fluorescence intensity (MFI) increase compared to the liposomes without ligand is shown. Different numbers of ligands per liposome were used. Liposome concentration was 1500 nmol lipid per ml. Liposome characteristics are shown in table II. Mean±s.d, n=3.*

The results presented in this chapter demonstrate that taking a peptide out of its original environment can result in reduction of the peptide binding capacity, and that this binding may be improved or restored when the peptide is placed back into its natural environment, being the phage p3 minor coat protein. It is possible that the coat protein brings the GLA peptide back to its original conformation as it was on the phage. Alternatively, restored amino acids that flank the GLA peptide may play a role in enhancing target interaction. Finally, the p3 protein may cause the peptide to stick out further from the surface of the liposome, or may introduce more flexibility in the distance between adjacent peptides, to adopt an optimal position for receptor interaction [29].

It is of interest to find out if p3 fusion could also improve or restore peptide properties of other phage display-selected peptides. In literature, several brain-targeting peptides have been selected by phage display. For example, Kolonin *et al.* [30] identified phage clones *in vivo* that showed selectivity for the brain compared to other organs. Especially the tripeptide motifs LGG, RGF, DSY, GIW, and HGL were frequently found. However, none of these peptides have been described in later literature for brain-targeting purposes. This is remarkable, given the fact that there is a need for new efficient brain-targeting systems [31-33]. It is unknown to us whether these tripeptides, when produced synthetically, still possess their brain-targeting properties. If this is not the case, it could be interesting to investigate whether p3 fusion could restore the binding properties of such peptides.

Next to the p3 coat protein, peptide fusion can also be accomplished with the p8 major coat protein. Jayanna *et al.* [34]. separated the whole p8 coat protein, fused to a foreign peptide, from a landscape phage which displays the peptide on all copies of the p8 major

coat protein. The amphiphilic coat protein was able to spontaneously insert into liposomes and retain targeting properties [35], supporting our finding that phage protein-fused peptides can act as targeting ligands.

Conclusion

When target-binding peptides have been selected by phage display, this does not necessarily mean that the synthetically produced form of the peptide will have the same properties or the same extent of target binding, as was the case for our previously phage display-selected GLA peptide. To some extent, the peptide density plays a role on the binding capacity of the peptide. To a higher extent, the presence of the p3 minor coat protein has an influence on the binding capacity of the peptide. To which degree and by which mechanism this occurs remains to be determined, and further experiments are needed to elucidate the possible role of p3 on phage-displayed peptide properties. The results presented in this chapter indicate that the GLA peptide has potential to be used as a liposomal brain-targeting ligand.

Acknowledgements

We thank Pierre-Olivier Couraud, Ignacio Romero, and Babette Weksler for providing the hCMEC/D3 cells. This work was performed within the framework of the Dutch Top Institute Pharma, project T5-105-1: nanoscience as a tool for improving bioavailability and blood-brain barrier penetration.

References

[1] A.G. de Boer, P.J. Gaillard. Drug Targeting to the Brain, Annu Rev Pharmacol Toxicol. 47 (2007) 323-355.
[2] W.M. Pardridge. Drug targeting to the brain, Pharm.Res. 24 (2007) 1733-1744.
[3] I. van Rooy, S. Cakir-Tascioglu, W.E. Hennink, G. Storm, R.M. Schiffelers, E. Mastrobattista. In Vivo Methods to Study Uptake of Nanoparticles into the Brain, Pharm.Res. 28 (2011) 456-471.
[4] A.G. de Boer, I.C. van der Sandt, P.J. Gaillard. The role of drug transporters at the blood-brain barrier, Annu Rev Pharmacol Toxicol. 43 (2003) 629-656.
[5] N. Shi, Y. Zhang, C. Zhu, R.J. Boado, W.M. Pardridge. Brain-specific expression of an exogenous gene after i.v. administration, Proc.Natl.Acad.Sci.U.S.A. 98 (2001) 12754-12759.
[6] Y. Xie, L. Ye, X. Zhang, W. Cui, J. Lou, T. Nagai, et al. Transport of nerve growth factor encapsulated into liposomes across the blood-brain barrier: in vitro and in vivo studies, J.Control.Release. 105 (2005) 106-119.
[7] A. Schnyder, S. Krahenbuhl, J. Drewe, J. Huwyler. Targeting of daunomycin using biotinylated immunoliposomes: pharmacokinetics, tissue distribution and in vitro pharmacological effects, J.Drug Target. 13 (2005) 325-335.

[8] E. Afergan, H. Epstein, R. Dahan, N. Koroukhov, K. Rohekar, H.D. Danenberg, et al. Delivery of serotonin to the brain by monocytes following phagocytosis of liposomes, J.Control.Release. 132 (2008) 84-90.
[9] R.J. Kok, A.J. Schraa, E.J. Bos, H.E. Moorlag, S.A. Asgeirsdottir, M. Everts, et al. Preparation and functional evaluation of RGD-modified proteins as alpha(v)beta(3) integrin directed therapeutics, Bioconjug.Chem. 13 (2002) 128-135.
[10] G.A. Koning, R.M. Schiffelers, M.H.M. Wauben, R.J. Kok, E. Mastrobattista, G. Molema, et al. Targeting of angiogenic endothelial cells at sites of inflammation by dexamethasone phosphate-containing RGD peptide liposomes inhibits experimental arthritis, Arthritis & Rheumatism. 54 (2006) 1198-1208.
[11] D. Kirpotin, J.W. Park, K. Hong, S. Zalipsky, W.L. Li, P. Carter, et al. Sterically stabilized anti-HER2 immunoliposomes: design and targeting to human breast cancer cells in vitro, Biochemistry. 36 (1997) 66-75.
[12] G. Rouser, S. Fleischer, A. Yamamoto. Two dimensional then layer chromatographic separation of polar lipids and determination of phospholipids by phosphorus analysis of spots, Lipids. 5 (1970) 494-496.
[13] X. Gao, P. Kouklis, N. Xu, R.D. Minshall, R. Sandoval, S.M. Vogel, et al. Reversibility of increased microvessel permeability in response to VE-cadherin disassembly, Am J Physiol Lung Cell Mol Physiol. 279 (2000) L1218-1225.
[14] M. Shayo, R.N. McLay, A.J. Kastin, W.A. Banks. The putative blood-brain barrier transporter for the [beta]-amyloid binding protein apolipoprotein j is saturated at physiological concentrations, Life Sciences. 60 (1997) PL115.
[15] D. Triguero, J. Buciak, W.M. Pardridge. Capillary depletion method for quantification of blood-brain barrier transport of circulating peptides and plasma proteins, J.Neurochem. 54 (1990) 1882-1888.
[16] E.G. Gutierrez, W.A. Banks, A.J. Kastin. Murine tumor necrosis factor alpha is transported from blood to brain in the mouse, J.Neuroimmunol. 47 (1993) 169-176.
[17] K.H. Diehl, R. Hull, D. Morton, R. Pfister, Y. Rabemampianina, D. Smith, et al. A good practice guide to the administration of substances and removal of blood, including routes and volumes, J.Appl.Toxicol. 21 (2001) 15-23.
[18] I. van Rooy, S. Cakir-Tascioglu, P.O. Couraud, I.A. Romero, B. Weksler, G. Storm, et al. Identification of peptide ligands for targeting to the blood-brain barrier, Pharm.Res. 27 (2010) 673-682.
[19] G.P. Smith, V.A. Petrenko. Phage Display, Chem. Rev. 97 (1997) 391-410.
[20] W.G.T. Willats. Phage display: practicalities and prospects, Plant Molecular Biology. 50 (2002) 837-854.
[21] K. Zhang, H. Fang, Z. Chen, J.S. Taylor, K.L. Wooley. Shape effects of nanoparticles conjugated with cell-penetrating peptides (HIV Tat PTD) on CHO cell uptake, Bioconjug.Chem. 19 (2008) 1880-1887.
[22] P. Chaudhuri, R. Harfouche, S. Soni, D.M. Hentschel, S. Sengupta. Shape effect of carbon nanovectors on angiogenesis, ACS Nano. 4 (2010) 574-582.
[23] S. Gelperina, O. Maksimenko, A. Khalansky, L. Vanchugova, E. Shipulo, K. Abbasova, et al. Drug delivery to the brain using surfactant-coated poly(lactide-co-glycolide) nanoparticles: influence of the formulation parameters, Eur.J.Pharm.Biopharm. 74 (2010) 157-163.
[24] A. Fakhari, A. Baoum, T.J. Siahaan, K.B. Le, C. Berkland. Controlling ligand surface density optimizes nanoparticle binding to ICAM-1, J.Pharm.Sci. (2010).
[25] Kremser, I. Rasched. The adsorption protein of filamentous phage fd: assignment of its disulfide bridges and identification of the domain incorporated in the coat, Biochemistry. 33 (1994) 13954-13958.
[26] H. Kumagai, M. Tajima, Y. Ueno, Y. Giga-Hama, M. Ohba. Effect of cyclic RGD peptide on cell adhesion and tumor metastasis, Biochem.Biophys.Res.Commun. 177 (1991) 74-82.
[27] E. Koivunen, D.A. Gay, E. Ruoslahti. Selection of peptides binding to the alpha 5 beta 1 integrin from phage display library, J.Biol.Chem. 268 (1993) 20205-20210.

[28] J. Lubkowski, F. Hennecke, A. Pluckthun, A. Wlodawer. The structural basis of phage display elucidated by the crystal structure of the N-terminal domains of g3p, Nat.Struct.Biol. 5 (1998) 140-147.
[29] V. Olivier, I. Meisen, B. Meckelein, T.R. Hirst, J. Peter-Katalinic, M.A. Schmidt, et al. Influence of targeting ligand flexibility on receptor binding of particulate drug delivery systems, Bioconjug.Chem. 14 (2003) 1203-1208.
[30] M.G. Kolonin, J. Sun, K. Do, C.I. Vidal, Y. Ji, K.A. Baggerly, et al. Synchronous selection of homing peptides for multiple tissues by in vivo phage display, FASEB J. 20 (2006) 979-981.
[31] V. Nienaber. Start small and stay small. Minimizing attrition in the clinic with a focus on CNS therapeutics, Curr.Top.Med.Chem. 9 (2009) 1688-1704.
[32] D. Refojo, F. Holsboer. CRH signaling. Molecular specificity for drug targeting in the CNS, Ann.N.Y.Acad.Sci. 1179 (2009) 106-119.
[33] M.I. Alam, S. Beg, A. Samad, S. Baboota, K. Kohli, J. Ali, et al. Strategy for effective brain drug delivery, Eur.J.Pharm.Sci. 40 (2010) 385-403.
[34] P.K. Jayanna, D. Bedi, J.W. Gillespie, P. DeInnocentes, T. Wang, V.P. Torchilin, et al. Landscape phage fusion protein-mediated targeting of nanomedicines enhances their prostate tumor cell association and cytotoxic efficiency, Nanomedicine. 6 (2010) 538-546.
[35] T. Wang, G.G. D'Souza, D. Bedi, O.A. Fagbohun, L.P. Potturi, B. Papahadjopoulos-Sternberg, et al. Enhanced binding and killing of target tumor cells by drug-loaded liposomes modified with tumor-specific phage fusion coat protein, Nanomedicine (Lond). 5 (2010) 563-574.

Supplementary information to chapter 5

Introduction

Ultra performance liquid chromatography (UPLC) analysis was performed to confirm that thiolated peptides and proteins could be coupled to the maleimide-containing liposomes. Results are shown for one representative peptide (GYR).

Materials and Methods

Liposomes were prepared with either a composition of DPPC, cholesterol, DSPE-PEG_{2000}, and DSPE-PEG_{2000}-maleimide, in a 1.85:1:0.075:0.075 molar ratio, or a composition of DPPC, cholesterol, and DSPE-PEG_{2000} in a 1.85:1:0.15 molar ratio. Final total lipid concentration was 100 µmol/ml. Peptide GYR was reduced and added at a concentration of 1 mg/ml (12.5 nmol protein/µmol total lipid, corresponding to a peptide:maleimide rato of 1:1 for the maleimide-containing liposomes) or 1.5 mg/ml. After overnight incubation, liposomes and a GYR peptide calibration curve were applied to a Waters Acquity UPLC system (Waters corporation, Milford, MA) using a BEH300 C18 1.7µm column, at a flow rate of 0.25 ml/min. All samples were applied to the UPLC undiluted, except for the sample which contained liposomes without maleimide, this sample was 2x diluted. Gradient mobile phase was changed during 10 minutes from 100% solvent A (acetonitrile:H2O 5:95) to 100% solvent B (acetonitrile), and ran additionally for 2 minutes at 100% solvent B. Both solvents contained 0.1% trifluoroacetic acid. UV detection was performed at 210 nm.

Results and Discussion

The GYR peptide was incubated with either maleimide-containing or maleimide-free liposomes. The amount of uncoupled peptide in the samples was analyzed, to indirectly determine the amount that was coupled [1]. The GYR peptide had a retention time (RT) of 2.36 min (Figure 1A). When the peptide was incubated with liposomes containing no maleimide, 100% of the added peptide could be detected as uncoupled peptide in the liposomal sample, at the same RT as the free peptide (Figure 1B). When maleimide-containing liposomes were incubated with the peptide, only 5% could be detected as uncoupled peptide, indicating that 95% of the peptide was coupled to the liposomes (Figure 1C). A new peak appeared at a RT of 10.45 min, probably representing the peptide-DSPE-PEG_{2000}-maleimide conjugate. When an excess of peptide was added to the maleimide liposomes (1.5:1), free peptide could be detected again in the liposomal solution (Figure 1D), indicating saturation of maleimide. For all peptides and proteins used in this study, coupling efficiencies between 90 and 99% were obtained.

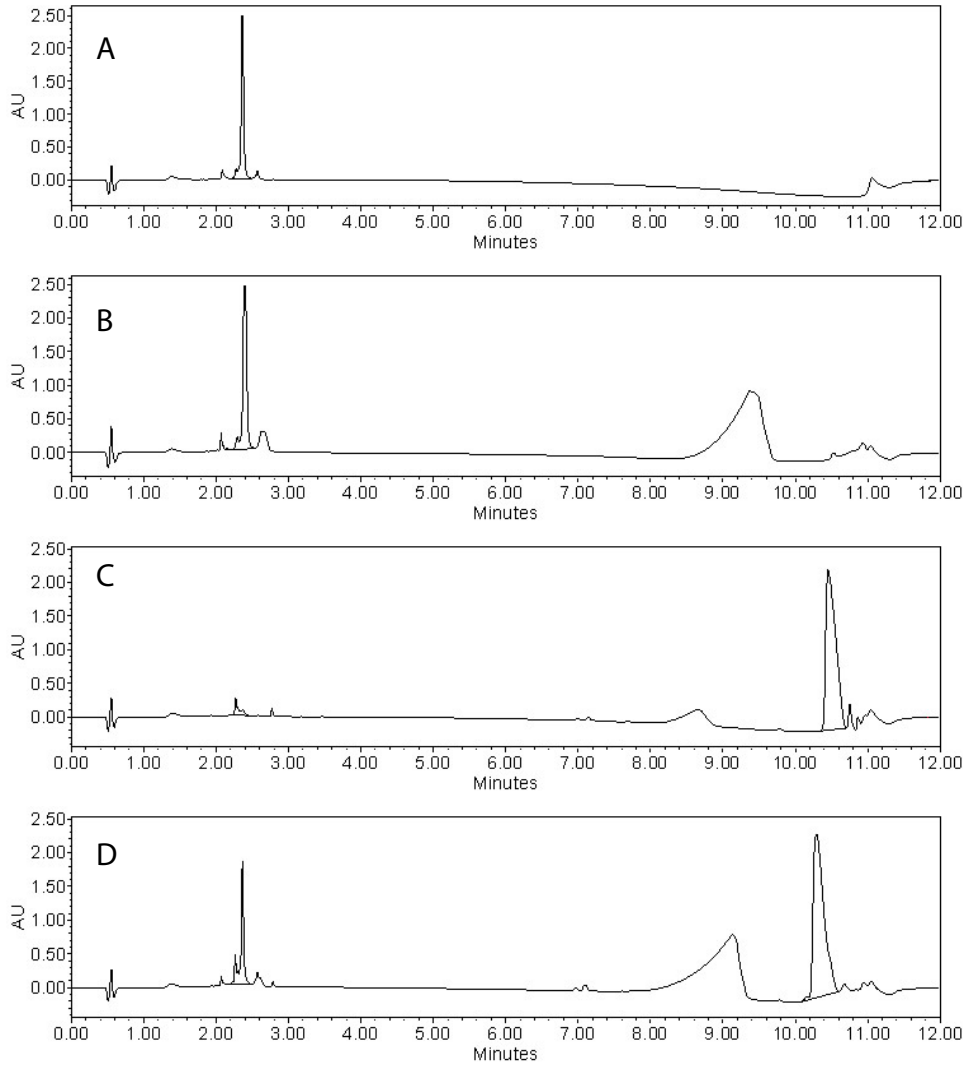

Figure 1. *UPLC chromatograms of GYR peptide and liposomes, detected by UV absorbance at 210 nm. Retention times (RT) and area under the curve (AUC) of peptide peaks are shown in chromatogram. (**A**) Peptide only, 0.375 mg/ml. (**B**) Liposomes without maleimide, incubated overnight with 1 mg/ml GYR peptide (2x diluted before measurement). (**C**) Liposomes containing maleimide, incubated overnight with 1 mg/ml GYR peptide. (**D**) Liposomes with maleimide, incubated overnight with 1.5 mg/ml GYR peptide.*

Reference

[1] G.A. Koning, R.M. Schiffelers, M.H.M. Wauben, R.J. Kok, E. Mastrobattista, G. Molema, et al. Targeting of angiogenic endothelial cells at sites of inflammation by dexamethasone phosphate-containing RGD peptide liposomes inhibits experimental arthritis, Arthritis & Rheumatism. 54 (2006) 1198-1208.

Chapter 6

Preparation and characterization of liposomal formulations of neurotensin-degrading enzyme inhibitors

Inge van Rooy
Shin-Ying Wu
Gert Storm
Wim E Hennink
Heike Dinter-Heidorn
Raymond M Schiffelers
Enrico Mastrobattista

International Journal of Pharmaceutics (2011), in press

Abstract

Neurotensin-degrading enzyme (NTDE) inhibitors hold great potential for treating psychotic disorders. However, brain uptake of such compounds *in vivo* is generally low due to the presence of the blood-brain barrier. In this study, liposomal formulations of two NTDE inhibitors, named compound 1 (C1) and compound 2 (C2) were prepared. Association of these compounds with the liposomal bilayer, subsequent liposomal stability, and compound release in the presence of albumin were studied. Entrapment of the compounds in the liposomal bilayer showed the solubilizing properties of the liposomes. Size and polydispersity index of the compound-entrapped liposomes did not change over 1 month, showing colloidal stability of the liposomal drug formulations. The amount of compounds associated with the liposomes decreased within one day. After this, the association remained stable at 4°C. For C1, association remained stable at 37°C in HEPES buffered saline, and the compound was gradually released in the presence of albumin. For C2, the release was rapid in both HBS and BSA at 37°C. In conclusion, the formulation of NTDE inhibitors C1 and C2 in liposomes has been demonstrated and holds promise to deliver NTDE inhibitors *in vivo*.

Introduction

Neurotensin is a tridecapeptide found within the central nervous system (CNS) and the gastrointestinal tract. Three main neurotensin receptors have been identified (NTS1, NTS2, and NTS3). In the gastrointestinal tract, neurotensin is involved in gut motility. In the brain, it is highly expressed in the limbic system, and is involved as a neurotransmitter in many processes, including antinociception, hypothermia, control of anterior pituitary hormone secretion, and muscle relaxation [1]. In addition, neurotensin acts as a neuromodulator affecting the dopaminergic pathways in the brain. Dopamine receptors are divided into the D1 and D2 subfamilies, and neurotensin antagonizes dopamine effects at the D2 receptors. Neuronal D2 receptors are located on both the presynaptic and the postsynaptic site. At the presynaptic site, D2 regulates synthesis and release of dopamine. Postsynaptically, D2 inhibits downstream effects of dopamine, by inhibiting adenylyl cyclase and the cAMP pathway [2]. Presynaptic neurotensin antagonism of D2 receptors leads to an increase of dopamine release, enhancing postsynaptic dopamine D2 action. In contrast, postsynaptic neurotensin antagonism of D2 receptors results in a reduction of dopamine D2 neurotransmission [3]. This resembles the action of antipsychotic drugs, which block D2 receptors [4], making neurotensin a possible endogenous antipsychotic [3,5]. Because of the close interaction of neurotensin and the dopamine pathways, neurotensin may be involved in many dopamine-related disorders, such as Huntington's disease, Parkinson's disease, and drug abuse. For this reason, modulating the concentration of neurotensin in the brain is of therapeutic interest, and several neurotensin analogs have been developed [1].

When neurotransmitters and neuropeptides are released from the cells that store them, they are meant to produce rapid peak signals that last only shortly. Therefore, after release, neurotensin is cleaved and inactivated by metallo-endopeptidases in the extracellular space near the target cells. There are 3 major neurotensin-degrading enzymes: EP 24.11, EP 24.15, and EP 24.16. Their cleavage sites are indicated in Figure 1. Cleavage by these enzymes leads to complete biological inactivation of neurotensin [6]. In order to prevent neurotensin degradation, NTDE inhibitors have been synthesized. This approach is an alternative to the use of neurotensin analogs, and is meant to increase the effects of endogenous neurotensin. *In vivo* experiments have shown that an intracerebroventricularly (icv) injected mixed inhibitor of all three major NTDEs was able to potentiate the hypothermic effects of icv injected neurotensin [7]. In another study, an icv injected inhibitor selective for EP 24.25 and EP 24.16 was able to potentiate the antinociceptive effects of icv injected neurotensin [8].

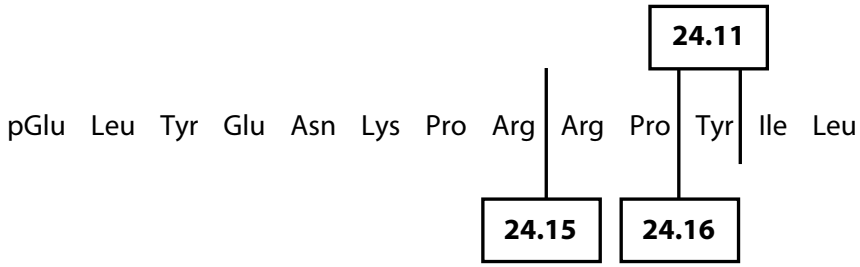

Figure 1. *Neurotensin amino acid sequence and cleavage sites for endopeptidases EP 24.11, EP 24.15, and EP 24.16.*

The *in vivo* experiments performed with NTDE inhibitors only showed effects when the drug was administered by icv injection. Lack of sufficient effect after intravenous administration is due to the blood-brain barrier (BBB). This barrier is formed by the brain endothelial cells that surround the microvessels of the brain. Additionally, other cell types surrounding the endothelium, such as astrocytes and pericytes, contribute to the formation of the BBB [9]. Due to the tightness and strict transport regulation of the barrier, less than 98% of small molecule drugs can enter the brain [10]. For clinical applications, icv injection is not an option [11]. Therefore, a drug delivery vehicle is needed to transport peripherally administered NTDE inhibitors to the brain. Liposomes have been widely used as delivery vehicles to increase uptake into the brain *in vivo* [12-15]. By coupling specific BBB targeting ligands to the outside of the liposomes, they can enter the brain endothelial cells through receptor-mediated endocytosis, followed by transcytosis to the brain [16].

In this study, liposomal formulations of two 2,3-diaryl-pyparazolidine derivatives, named compound 1 (C1) and compound 2 (C2) [17] were prepared. These lipophilic compounds act as neurotensin-degrading enzyme (NTDE) inhibitors in the brain, but show poor brain uptake *in vivo*. Association of C1 and C2 with liposomes, subsequent liposomal stability, and compound release in the presence of albumin was studied. The structural formulas and characteristics of C1 and C2 are shown in table I.

Name	Structural formula	MW (Da)	IC_{50} (nM)*	AlogP	Oral bioavail-ability (%)	CNS/plasma ratio
C1	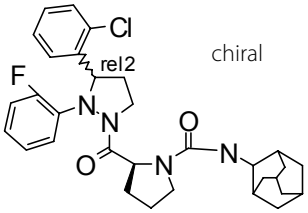 chiral	551	100	5.9	0.7	0.2-0.5
C2	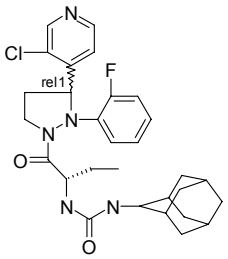	540	20	4.9	18	0.02

Table I. *Structural formulas and characteristics of NTDE inhibitors C1 and C2 [17]. Characteristics are based on unpublished results. *IC50 values were obtained according to the methods described in [18].*

Materials and Methods

Materials

Cholesterol was obtained from Sigma (St. Louis, MO). Dipalmitoyl phosphatidylcholine (DPPC) and distearoyl phosphatidylethanolamine-polyethyleneglycol$_{2000}$ (DSPE-PEG$_{2000}$) were obtained from Lipoid GmbH (Ludwigshafen, Germany). Compounds 1 and 2 were obtained from Abbott Healthcare Products B.V. (formerly Solvay Pharmaceuticals B.V., Weesp, The Netherlands).

HPLC detection of compounds

Drugs were dissolved in pure ethanol to yield 10 mg/ml stock solutions. UV-Vis absorption at a wavelength range from 220 to 400 nm determined the optimal detection wavelength at 233 nm for both compounds. Compound concentration determinations were performed by high-performance liquid chromatography (HPLC, Waters corporation, Milford, MA), using a C18, 4.6x150 mm column (Sunfire), at a flow rate of 1 ml/min. Gradient mobile phase consisted of solvent A (methanol:H_2O 5:95) and solvent B (methanol), and was changed during 15 minutes from 50/50 solvent A/B to 100% solvent B, and ran additionally for 3 minutes at 100% solvent B. Both solvents contained 0.1% perchloric acid. UV detection was performed at 233 nm. Compounds showed a retention time of 12 min (C2) and 15 min (C1). HPLC sample injection volume was 50 µl and for

liposomes proper sample dilutions were made to obtain a concentration estimated to fit within a free drug standard curve.

Liposome preparation

Liposomes were prepared by the film hydration method. Lipids (DPPC, cholesterol and DSPE-PEG_{2000}) were dissolved in chloroform, in a 1.85:1:0.15 molar ratio. Compounds were mixed with the lipid solution to achieve a final compound concentration of either 1 mol % or 5 mol % of total lipids. A lipid film was made by rotary evaporation. The lipid film was hydrated in HBS (10 mM HEPES, 146 mM NaCl, pH 7.4) to a final lipid concentration of 30 µmol/ml. Liposomes were sized by probe sonication at 100% amplitude, 0.5 cycles for 20 min on ice (Labsonic P, 50/60 Hz, Satorius). To remove drugs that did not associate with the liposomes, the liposome solution was centrifuged at 20,000xg for 10 min. Supernatant containing the liposomes was collected. Precipitated drug pellet was resuspended in ethanol. A phosphate determination [19] of both the pellet and the supernatant confirmed that all liposomes were in the supernatant, and no liposomes were present in the pellet. Both pellet and supernatant were subjected to HPLC for compound determination.

Characterization of liposomes

The mean particle size distribution (z-average) and the polydispersity index of the liposomes were determined by dynamic light scattering (DLS) in a Malvern ALV CGS-3 (Malvern Instruments, Malvern, UK) containing a He-Ne laser source (λ=632.8 nm, 22 mW output power) under an angle of 90°. Measurements were performed in HBS (10 mM HEPES, 146 mM NaCl, pH 7.4). When size distribution and polydispersity index were measured over time, liposomes were subjected to centrifugation at 20,000xg for 10 min before each measurement.

Compound association at 4°C

Liposomes were stored at 4°C. At various time points, liposomes were centrifuged at 20,000xg for 10 min. Drug concentrations in both liposomal supernatant and free drug pellet were measured by HPLC. The total amount of drugs added to the liposomes was set at 100%.

Compound leakage at 37°C

Drug release from liposomes was studied over 7 days at 37°C, in the presence of either HBS or BSA, as modified from Peschka *et al*. [20]. One day old liposomes (30 µmol/ml lipid) were centrifuged at 20,000xg for 10 min to remove unassociated drugs. Two % of agarose was dissolved in water and liquefied by heating. Equal volumes (250 µl) of agarose solution and liposomes were mixed in glass vials. After this layer solidified, a second layer

of 2% agarose (150 µl) was added on top. A receptor solution of 4.5 ml HBS (10 mM HEPES, 146 mM NaCl, pH 7.4), or 4.5 ml BSA in HBS (40 mg/ml) was poured on top. In this way, the agarose-embedded liposomes were physically separated from the buffer by the 2% agarose layer. The liposomes were trapped in the agarose, while the HBS and albumin were able to penetrate into it. The vials were incubated at 37°C while shaking at 250 rpm and the receptor solution was replaced at various time points. The concentration of compound in the replaced solutions was determined by HPLC. The amount of drugs in the liposomes after centrifugation (before agarose embedding) was set at 100%. Peschka *et al*. showed that 98.7% of liposomes remained intact after 5 days using this method [20].

Results

Preparation of liposomal drug formulations

The solubility of NTDE inhibitors C1 and C2 in aqueous buffer is extremely poor. To determine whether encapsulation in a liposomal bilayer could increase the solubility, suspensions of both free and liposomal drugs in aqueous buffer (HBS) were prepared. Liposomes were composed of phosphatidylcholine, cholesterol and DSPE-PEG_{2000}, as this liposomal composition has been used before to target to the brain [13,14,21,22]. After preparation, liposomal suspensions were centrifuged to spin down non-dissolved drugs, and the amount of drugs in pellet and supernatant was determined. As shown in Figure 2, about 50% of the free C1 and C2 in the suspension could be recovered. This was probably due to the highly lipophilic nature of both compounds, which makes them stick to polypropylene disposables used for preparation and detection [23]. When the free drug suspension was centrifuged, all of C1 and most of C2 was pelleted, underlining the poor solubility. When liposomal formulations of these drugs were prepared, a much higher amount of drug could be recovered from the suspension, showing the solubilizing properties of the liposomes. When the liposomes were centrifuged, a high percentage of free drug was pelleted, indicating that not all of the solubilized drug had been encapsulated inside the liposomes. The total association percentage was 25 to 55%, depending on the compound concentration, indicating that there is an association plateau.

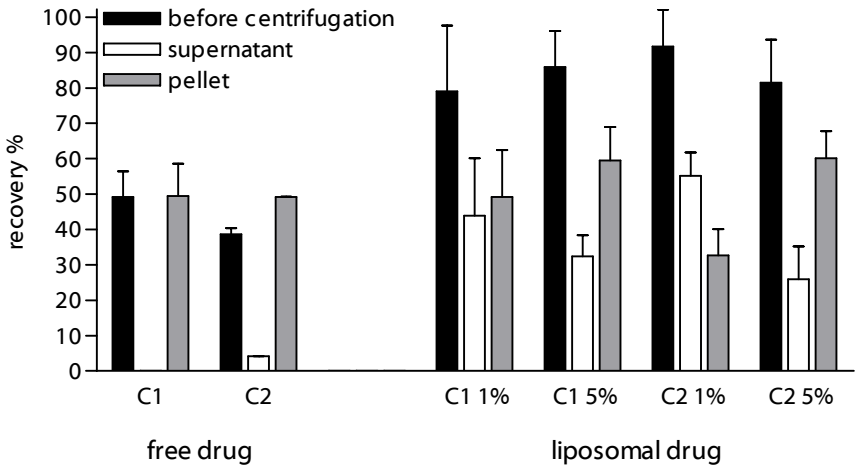

Figure 2. *Recovery percentage of compounds C1 and C2 from free and liposomal drug suspensions. In the liposomal formulations, the amount of drugs added was 1 or 5 mol % of total lipid. The total amount of drugs added to the suspensions was set at 100%. Concentrations were determined by HPLC before and after centrifugation. After centrifugation (10,000 xg, 10 min), the amount of drug was determined in the pellet (precipitated drug) and supernatant (free or liposomal drug in suspension). Mean±s.d. n=3.*

Characterization and stability of liposomal drug formulations

Stability of the liposomal formulations in terms of size, polydispersity, and drug association was monitored over a one month period. During this time the liposomes were stored at 4°C. As shown in Figure 3, the average size of all four liposomal formulations was stable at around 130 to 140 nm. The polydispersity index (PDI) was in the range of 0.1 to 0.2.

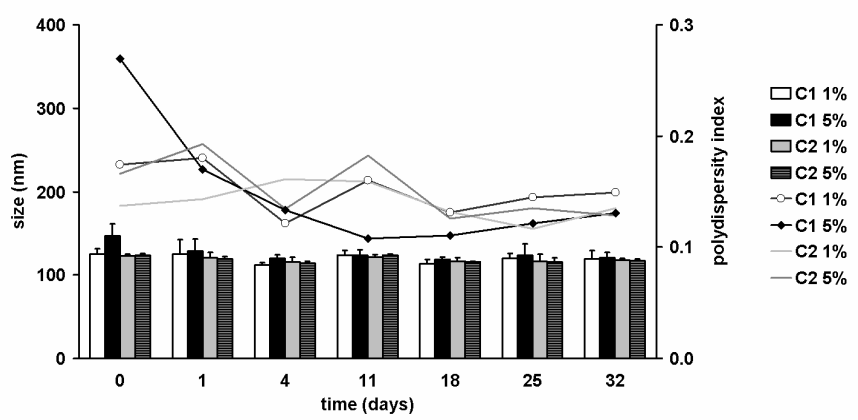

Figure 3. *Size (bars) and polydispersity index (lines) of liposomal preparations of compounds C1 and C2, measured over a period of 32 days while liposomes were stored at 4°C. The amount of drug added to the liposomes was 1 or 5 mol % of total lipid.*

The release of compounds C1 and C2 from these liposomes was determined over one month. As shown in Figure 4, both C1 and C2 showed an initial burst release of the compounds within the first 24 hours. After this release, the association of the drugs with the liposomes stabilized.

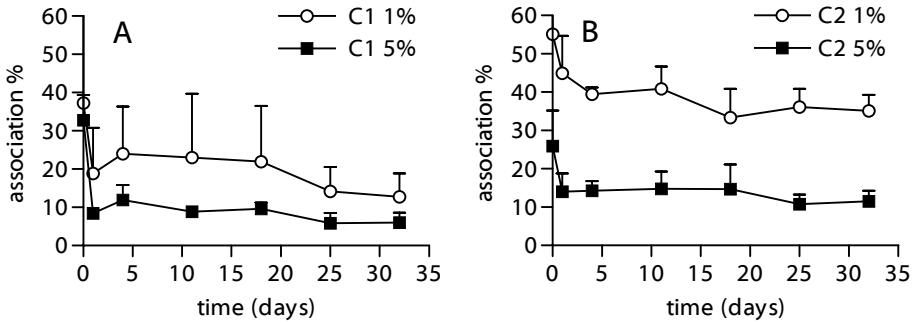

Figure 4. *Association percentage of compounds C1 (**A**) and C2 (**B**) to liposomes, measured over a period of 32 days while liposomes were stored at 4°C in HBS buffer. The total amount of drugs added to the liposomes was set at 100%. The added drug amount was 1 or 5 mol % of total lipid. The percentage of drugs associated with the liposomes was measured by HPLC. Mean±s.d. n=3.*

Drug release at 37°C in the presence of albumin

Drug release of compounds C1 and C2 from the liposomes was studied at 37°C in the presence of buffer (HBS), with or without albumin. Albumin is the most abundant plasma protein and is known to interact with many drugs, due to its hydrophobic pockets [24]. To study the release of the compounds in the presence of HBS and BSA, one day old liposomes were centrifuged to remove unassociated drugs, and were embedded in a 1% agarose gel, and covered by a physical protection layer of 2% agarose gel. A receptor solution consisting of either HBS or BSA solution was poured on top. The solution was replaced at several time points during 7 days. The drug concentration in the replaced solution was measured. Figure 5 shows the cumulative release of the drugs from the liposomes into the receptor solutions. C1 was not released in HBS during the time period measured (Figure 5A), which was comparable to the previous experiment at 4°C (Figure 4A). When liposomes were incubated with BSA solution, release of C1 was first measured after 8 hours, and continued gradually over 7 days. For compound C2, release was detected at the first time point measured (1 hour), regardless of the receptor solution composition (Figure 5B), implicating that the release of C2 was not related to protein interaction. Release of C2 reached a maximum within 1 day. Although only 30-50% of C2 could be recovered, this probably represents 100% of the drug, as the remaining 50-70% was not found within the agarose gel after 7 days. Again, the lipophilic nature of the compound probably resulted in loss of compound during preparation and measurement.

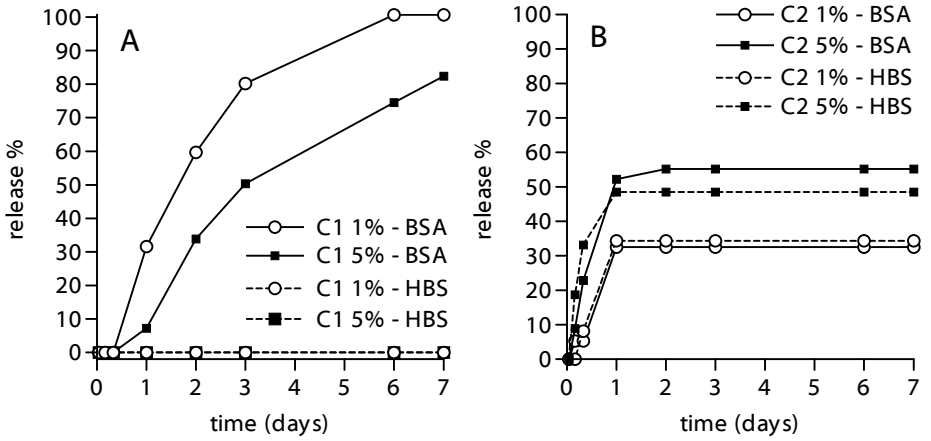

Figure 5. *Cumulative dissociation of compounds C1 (**A**) and C2 (**B**) from liposomes embedded in agarose, measured over a period of 7 days while liposomes were shaken at 37°C. The amount of drugs in 1 day old liposomes (after centrifugation, before agarose embedding) was set at 100%. The added drug amount was 1 or 5 mol % of total lipid. Dissociation was measured in either HBS or BSA. t=0 is the time point of embedding.*

Discussion

Liposomal formulations of two NTDE inhibiting compounds with poor aqueous solubility were prepared. Although entrapping these compounds in the bilayer of liposomes clearly increased the solubility of these compounds, the association efficiency of C1 and C2 decreased after 1 day, resulting in a low final amount of drugs associated to the liposomes. The reason for the rapid dissociation of the compounds remains unclear. It is known that lipophilic compounds are able to destabilize the bilayer and can lead to the disintegration of the liposomes [25]. However, size and polydispersity index of the liposomes remained stable. Possibly the drug aggregated and precipitated.

After the initial release, the liposomal association of C1 in HBS remained stable. In conditions mimicking the circulation (a 37°C shaking BSA solution), C1 release commenced after 8 hours, and the compound was gradually released over 7 days. This is of interest for the *in vivo* situation since a substantial part of these type of liposomes will be taken up into the brain within 8 hours after iv administration, and the majority will usually be taken up within 24 hours [26,27]. Drug release from the carrier at the target site (brain) is of major importance [28]. Therefore, a liposome gradually releasing the drug could be an interesting vehicle for delivering the NTDE inhibitor to the brain. For compound C2, release under these conditions started immediately. Therefore, this formulation is probably less suitable for *in vivo* applications.

To induce uptake of C1 liposomes into the brain, they should preferentially be coupled to a brain-targeting ligand. For example, anti-transferrin receptor antibodies such as OX26 or RI7217 are good candidates for liposomal targeting to the brain [21,29]. Once the ligands bind to the brain endothelial cells, the liposomes can be taken up by receptor-mediated endocytosis, and release their contents [30].

Conclusion

We have demonstrated that encapsulation of compounds C1 and C2 in liposomes results in a higher solubility of these compound in aqueous media and a gradual release of C1 under physiological conditions over a period of 7 days. This formulation may solve the problem of poor solubility and difficulty to cross the blood-brain barrier. Further investigation is needed to show proof-of-concept that liposomal formulations of NTDE inhibitors can be used to deliver sufficient amounts of these inhibitors to the brain to modify the dopaminergic pathways, and act as future therapeutics for psychotic disorders.

Acknowledgements

We thank Abbott Healthcare Products B.V. (formerly Solvay Pharmaceuticals B.V.) for providing the NTDE inhibitors (P. Smid and R.W. Feenstra) and the data described in table I (J.A.R. Dijksman and P. Spaans). This work was performed within the framework of the Dutch Top Institute Pharma project T5-105-1: nanoscience as a tool for improving bioavailability and blood-brain barrier penetration.

References

[1] M. Boules, P. Fredrickson, E. Richelson. Bioactive analogs of neurotensin: focus on CNS effects, Peptides. 27 (2006) 2523-2533.

[2] C. De Mei, M. Ramos, C. Iitaka, E. Borrelli. Getting specialized: presynaptic and postsynaptic dopamine D2 receptors, Curr.Opin.Pharmacol. 9 (2009) 53-58.

[3] R. Caceda, B. Kinkead, C.B. Nemeroff. Neurotensin: role in psychiatric and neurological diseases, Peptides. 27 (2006) 2385-2404.

[4] P. Seeman. Dopamine D2 receptors as treatment targets in schizophrenia, Clin.Schizophr.Relat.Psychoses. 4 (2010) 56-73.

[5] B. Kinkead, C.B. Nemeroff. Neurotensin: an endogenous antipsychotic? Curr.Opin.Pharmacol. 2 (2002) 99-103.

[6] P. Kitabgi. Inactivation of neurotensin and neuromedin N by Zn metallopeptidases, Peptides. 27 (2006) 2515-2522.

[7] S. Doulut, I. Dubuc, M. Rodriguez, F. Vecchini, H. Fulcrand, H. Barelli, et al. Synthesis and analgesic effects of N-[3-[(hydroxyamino) carbonyl]-1-oxo-2(R)-benzylpropyl]-L-isoleucyl-L-leucine, a new potent inhibitor of multiple neurotensin/neuromedin N degrading enzymes, J.Med.Chem. 36 (1993) 1369-1379.

[8] B. Vincent, V. Dive, A. Yiotakis, C. Smadja, R. Maldonado, J.P. Vincent, et al. Phosphorus-containing peptides as mixed inhibitors of endopeptidase 3.4.24.15 and 3.4.24.16: effect on neurotensin degradation in vitro and in vivo, Br.J.Pharmacol. 115 (1995) 1053-1063.
[9] A.G. de Boer, I.C. van der Sandt, P.J. Gaillard. The role of drug transporters at the blood-brain barrier, Annu Rev Pharmacol Toxicol. 43 (2003) 629-656.
[10] W.M. Pardridge. Blood-brain barrier delivery, Drug Discovery Today. 12 (2007) 54-61.
[11] A.G. de Boer, P.J. Gaillard. Drug Targeting to the Brain, Annu Rev Pharmacol Toxicol. 47 (2007) 323-355.
[12] N. Shi, Y. Zhang, C. Zhu, R.J. Boado, W.M. Pardridge. Brain-specific expression of an exogenous gene after i.v. administration, Proc.Natl.Acad.Sci.U.S.A. 98 (2001) 12754-12759.
[13] Y. Xie, L. Ye, X. Zhang, W. Cui, J. Lou, T. Nagai, et al. Transport of nerve growth factor encapsulated into liposomes across the blood-brain barrier: in vitro and in vivo studies, J.Control.Release. 105 (2005) 106-119.
[14] A. Schnyder, S. Krahenbuhl, J. Drewe, J. Huwyler. Targeting of daunomycin using biotinylated immunoliposomes: pharmacokinetics, tissue distribution and in vitro pharmacological effects, J.Drug Target. 13 (2005) 325-335.
[15] E. Afergan, H. Epstein, R. Dahan, N. Koroukhov, K. Rohekar, H.D. Danenberg, et al. Delivery of serotonin to the brain by monocytes following phagocytosis of liposomes, J.Control.Release. 132 (2008) 84-90.
[16] I. van Rooy, S. Cakir-Tascioglu, W.E. Hennink, G. Storm, R.M. Schiffelers, E. Mastrobattista. In Vivo Methods to Study Uptake of Nanoparticles into the Brain, Pharm.Res. 28 (2011) 456-471.
[17] R.W. Feenstra, J.H.M. Lange, M. Pras-Raves L., C.G. Kruse, H.H. Van Stuivenberg, T. Tuinstra, et al. Neurotensin active 2,3-diaryl-pyparazolidine derivatives, PCT/EP2003/050064 (2003).
[18] P. Dauch, H. Barelli, J.P. Vincent, F. Checler. Fluorimetric assay of the neurotensin-degrading metalloendopeptidase, endopeptidase 24.16, Biochem.J. 280 (Pt 2) (1991) 421-426.
[19] G. Rouser, S. Fleischer, A. Yamamoto. Two dimensional then layer chromatographic separation of polar lipids and determination of phospholipids by phosphorus analysis of spots, Lipids. 5 (1970) 494-496.
[20] R. Peschka, C. Dennehy, F.C. Szoka Jr. A simple in vitro model to study the release kinetics of liposome encapsulated material, J.Control.Release. 56 (1998) 41-51.
[21] S. Gosk, C. Vermehren, G. Storm, T. Moos. Targeting anti-transferrin receptor antibody (OX26) and OX26-conjugated liposomes to brain capillary endothelial cells using in situ perfusion, J.Cereb.Blood Flow Metab. 24 (2004) 1193-1204.
[22] X. Zhang, Y. Xie, Y. Jin, X. Hou, L. Ye, J. Lou. The effect of RMP-7 and its derivative on transporting Evans blue liposomes into the brain, Drug Deliv. 11 (2004) 301-309.
[23] L. Pan, Q. Ho, K. Tsutsui, L. Takahashi. Comparison of chromatographic and spectroscopic methods used to rank compounds for aqueous solubility, J.Pharm.Sci. 90 (2001) 521-529.
[24] F. Kratz. Albumin as a drug carrier: Design of prodrugs, drug conjugates and nanoparticles, J.Controlled Release. 132 (2008) 171-183.
[25] B. McCormack, G. Gregoriadis. Entrapment of cyclodextrin-drug complexes into liposomes: potential advantages in drug delivery, J.Drug Target. 2 (1994) 449-454.
[26] J. Wu, Q. Liu, R.J. Lee. A folate receptor-targeted liposomal formulation for paclitaxel, Int.J.Pharm. 316 (2006) 148-153.
[27] D. Paolino, D. Cosco, L. Racanicchi, E. Trapasso, C. Celia, M. Iannone, et al. Gemcitabine-loaded PEGylated unilamellar liposomes vs GEMZAR®: Biodistribution, pharmacokinetic features and in vivo antitumor activity, J.Controlled Release. 144 (2010) 144-150.
[28] L.H. Lindner, M. Hossann. Factors affecting drug release from liposomes, Curr.Opin.Drug Discov.Devel. 13 (2010) 111-123.

[29] I. van Rooy, E. Mastrobattista, G. Storm, W.E. Hennink, R.M. Schiffelers. Comparison of five different targeting ligands to enhance accumulation of liposomes into the brain, J.Control.Release. 150 (2011) 30-36.

[30] W.M. Pardridge. The blood-brain barrier: bottleneck in brain drug development, NeuroRx. 2 (2005) 3-14.

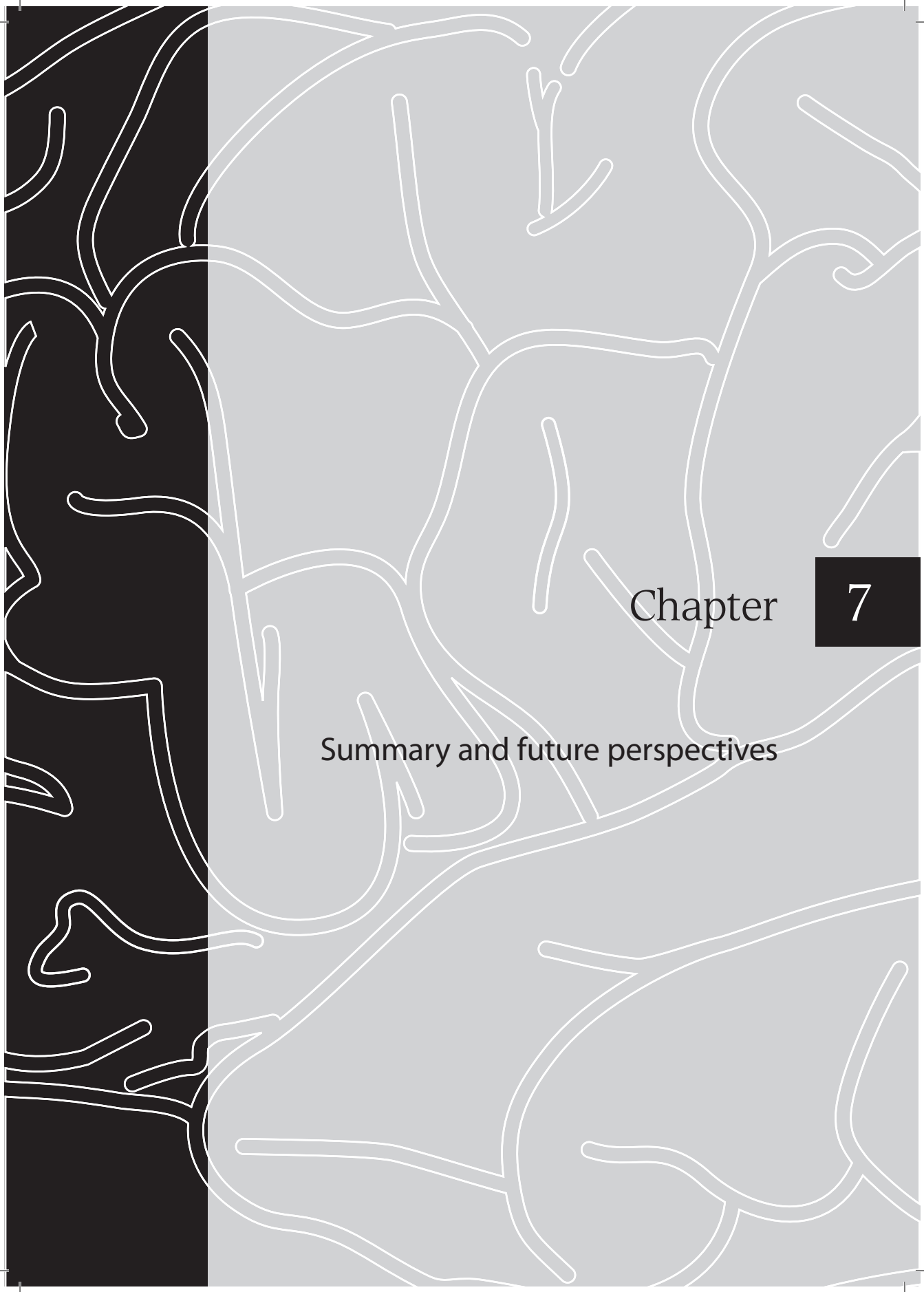

Chapter 7

Summary and future perspectives

Summary

The transport of many central nervous system (CNS) therapeutics to the brain is limited by the presence of the blood-brain barrier (BBB). In this thesis, liposomes modified with brain-targeting ligands were studied for their potential to target to the brain. Additionally, new brain-targeting ligands were identified by phage display and their targeting potential was investigated.

Chapter 1 provides a general introduction on the blood-brain barrier. This barrier is formed by specialized endothelial cells of the brain vasculature, and is supported by cells that are in close contact with the endothelial cells, such as pericytes and astrocytes. The barrier prevents toxic substances from entering the brain and maintains brain homeostasis. However, the downside is that many drugs that are developed to cure brain diseases, cannot substantially cross this barrier and therefore therapeutic concentrations in the brain are not reached. Various strategies have been attempted to tackle this problem. Next to some invasive methods, nanoformulations have been developed with the aim to specifically transport drugs into the brain. In this strategy, particles with nanoscale dimensions carry the drug through the circulation. A targeting ligand on the outside of the particle induces specific uptake of the drug-loaded particle into the endothelial cells of the BBB, after which the drug can be released into the brain. To measure whether a drug or particle has indeed been taken up into the BBB, or even crossed the BBB and entered the brain parenchyma is quite a challenge, especially *in vivo*.

Chapter 2 reviews the methods that have been used to measure the uptake of drugs and nanoparticles into the brain *in vivo*. For drugs that substantially cross the BBB via transmembrane diffusion or carrier-mediated transcytosis, measuring brain uptake is relatively easy because brain entry is rapid, and brain concentrations can reach detectable levels. For these drugs, techniques have been developed to determine various uptake parameters, including the blood to brain influx constant (K_{in}), the permeability-surface area (PS) product, and the brain uptake index (BUI). Nanoparticles are very different from these drugs in size, composition, physicochemical properties and uptake mechanisms. This has led to different methods and approaches to study their brain uptake *in vivo*. Because particles are larger than low molecular weight drug molecules, they can be easily labeled for visualization by microscopy. Therefore, fluorescence and electron microscopy have been used to visualize particles in brain sections. Fluorescence imaging *in vivo* has also been used. A unique aspect of the brain is its role in regulating behavior. Some drugs are able to modulate behavior, which can be used to study their uptake. For example, the opiate antagonist loperamide has an antinociceptive effect in the brain, but normally does

not cross the BBB to reach the brain, so these effects are not seen upon regular intravenous (iv) administration. However, loperamide can be encapsulated into nanoparticles, and if the particles are able to cross the BBB, the antinociceptive effects will occur. These effects can be detected in specifically designed behavioral test, such as the tail-flick test. The final method to study particle uptake into the brain involves quantitative methods, such as determination of pharmacokinetic (PK) parameters, and biodistribution studies. For both of these studies either the particle itself, or an entrapped compound is labeled. In our studies, we used liposomes as nanoformulation. The liposomes were labeled with the metabolically inert [^{3}H]cholesteryl hexadecyl ether, and biodistribution studies were performed to quantify the percentage of liposomes in the blood, brain, and other organs.

In **chapter 3**, these liposomes were modified with five different ligands that were described in literature for brain targeting. This study was performed to estimate the capacity of these ligands to target liposomes to the brain, and to make a comparison to establish which one of these ligands works best. Liposomes were chosen as a delivery vehicle in our studies, because they have been successfully used for brain delivery *in vivo*. The selected ligands were holo-transferrin, RI7217, COG133, angiopep-2, and CRM197. Liposomes surface-modified with these ligands were tested for their brain-targeting capacity *in vitro* and *in vivo*. *In vitro*, only CRM197-modified liposomes were able to bind to murine brain endothelial cells (bEnd.3). Both CRM197 and RI7217-modified liposomes bound to human brain endothelial cells (hCMEC/D3). *In vivo*, uptake of targeted liposomes was tested at 12 hours after iv injection. For some of the ligands, additional time points of 1 and 6 hours were tested. To differentiate between liposomes internalized by the brain endothelial cells, and liposomes that crossed into the brain parenchyma, a brain capillary depletion technique was used to separate these fractions. Only the RI7217 antibody, which is directed against the transferrin receptor, was able to significantly enhance brain uptake *in vivo* at all time points. Uptake in the brain capillaries was up to 10 times higher compared to untargeted liposomes, and uptake in the brain parenchyma was up to 4.3 times higher. The results demonstrated that a fraction of these RI7217 liposomes was able to transcytose from the endothelial cells into the brain parenchyma. Although it has to be noted that changing the formulation parameters, e.g. the ligand density, could yield a different outcome, the results showed the ability of liposomes to target to the transferrin receptor and to mediate brain targeting *in vivo*. Additionally, this chapter showed that measuring brain uptake of nanoparticles is challenging, and that none of the tested targeting ligands were able to get high quantities (>1% of the injected dose) of liposomes into the brain.

In **chapter 4**, we searched for a new specific brain-targeting ligand, using the technique of phage display. A 15-amino acid random peptide phage library was perfused through mouse brain capillaries *in situ*. The phage were infused via the heart, so they would come into contact with multiple endothelial sites (i.e. aorta and carotid arteries) before reaching the brain, allowing for a negative selection of ubiquitous endothelial-binding phage. Two phage clones, displaying 15-amino acid peptides GLAHSFSDFARDFVA (GLA) and GYRPVHNIRGHWAPG (GYR) were selected for brain binding in the *in situ* model. These phage were tested for cross-reactivity with human brain endothelial cells (hCMEC/D3) *in vitro*, and showed significant binding to these cells compared to a random control phage (RVR). This binding was not seen to human endothelial cells of non-brain origin (HUVEC). Binding to hCMEC/D3 cells was dose dependent, and when phage GLA and GYR were individually perfused through a murine brain, their ability to bind to the brain was 6-fold (GLA) and 5-fold (GYR) higher than the control phage, which was not seen when these phage were perfused through a murine lung, which also contains microvascular endothelium. Finally, binding of phage GLA and GYR to hCMEC/D3 cells was visualized by fluorescence microscopy, using a labeled anti-phage antibody. This showed enhanced binding of selected phage GLA and GYR compared to the control phage RVR. Although the GLA and GYR binding sites were unknown, the results indicated that two new phage-displayed peptides had been identified with BBB-targeting properties. To eventually use these displayed peptides as targeting ligands, they need to be coupled to a delivery vehicle.

Therefore, in **chapter 5**, peptides GLA and GYR were synthetically produced. Liposomes were used as a delivery vehicle. A C-terminal cysteine was added to the peptide sequences to enable coupling to maleimide-functionalized phospholipids in the liposomal bilayer. The capacity of the peptides to target the liposomes to the brain was investigated both *in vitro* and *in situ*. Flow cytometry studies with hCMEC/D3 cells showed that these targeted liposomes showed weak binding to the endothelial cells *in vitro*. Also *in situ* perfusion did not result in brain binding, which was surprising since the phage-displayed GLA and GYR did show binding in these settings. We hypothesized that the weak binding of these peptide-coupled liposomes could be ascribed to three main factors that were changed when the peptides were 'moved' from phage to liposome: change of vehicle shape, change of peptide density, and change of peptide conformation. In this chapter we showed that the peptide density on the liposomes influenced the binding of the liposomes to the cells. However, this effect was minor. To study the influence of the peptide conformation, the GLA peptide was recombinantly produced fused to the N1-N2 domains of the phage p3 minor coat protein (p3-GLA) to mimic its conformation when displayed on phage particles. Binding of liposomes modified with either the GLA peptide or the p3-GLA protein to hCMEC/D3 cells was studied, and the p3-

GLA-liposomes showed a higher binding to the cells compared to the GLA-liposomes. The experiments indicated that bringing the GLA peptide into the original phage protein environment improved peptide binding capacity. This could indicate that the GLA peptide, with some modifications, may be used as a brain-targeting ligand in the future. The exact mechanism by which the p3 phage protein influenced the binding capacity of the GLA peptide remains to be determined.
To this end, the liposomes were tested for their targeting capacity. The ultimate clinical aim is to encapsulate drugs into the liposomes, in order to transport them into the brain.

Therefore, in **chapter 6**, liposomal formulations of two new neurotensin-degrading enzyme (NTDE) inhibitors were prepared. These central nervous system (CNS) drugs hold great potential for treating psychotic disorders, however, they show poor brain uptake *in vivo*. Therefore, liposomal formulations of these two hydrophobic drugs, named compound 1 (C1) and compound 2 (C2) were prepared. Association of these compounds with the liposomal bilayer, subsequent liposomal stability, and compound release in the presence of albumin were studied. Entrapment of the compounds in the liposomal bilayer showed the solubilizing properties of the liposomes. Size and polydispersity index of the compound-entrapped liposomes did not change over 1 month, showing good colloidal stability of the formulations. The amount of compounds associated with the liposomes decreased within one day. After this, the association remained stable at 4°C. For C1, association remained stable at 37°C in HEPES buffered saline, and the compound was gradually released in the presence of bovine serum albumin. For C2, the release was rapid in both HBS and BSA at 37°C. Therefore, C1 was more suitable for this liposome formulation than C2. The formulation may solve the problem of poor solubility, and carry the drugs in the circulation. To induce uptake of the liposomes into the brain, they should preferentially be coupled to a brain-targeting ligand like p3-GLA. Further investigations are needed to show that liposomal formulations of NTDE inhibitors can be used to deliver sufficient amounts of these inhibitors to the brain, to act as future therapeutics for psychotic disorders.

Future perspectives

Brain diseases

Over the past decades, it has become obvious that the major hurdle for the development of new CNS drugs is the blood-brain barrier. For some brain diseases, including depression, epilepsy, and pain, traditional small-molecule pharmaceuticals have been developed that were able to cross the BBB to a sufficient extent to provide treatment. However, for some of the most severe CNS diseases, including Alzheimer's disease, Huntington's disease, stroke, and brain cancer, small molecules that cross the BBB have been unable to satisfactorily treat these diseases. Therapeutics that are effective against these diseases are continuously under development. However, since the vast majority of small molecule drugs (>98%) do not cross the BBB, new drugs to treat these diseases will very likely not reach the brain [1].

Major hurdles

As described in chapter 1 and 2, many strategies have been attempted to get these drugs across the BBB. One of the most innovative methods is by the incorporation of drugs into a targeted nanosized delivery vehicle, after which the drugs can be administered intravenously. Intravenous administration is safer than injection directly into the brain or CSF and results in a more widespread brain distribution because every neuron is in close proximity to a brain capillary [2]. Therefore, strategies to get therapeutics from the blood into the brain are extremely important.

The ideal brain-targeting nanoparticle should be non-toxic, biodegradable, small in size (<150 nm), able to incorporate large quantities of drugs, have a strong affinity to a receptor expressed highly on the BBB, be taken up by receptor-mediated endocytosis, and mediate transcytosis and exocytosis of the drug at the brain side of the BBB. Such a delivery device for brain therapeutics is still lacking today. Although a lot of these requirements have been reached, especially binding to a receptor and endocytosis into the brain endothelial cells are the crucial steps that are the most difficult to accomplish (figure 1).

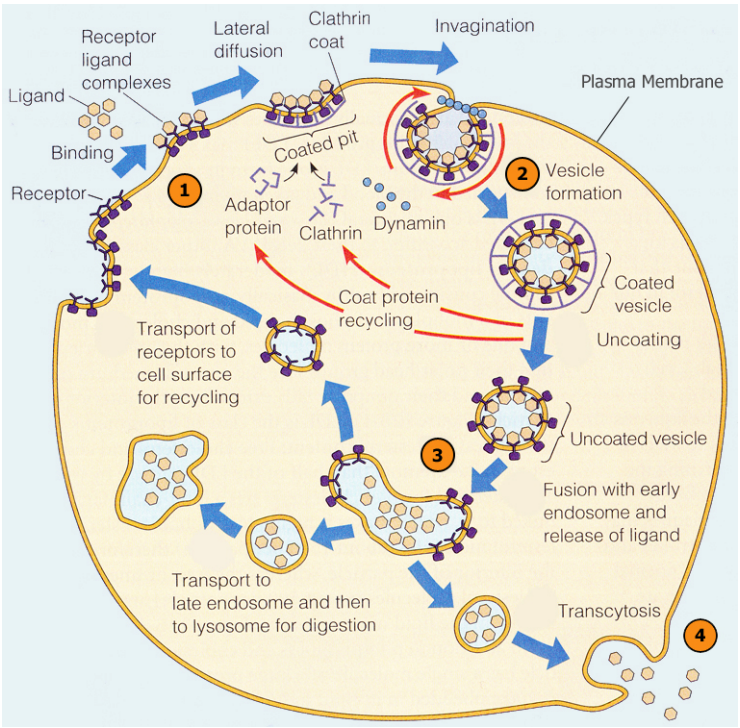

Figure 1. *Schematic representation of receptor-mediated endocytosis, and subsequent intracellular trafficking pathways. (**1**) receptor binding. (**2**) endocytosis. (**3**) movement through the cell. (**4**) exocytosis.*

Targeting ligands

In chapter 3, we found that out of five ligands that were tested for brain targeting, only the anti-transferrin receptor monoclonal antibody RI7217 was able to target liposomes across the BBB. Because this antibody enters the BBB by receptor-mediated endocytosis, a nanoparticle such as a liposome can be taken up by this mechanism, because its size allows internalization in the endosome [3]. For the peptides that were able to bind to brain endothelium in chapter 4 and 5 (GYR, GLA, and p3-fused GLA), it is unknown to which structure on the surface of the endothelial cells they bind. Binding to a receptor would be preferable, because this could mediate uptake of drug-loaded particles. Another type of transporter that could be a possible binding site is a carrier, which could induce carrier-mediated transcytosis. As described in chapter 2, carriers are membrane-fixed transporters that can mediate the uptake of endogenous substrates such as nutrients. For other molecules to be taken up via such carriers, they have to be small in size (<600 Da) and closely mimic the endogenous ligand. Therefore, it would not be preferable for a ligand that is attached to a nanoparticle to target to a carrier, because this could not lead

to endocytosis of the particle. However, brain targeting exploiting carriers has been accomplished by using a different strategy: drug-ligand conjugation. For example, Gynther et al. [4] conjugated the anti-inflammatory drug ketoprofen to L-tyrosine, which is specifically transported into the brain via the large neutral amino acid transporter (LAT1). It was shown by rat brain perfusion that the conjugate was concentration-dependently taken up into the brain by the LAT1 transporter. For our peptides GLA and GYR, further investigation is needed into the binding and/or uptake mechanism, to find out whether the endothelial association could be mediated through a carrier. Drug-ligand conjugates can also be targeted to a receptor, to mediate uptake via endocytosis. Even when the strategy of nanoparticle conjugation does not result in targeting, drug-ligand conjugation may be a suitable option. For example, the 19-amino acid peptide angiopep-2 that we used in chapter 3, did not induce uptake of liposomes into the brain *in vitro* or *in vivo* in our experiments. However, a conjugate of angiopep-2 and paclitaxel (named ANG1005), was shown to be transported across the BBB, via the low-density lipoprotein receptor-related protein (LRP) [5]. This conjugate is now in clinical trials, and a Phase I study in patients with recurrent glioblastomas showed that the drug was fairly well tolerated and displayed good activity [6]. For GYR, GLA, and p3-fused GLA, a conjugation strategy could also be interesting to explore in further investigations.

For p3-fused GLA, it remains questionable whether this protein could eventually be used as a targeting ligand *in vivo*, because the phage-derived 240-amino acid protein is likely to cause an immunogenic reaction [7,8]. Nevertheless, it is of interest to find out if specific peptide properties can be restored or enhanced by putting the peptide back into its initial environment used for screening. If this strategy works, a less immunogenic approach could later on be applied that mimics the p3 environment, such as the addition of a few flanking p3 amino acids to the peptide, or the introduction of conformation restraints to the peptide, for example by introducing cysteine residues which change the conformation by forming disulfide bonds [9].

Another molecule that has been explored for targeted delivery to the BBB is the antioxidant glutathione, which is thought to be transported into brain endothelial cells via carrier-mediated transport [10,11]. More *et al.* [12] synthesized a glutathione analog, and conjugated this to the anti-Parkinson drugs dopamine and adamantamine, and showed transport of these prodrugs through cell monolayers. The Dutch biotechnology company to-BBB is currently developing a liposomal formulation coated with glutathione-conjugated polyethylene glycol (G-Technology®) for the delivery of anticancer drugs and analgesic peptides to the brain [13]. They expect to initiate a phase I/II clinical trial within a year. This shows that research and progress in the field of BBB drug delivery is ongoing,

which is highly needed because the number of individuals with CNS diseases is expected to increase in the future [1].

Brain cancer

Several companies that are developing brain drug delivery systems are aiming at the treatment of brain tumors. In fact, brain drug delivery systems for anticancer drugs are predominant in clinical trials compared to drugs against any other brain disease. The most frequent primary CNS tumors are gliomas. In these tumors, the endothelial cells, astrocytes, and pericytes show significant abnormalities compared to healthy BBB cells. This can lead to an increased number of fenestrations, tight junction opening, and increased non-selective transendothelial transport [2,14]. Next to brain cancer, other diseases that affect the BBB integrity include cerebrovascular diseases (e.g. ischemia) and inflammatory diseases (e.g. multiple sclerosis). Although partial BBB disruption may result in increased BBB transport activity, sufficient brain penetration and diffusion of drugs is still limited in these situations [15]. Therefore, these clinical trials are majorly important to find a new efficient drug delivery systems to treat these devastating diseases. Hopefully some of these trials will be successful, and result in a translation of drug delivery systems to the market.

Drugs

As was demonstrated in chapter 6, the encapsulation of a drug into a nanoparticle can be difficult, especially when highly hydrophobic drug molecules are incorporated in the bilayer of a liposome. If the drug and nanoparticle are not a perfect match, other options can be explored. In the case of our liposomes (p3-GLA or RI7217-targeted), drugs that are either less hydrophobic compared to the NTDE inhibitors used in chapter 6, or hydrophilic drugs that can be encapsulated inside the core of the liposomes, may be more suitable options. Possibilities for liposome encapsulation in future experiments include drugs to treat brain cancers (e.g. doxorubicin, 5-fluorouracil, topotecan or gemcitabine), and drugs to treat inflammatory brain diseases (e.g. amphotericin B or prednisolone) [15,16].

Antibodies

In our studies, the ligand that induced the highest uptake of liposomes into the brain was the RI7217 antibody (chapter 3). Antibodies against BBB receptors are generally regarded as good targeting ligands for the brain [17,18]. In order to create new targeting ligands for BBB targeting, phage display can be a useful tool, especially if a screening method is performed in which the exact binding site you are screening for is unknown (as was the case in our perfusion screenings in chapter 4). In our studies, a phage library displaying 15-mer peptides was used, but phage libraries displaying antibodies have also been generated, and may be useful in future studies to generate high affinity targeting ligands.

Initially, libraries have been constructed which display the binding fragments of conventional antibodies (VH+VL domain). More recently, libraries expressing the VHH domains of camelid heavy-chain antibodies have been created (figure 2). These domains are smaller, and easier to construct [19]. Studies have even shown that some of these 15 kDa VHH domains were able to cross the BBB, even if they were not specifically selected to do so [20]. Although the mechanism by which this transport occurs remains to be elucidated, such findings may result in an important role for VHH domains as brain targeting ligands in the near future.

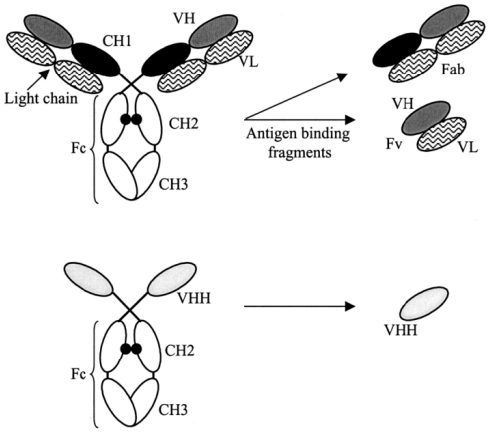

Figure 2. *Schematic illustration of the conventional (top) and camelid heavy-chain antibodies (bottom). To the right of the arrows the minimal intact antigen-binding fragments are represented. CH: constant domain. VH: variable domain of heavy chain of conventional antibodies. VL: variable domain of light chain of conventional antibodies. Fv: variable fragments of conventional antibodies. VHH: variable domain of heavy chain of camelid antibodies. Reprinted from Reviews in molecular biotechnology [19].Copyright (2001), with permission from Elsevier.*

Detection techniques

In recent years, reliable *in vitro* models of the BBB have been developed to assist in the determination of BBB transport [21]. However, testing *in vivo* whether a targeting ligand, drug, or nanoparticle has successfully crossed the BBB and entered the brain parenchyma remains to be difficult. The main factors contributing to these difficulties are the generally low percentages of drug or vehicle that enter the brain, the concentration present in the blood within the brain capillaries, and the challenge to discriminate between substances within the brain endothelium and the brain parenchyma. However, it has to be stressed that when *in vivo* experiments are carried out, proper measures need to be taken to deal with these difficulties, as was discussed in chapter 2. Sensitive detection assays, perfusion techniques to remove remaining blood from the brain capillaries, and capillary depletion techniques are essential in such experiments. Because these techniques are technically difficult and laborious, easier and quick detection methods are needed to provide sensitive and quantitative values for brain uptake studies. Progression in the field of *in vivo* imaging could provide a noninvasive solution for these issues [22,23], if the technique develops in such a way that high resolution images can be obtained in which

discrimination between endothelium and parenchyma is possible, and if quantitative uptake values can be obtained.

Administration routes

Next to intravenous administration, as was used in our studies (chapter 3 and 5), alternative drug administration routes should also be explored, such as intranasal delivery. Small lipophilic molecules like cocaine and morphine are able to reach the brain after intranasal administration. Direct pathways from the nasal cavity into the brain have been suggested, possibly bypassing the circulation and the BBB [24]. The exact mechanism of brain entry via the nasal route remains unclear, however, this pathway has been successfully explored for the delivery of lipid nanoparticles to the brain [25,26], and could provide a noninvasive alternative to intravenous injection.

Conclusion

To date, no single delivery strategy can provide a conclusive solution to all the challenges associated with brain drug delivery. The brain is extremely efficient in keeping foreign substances out, making drug delivery exceedingly difficult. Recent and future advances in drug delivery systems, targeting ligands, administration routes, and detection techniques could provide new insights and should eventually lead to the development of safe and efficient brain drug delivery systems.

References

[1] W.M. Pardridge. Why is the global CNS pharmaceutical market so under-penetrated? Drug Discov.Today. 7 (2002) 5-7.

[2] K.E. Schlageter, P. Molnar, G.D. Lapin, D.R. Groothuis. Microvessel organization and structure in experimental brain tumors: microvessel populations with distinctive structural and functional properties, Microvasc.Res. 58 (1999) 312-328.

[3] W.M. Pardridge. The blood-brain barrier: bottleneck in brain drug development, NeuroRx. 2 (2005) 3-14.

[4] M. Gynther, K. Laine, J. Ropponen, J. Leppanen, A. Mannila, T. Nevalainen, et al. Large neutral amino acid transporter enables brain drug delivery via prodrugs, J.Med.Chem. 51 (2008) 932-936.

[5] A. Regina, M. Demeule, C. Che, I. Lavallee, J. Poirier, R. Gabathuler, et al. Antitumour activity of ANG1005, a conjugate between paclitaxel and the new brain delivery vector Angiopep-2, Br J Pharmacol. 155 (2008) 185-197.

[6] P.Y. Wen. American Society of Clinical Oncology 2010: report of selected studies from the CNS tumors section, Expert Rev.Anticancer Ther. 10 (2010) 1367-1369.

[7] Y.L. Yip, G. Smith, R.L. Ward. Comparison of phage pIII, pVIII and GST as carrier proteins for peptide immunisation in Balb/c mice, Immunol.Lett. 79 (2001) 197-202.

[8] N.E. van Houten, K.A. Henry, G.P. Smith, J.K. Scott. Engineering filamentous phage carriers to improve focusing of antibody responses against peptides, Vaccine. 28 (2010) 2174-2185.

[9] V.J. Hruby. Conformational restrictions of biologically active peptides via amino acid side chain groups, Life Sci. 31 (1982) 189-199.

[10] R. Kannan, J.F. Kuhlenkamp, E. Jeandidier, H. Trinh, M. Ookhtens, N. Kaplowitz. Evidence for carrier-mediated transport of glutathione across the blood-brain barrier in the rat, J.Clin.Invest. 85 (1990) 2009-2013.
[11] A. Tsuji, I.I. Tamai. Carrier-mediated or specialized transport of drugs across the blood-brain barrier, Adv.Drug Deliv.Rev. 36 (1999) 277-290.
[12] S.S. More, R. Vince. Design, synthesis and biological evaluation of glutathione peptidomimetics as components of anti-Parkinson prodrugs, J.Med.Chem. 51 (2008) 4581-4588.
[13] to-BBB: developing targeted CNS drugs. www.tobbb.com (2010).
[14] M.C. Papadopoulos, S. Saadoun, C.J. Woodrow, D.C. Davies, P. Costa-Martins, R.F. Moss, et al. Occludin expression in microvessels of neoplastic and non-neoplastic human brain, Neuropathol.Appl.Neurobiol. 27 (2001) 384-395.
[15] E. Garcia-Garcia, K. Andrieux, S. Gil, P. Couvreur. Colloidal carriers and blood-brain barrier (BBB) translocation: A way to deliver drugs to the brain? International Journal of Pharmaceutics. 298 (2005) 274-292.
[16] S. Pasha, K. Gupta. Various drug delivery approaches to the central nervous system, Expert Opin.Drug Deliv. 7 (2010) 113-135.
[17] R.J. Boado, Q.H. Zhou, J.Z. Lu, E.K. Hui, W.M. Pardridge. Pharmacokinetics and brain uptake of a genetically engineered bifunctional fusion antibody targeting the mouse transferrin receptor, Mol.Pharm. 7 (2010) 237-244.
[18] W.M. Pardridge. Drug targeting to the brain, Pharm.Res. 24 (2007) 1733-1744.
[19] S. Muyldermans. Single domain camel antibodies: current status, Reviews in Molecular Biotechnology. 74 (2001) 277-302.
[20] U. Iqbal, U. Trojahn, H. Albaghdadi, J. Zhang, M. O'Connor-McCourt, D. Stanimirovic, et al. Kinetic analysis of novel mono- and multivalent VHH-fragments and their application for molecular imaging of brain tumours, Br.J.Pharmacol. 160 (2010) 1016-1028.
[21] M.M. Ribeiro, M.A. Castanho, I. Serrano. In vitro blood-brain barrier models--latest advances and therapeutic applications in a chronological perspective, Mini Rev.Med.Chem. 10 (2010) 262-270.
[22] C. von Zur Muhlen, N.R. Sibson, K. Peter, S.J. Campbell, P. Wilainam, G.E. Grau, et al. A contrast agent recognizing activated platelets reveals murine cerebral malaria pathology undetectable by conventional MRI, J.Clin.Invest. 118 (2008) 1198-1207.
[23] T.J. Moriarty, M.U. Norman, P. Colarusso, T. Bankhead, P. Kubes, G. Chaconas. Real-time high resolution 3D imaging of the lyme disease spirochete adhering to and escaping from the vasculature of a living host, PLoS Pathog. 4 (2008) e1000090.
[24] S.V. Dhuria, L.R. Hanson, W.H. Frey 2nd. Intranasal delivery to the central nervous system: mechanisms and experimental considerations, J.Pharm.Sci. 99 (2010) 1654-1673.
[25] S. Patel, S. Chavhan, H. Soni, A.K. Babbar, R. Mathur, A.K. Mishra, et al. Brain targeting of risperidone-loaded solid lipid nanoparticles by intranasal route, J.Drug Target. (2010).
[26] J. Ali, M. Ali, S. Baboota, J.K. Sahani, C. Ramassamy, L. Dao, et al. Potential of nanoparticulate drug delivery systems by intranasal administration, Curr.Pharm.Des. 16 (2010) 1644-1653.

Appendices

Nederlandse samenvatting

List of abbreviations

List of publications

Affiliations of collaborating authors

Curriculum vitae

Dankwoord

Nederlandse Samenvatting

Geneesmiddelen en de bloed-hersenbarrière

Er bestaan vele hersenziekten waarvoor toediening van geneesmiddelen noodzakelijk is voor de behandeling. Voorbeelden hiervan zijn de ziekte van Alzheimer, de ziekte van Parkinson, hersenkanker, epilepsie, depressie en schizofrenie. Als deze geneesmiddelen aan de patiënt worden toegediend, komen ze in het bloed terecht, waarna ze door het hele lichaam vervoerd worden. In de hersenen is een groot netwerk van bloedvaatjes aanwezig. Deze voorzien alle hersencellen van zuurstof en voedingsstoffen. Ook geneesmiddelen die aan de patiënt worden toegediend komen in deze bloedvaatjes terecht. Om hun werking uit te voeren moeten de geneesmiddelen vanuit de bloedvaatjes door de bloedvatwand heen om in het hersenweefsel (hersenparenchym) terecht te komen. Dit is echter niet makkelijk. In Figuur 1 is een dwarsdoorsnede van zo'n hersenbloedvat te zien. De wand van het bloedvat bestaat uit zogenaamde endotheelcellen. In vele andere organen in het lichaam kunnen geneesmiddelen tussen deze endotheelcellen door om het orgaanweefsel te bereiken. Echter, in de hersenen zijn deze cellen zeer stevig aan elkaar vast geregen met structuren die 'tight junctions' worden genoemd. Daarom spreekt men ook wel van de bloed-hersenbarrière (BHB). Vanwege deze barrière kan bijna geen enkel geneesmiddel tussen deze cellen passeren om in de hersenen te komen. Bovendien zijn er rond de hersenvaten nog astrocyten, pericyten en een basaal membraan aanwezig als extra barrière.

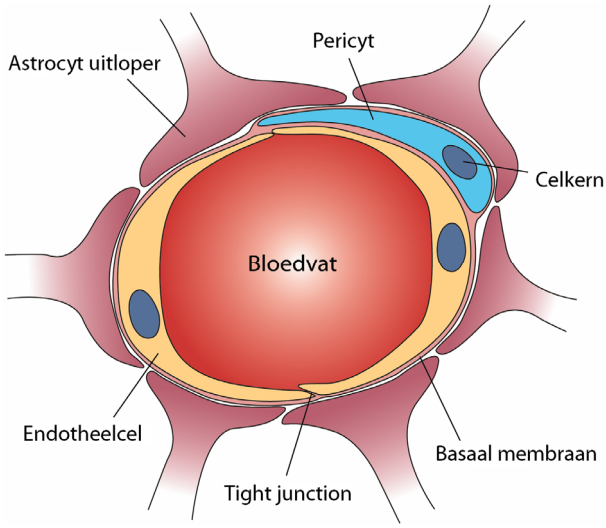

Figuur 1. *Schematische weergave van een dwarsdoorsnede door een hersenbloedvat. De bloedvatwand bestaat uit endotheelcellen, die aan elkaar vast geregen zijn met tight junctions. De endotheelcellen worden omgeven met pericyten en uitlopers van astrocyten.*

Transport over de bloed-hersenbarrière

Naast de route tussen de endotheelcellen door is er nog een andere manier voor stoffen om het parenchym te bereiken: door de endotheelcellen heen (transcytose). Een klein gasmolecuul zoals zuurstof kan door het celmembraan van de endotheelcellen heen diffunderen. Sommige kleine lipofiele geneesmiddelen kunnen dit ook. Echter, dit is slechts een heel klein gedeelte van alle potentiële hersengeneesmiddelen.

Een voedingsstof zoals een aminozuur kan binden aan speciale transportmoleculen. Dit zijn zeer selectieve kanaaltjes die zich op het celmembraan van de endotheelcellen bevinden. Na deze binding gaat het aminozuur door de transporter heen en komt hij aan de binnenkant (cytoplasma) van de endotheelcel terecht. Van daaruit kan hij vervoerd worden naar de andere kant van de endotheelcel en daar weer uitgescheiden worden in het hersenparenchym. Dit soort transportmoleculen in het membraan zijn zeer kieskeurig. Ze kunnen alleen stoffen binden en transporteren die er precies in passen. Zo'n stof wordt ook wel een ligand genoemd. Verder kunnen ze stoffen vervoeren die heel erg op het natuurlijke ligand lijken omdat ze even groot zijn en dezelfde eigenschappen hebben, dat zijn niet-originele liganden. In het verleden zijn er een aantal geneesmiddelen ontwikkeld die deze eigenschappen hebben, zoals L-DOPA dat naar de hersenen getransporteerd wordt via de grote neutrale aminozuur transporter (LAT) voor de behandeling van de ziekte van Parkinson.

Een andere manier voor een stof om in een hersenendotheelcel opgenomen te worden is via een receptor. Receptoren bevinden zich ook in het celmembraan van de endotheelcellen, maar ze werken anders dan de genoemde transportmoleculen. Receptoren zijn ook zeer kieskeurig en kunnen alleen een ligand binden dat precies op de receptor past. Als zo'n ligand aan de receptor gebonden is, ontstaat er een instulping in het celmembraan op de plaats van het receptor-ligand complex. Deze instulping vormt een blaasje die in de endotheelcel naar binnen gaat. Dit wordt ook wel endocytose genoemd (zie Figuur 1 uit hoofdstuk 7). In het blaasje bevindt zich het ligand, wat nu getransporteerd kan worden naar de andere kant van de endotheelcel, en uitgescheiden kan worden in het hersenparenchym. Liganden die op deze manier naar de hersenen gaan zijn vaak eiwitten die belangrijk zijn voor de hersenen, zoals insuline en transferrine. Het grote verschil met opname via een transporter is dat zo'n blaasje meer ruimte biedt dan de opening van een transporter. Hierdoor kunnen grote moleculen die aan het ligand gekoppeld zijn met het ligand meegetrokken worden de cel in. Van dit principe is gebruik gemaakt in dit proefschrift.

Gericht geneesmiddeltransport

In dit proefschrift zijn liganden die kunnen binden aan hersenendotheel gekoppeld aan liposomen (Figuur 2). Liposomen zijn vetbolletjes van meestal 100-200 nanometer in diameter, en zijn gemaakt van vetten die vergelijkbaar zijn met de vetten in de celmembranen in het lichaam. Daardoor zijn ze niet toxisch voor het lichaam. In deze liposomen kunnen geneesmiddelen verpakt worden die normaal niet de hersenen in gaan. Als het ligand op het liposoom aan de receptor op het hersenendotheel bindt, dan zal het ligand in een blaasje in de cel worden opgenomen. Het liposoom wat aan het ligand vast zit zal dan in het blaasje mee naar binnen gaan. Vanuit de endotheelcel kan het geneesmiddel naar het hersenparenchym vervoerd worden. Op deze manier kan een geneesmiddel wat bij normale toediening niet of nauwelijks in de hersenen komt, toch naar de hersenen gestuurd worden. Dit noemen we gericht geneesmiddeltransport.

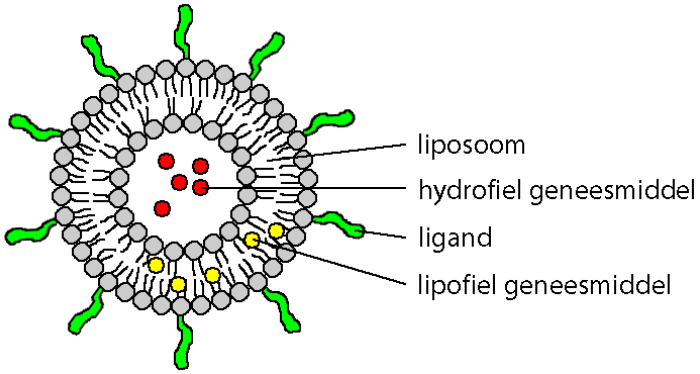

Figuur 2. *Schematische weergave van een doorsnede door een gericht liposoom. Het liposoom bestaat uit een dubbele laag van vetten met liganden gekoppeld aan de buitenkant. Binnenin het liposoom is een waterige holte waarin hydrofiele geneesmiddelen opgelost kunnen worden. Lipofiele geneesmiddelen kunnen opgelost worden in de vetlaag van het liposoom.*

Het onderzoek in dit proefschrift

In dit proefschrift zijn verschillende liganden gebruikt. Sommige liganden waren gekozen omdat ze in de literatuur waren beschreven als hersengericht ligand. Andere liganden hebben we zelf geïdentificeerd. Er is o.a. gekeken naar binding en opname van ligand-gekoppelde liposomen in gekweekte hersenendotheelcellen (*in vitro*) en naar opname van ligand-gekoppelde liposomen in muizenhersenen (*in vivo*).

In **hoofdstuk 1** wordt een algemene inleiding gegeven over de BHB. Behalve de genoemde endotheelcellen dragen ook andere cellen bij aan de vorming van de BHB, zoals pericyten en astrocyten. In het hoofdstuk wordt een aantal methodes besproken die gebruikt zijn om geneesmiddelen beter in de hersenen te krijgen. Het meten of een

geneesmiddel of nanodeeltje daadwerkelijk is opgenomen in hersenen is een hele uitdaging, vooral *in vivo*.

Hoofdstuk 2 geeft een overzicht van de methoden die in de literatuur zijn gebruikt om de opname van geneesmiddelen en nanodeeltjes te meten in de hersenen *in vivo*. Voor geneesmiddelen die in voldoende mate over de BHB getransporteerd worden (via transmembraan diffusie of via transporter-gemedieerde transcytose) is het meten van hersenopname relatief eenvoudig omdat de hersenenopname snel is en de hersenenconcentraties detecteerbare niveaus kunnen bereiken. Voor deze geneesmiddelen is een aantal technieken ontwikkeld om verschillende opname-parameters te bepalen, waaronder de bloed-naar-hersenen instroom constante, het permeabiliteit-oppervlakte product en de hersenopname index. Nanodeeltjes zijn zeer verschillend vergeleken met dit soort geneesmiddelen in termen van omvang, samenstelling, fysisch-chemische eigenschappen en opname mechanismen. Dit heeft geleid tot verschillende methodes en benaderingen om hun hersenopname to onderzoeken *in vivo*. Omdat de deeltjes relatief groot zijn (groter dan kleine geneesmiddelmoleculen), kunnen ze eenvoudig worden gelabeld voor visualisatie met behulp van microscopie. Daarom zijn fluorescentie- en elektronenmicroscopie gebruikt om deeltjes te visualiseren in hersenencoupes. Ook is fluorescentiebeeldvorming *in vivo* gebruikt. Een uniek aspect van de hersenen is de rol bij het reguleren van gedrag. Sommige geneesmiddelen kunnen gedrag moduleren, wat gebruikt kan worden om hun opname te bestuderen. Bijvoorbeeld, de opiaatantagonist loperamide heeft een pijnstillend effect in de hersenen, maar gaat normaal gesproken niet over de BHB om de hersenen te bereiken, zodat het pijnstillend effect niet wordt waargenomen na normale intraveneuze (iv) toediening. Echter, loperamide kan worden ingesloten in nanodeeltjes, en als deze deeltjes in staat zijn om de BHB te passeren, zal het pijnstillende effect optreden. Dit effect kan worden gemeten in speciaal ontworpen gedragstesten, zoals de staart-zwiep test. Andere methodes om deeltjesopname in de hersenen te bestuderen zijn kwantitatieve methodes, zoals de bepaling van farmacokinetische (PK) parameters en biodistributie studies. Voor beide van deze studies wordt ofwel het deeltje zelf, of een ingesloten stof gelabeld. In onze studies hebben we gebruik gemaakt van liposomen als nanodeeltje. De liposomen werden gelabeld met het metabolisch inerte [^{3}H] cholesteryl hexadecyl ether en biodistributie studies werden uitgevoerd om het percentage liposomen in het bloed, de hersenen, en andere organen te kwantificeren.

In **hoofdstuk 3** werden deze liposomen gekoppeld aan verschillende liganden die zijn beschreven in de literatuur voor doelgerichte hersenopname. Deze studie werd uitgevoerd om de capaciteit van deze liganden om liposomen te laten accumuleren in de hersenen te beoordelen, en om te bepalen welk van deze liganden het beste werkte. De

geselecteerde liganden waren holo-transferrine, RI7217, COG133, angiopep-2, en CRM197. *In vitro* waren alleen de CRM197-gekoppelde liposomen in staat om te binden aan muizen hersenendotheelcellen (bEnd.3). Zowel CRM197 als RI7217-gekoppelde liposomen waren in staat om te binden aan menselijke hersenendotheelcellen (hCMEC/D3). *In vivo* werd de opname van de hersengerichte liposomen getest op 12 uur na iv injectie. Voor een aantal van de liganden werd de opname ook op 1 en 6 uur na injectie getest. Om onderscheid te maken tussen liposomen die opgenomen waren door de hersenendotheelcellen en liposomen die terecht waren gekomen in het hersenparenchym, werden de hersenvaten en het parenchym van elkaar gescheiden door middel van centrifugatie in aanwezigheid van dextraan. Alleen het RI7217 antilichaam, dat gericht is tegen de transferrine receptor, was in staat om de hersenenopname *in vivo* op alle gemeten tijdstippen significant te verbeteren. Opname in de hersenvaten was tot 10 maal hoger in vergelijking met niet-gerichte liposomen en opname in het hersenparenchym was tot 4,3 keer hoger. De resultaten toonden aan dat een gedeelte van deze RI7217 liposomen kon worden overgedragen van de endotheelcellen naar het hersenparenchym. Hoewel moet worden opgemerkt dat het veranderen van de formuleringsparameters, zoals de ligand dichtheid, tot een andere uitkomst zou kunnen leiden, toonden de resultaten het vermogen aan van deze liposomen om te binden aan de transferrine receptor aanwezig op het hersenendotheel en daarmee doelgerichte sturing naar de hersenen *in vivo* te bemiddelen. Daarnaast liet dit hoofdstuk zien dat het meten van hersenopname van nanodeeltjes uitdagend is, en dat geen van de geteste liganden in staat was om de liposomen in grote hoeveelheden (>1% van de geïnjecteerde dosis) in de hersenen te krijgen.

In **hoofdstuk 4** hebben we gezocht naar nieuwe specifieke hersengerichte liganden, met behulp van de 'faagdisplay' techniek. Hierbij worden fagen (virussen die bacteriën infecteren) gebruikt om een eiwit of peptide te vinden dat kan binden aan een doelreceptor. In dit hoofdstuk werden de hersenvaten van muizen *in situ* doorgespoeld met een buffer die een willekeurige 15-aminozuur peptide faag bibliotheek bevatte. De fagen werden toegediend via het hart, zodat ze in contact konden komen met verscheidene endotheliale oppervlaktes (aorta en halsslagaders) vóór het bereiken van de hersenvaten, waardoor een negatieve selectie van alomtegenwoordige endotheelbindende fagen ontstond. Twee faagklonen, die de 15-aminozuur peptiden GLAHSFSDFARDFVA (GLA) en GYRPVHNIRGHWAPG (GYR) op hun oppervlakte weergaven, werden geselecteerd voor hersenbinding in het *in situ* model. Deze fagen werden getest op crossreactiviteit met menselijke hersenendotheelcellen (hCMEC/D3) *in vitro*, en toonden significante binding aan deze cellen ten opzichte van een willekeurige controlefaag (RVREPYPGMLERYRA). Deze binding werd niet waargenomen voor menselijke endotheelcellen van niet-hersen oorsprong (HUVEC). Binding aan de

hCMEC/D3 cellen was dosisafhankelijk, en wanneer faag GLA en GYR individueel geperfundeerd werden door muizenhersenen, was hun vermogen om aan de hersenen te binden 6 keer (GLA) en 5 keer (GYR) hoger dan de controlefaag, wat niet werd gezien toen deze fagen werden geperfundeerd door een muizenlong, dat ook microvasculair endotheel bevat. Ten slotte werd de binding van faag GLA en GYR aan hCMEC/D3 cellen gevisualiseerd door middel van fluorescentie microscopie, met behulp van een gelabeld anti-faag antilichaam. Dit liet een verhoogde binding van de geselecteerde fagen GLA en GYR zien in vergelijking met de controlefaag RVR. Hoewel de GLA en GYR bindingsplaatsen onbekend waren, lieten de resultaten zien dat twee nieuwe peptides met BHB-gerichte eigenschappen met behulp van faagdisplay waren geïdentificeerd. Om deze peptides uiteindelijk te gebruiken als doelgerichte liganden, moesten ze worden gekoppeld aan een geneesmiddeldragersysteem.

Daarom werden de peptides GLA en GYR in **hoofdstuk 5** synthetisch geproduceerd om ze vervolgens met een functionele groep (een C-terminale cysteïne) aan het oppervlak van liposomen te koppelen.. De capaciteit van de peptides om de liposomen doelgericht naar de hersenen te sturen werd zowel *in vitro* als *in situ* onderzocht. Flowcytometrie studies met hCMEC/D3 cellen toonden aan dat deze gerichte liposomen niet aan de gekweekte endotheelcellen bonden. Ook *in situ* perfusie resulteerde niet in hersenbinding, hetgeen verwonderlijk was aangezien GLA en GYR peptides op een faag wel binding lieten zien in dergelijke experimenten. We veronderstelden dat het gebrek aan binding van deze peptide-gekoppelde liposomen kon worden toegeschreven aan drie hoofdfactoren die werden gewijzigd toen de peptides waren 'verplaatst' van faag naar liposoom: verandering van de vorm van de drager, verandering van de peptide dichtheid, en verandering van de peptide conformatie. In dit hoofdstuk lieten we zien dat de peptide dichtheid op de liposomen van invloed was op de binding van de liposomen aan de cellen. Echter, dit effect was gering. Om de invloed van de peptide conformatie te onderzoeken, werd het GLA peptide recombinant geproduceerd, gefuseerd aan de N1-N2 domeinen van het faag p3 manteleiwit (p3-GLA). Op deze manier werd de conformatie die het peptide heeft wanneer deze wordt weergegeven op een faagdeeltje nagebootst. Binding van liposomen gekoppeld aan het GLA peptide of het p3-GLA eiwit aan hCMEC/D3 cellen werd bestudeerd, en de p3-GLA-liposomen lieten een hogere binding aan de cellen zien in vergelijking met de GLA-liposomen. Het experiment toonde aan dat het terugbrengen van het GLA peptide naar de originele faageiwit-omgeving de bindingscapaciteit van het peptide herstelde. Dit zou erop kunnen duiden dat het GLA peptide, met enkele wijzigingen, in de toekomst gebruikt zou kunnen worden als een hersengericht ligand. Het exacte mechanisme waarmee het p3 faageiwit het bindend vermogen van het GLA peptide beïnvloedde moet nog worden bepaald.

Tot hier werden de liposomen getest op hun doelgerichtheid. Het uiteindelijke klinische streven is om geneesmiddelen in te sluiten in deze liposomen, om ze te vervoeren naar de hersenen.

Daarom werden in **hoofdstuk 6** liposomen met geneesmiddelen bereid. De gebruikte geneesmiddelen waren twee nieuwe neurotensine-degraderende enzym (NTDE)-remmers. Deze CZS geneesmiddelen hebben grote mogelijkheden voor de behandeling van psychotische aandoeningen, maar ze laten slechte hersenopname *in vivo* zien. Daarom werden liposomale formuleringen bereid van deze twee hydrofobe geneesmiddelen, die verbinding 1 (C1) en verbinding 2 (C2) werden genoemd. De associatie van deze verbindingen met de liposomale bilaag, de daarop volgende liposomale stabiliteit en het vrijkomen van de verbindingen in de aanwezigheid van albumine werden bestudeerd. Insluiting van de verbindingen in de liposomale bilaag liet de oplossende eigenschappen van de liposomen zien. De grootte en polydispersiteitsindex van de verbindingsbevattende liposomen veranderde niet gedurende een maand, wat een goede colloïdale stabiliteit van de formuleringen betekende. De hoeveelheid van de verbindingen die geassocieerd was met de liposomen daalde binnen een dag. Daarna bleef de associatie stabiel bij 4 °C. Voor C1 bleef de associatie bij 37 °C stabiel in een HEPES gebufferde zoutoplossing en de verbinding kwam geleidelijk vrij in de aanwezigheid van albumine. Voor C2 was het vrijkomen snel in zowel de zoutoplossing als de albumine oplossing bij 37 °C. Daarom was C1 meer geschikt voor een liposomale formulering dan C2. De formulering kan de slechte oplosbaarheid van de verbinding verbeteren en de verbinding vervoeren in de bloedcirculatie. Voor het induceren van opname van de liposomen in de hersenen, moeten ze bij voorkeur worden gekoppeld aan een hersengericht ligand, zoals p3-GLA of RI7217. Verder onderzoek is nodig om aan te tonen dat de liposomale formuleringen van de NTDE-remmers gebruikt kunnen worden om voldoende hoeveelheden van deze verbindingen te transporteren naar de hersenen, om actief te zijn als toekomstige therapeutica voor psychotische aandoeningen.

In **hoofdstuk 7** werden de resultaten samengevat en nieuwe wegen voor veder onderzoek bediscussieerd.

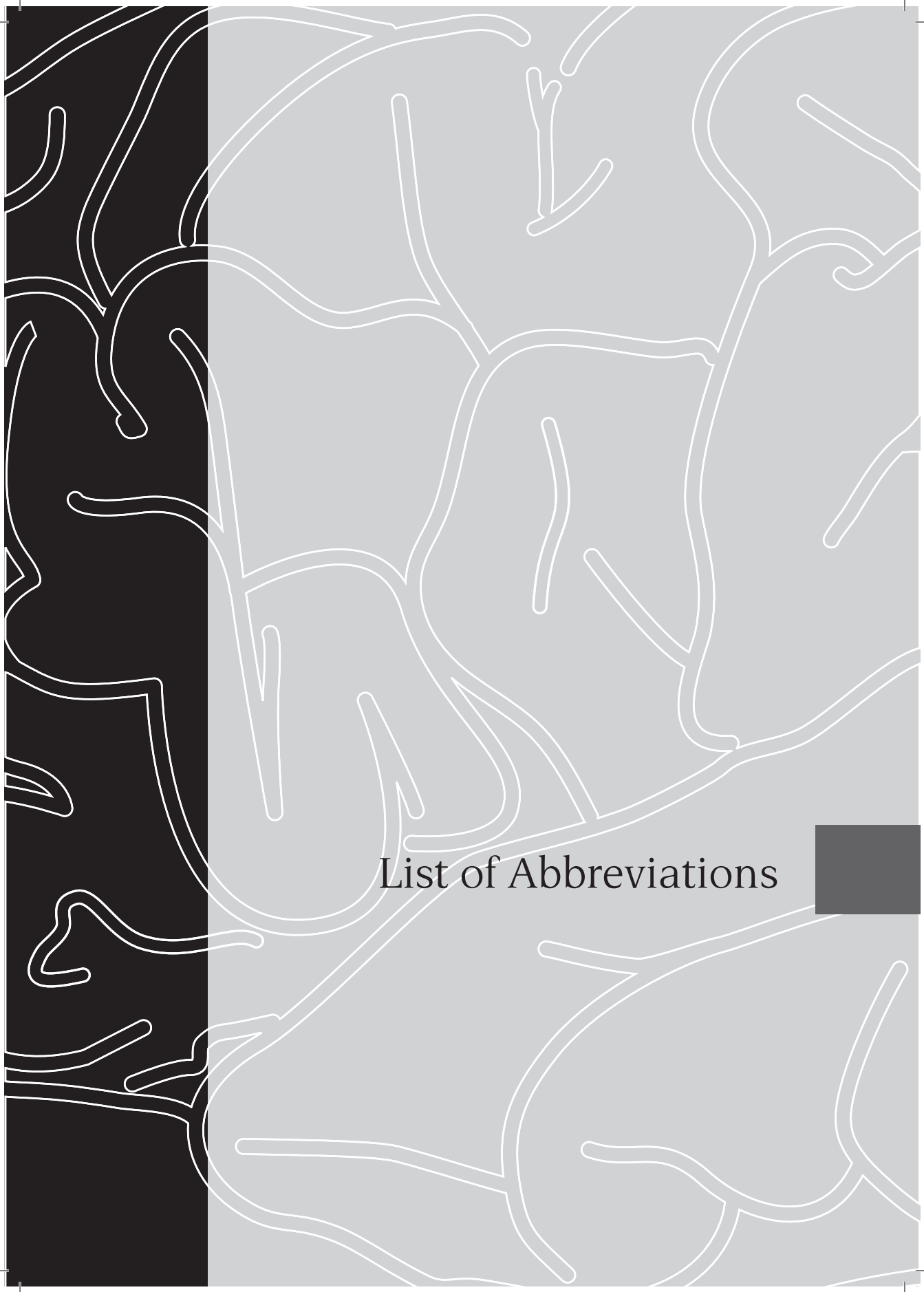

List of Abbreviations

%AD	percentage of added dose
%ID	percentage of injected dose
%MPE	percentage of maximal possible effect
AJ	adherens junction
ANG	angiopoetin
ApoE	apolipoprotein E
APP	β-amyloid precursor protein
BBB	blood-brain barrier
BDNF	brain-derived neurotrophic factor
bFGF	basic fibroblast growth factor
BSA	bovine serum albumin
BUI	brain uptake index
cHSA	cationized human serum albumin
CNS	central nervous system
CQ	clioquinol
CRM	cross reacting material
CSF	cerebrospinal fluid
DLS	dynamic light scattering
DPPC	dipalmitoyl phosphatidylcholine
DSPE	distearoyl phosphatidylethanolamine
DT	diphtheria toxin
DTR	diphtheria toxin receptor
EGF	epidermal growth factor
EM	electron microscopy
EPC	egg phosphatidylcholine
EPG	egg phosphotidylglycerol
FM	fluorescence microscopy
GDNF	glial-derived neurotrophic factor
GLUT	glucose transporter
HB-EGF	heparin-binding epidermal growth factor-like growth factor
HBS	HEPES-buffered saline
HBSS	Hank's balanced salt solution
hCMEC	human cerebral microvascular endothelial cells
HDL	high-density lipoprotein
HPLC	high-performance liquid chromatography
HSA	human serum albumin
HUVEC	human umbilical vein endothelial cells
ic	intracerebral
icv	intracerebroventricular
ISF	interstitial fluid
iv	intravenous
JAM	junctional adhesion molecule

K_{in}	brain influx constant
KPI	kunitz protease inhibitor
LAT	large neutral amino acid transporter
LDL	low-density lipoprotein
LDLR	low-density lipoprotein receptor
Lf	lactoferrin
LRP	low-density lipoprotein receptor-related protein
MAO	monoamine oxidase
MFI	mean fluorescence intensity
MPB	maleimidophenyl butyryl
MPE	maximal possible effect
MRP	multidrug resistance protein
NBD	N-(7-nitrobenz-2-oxa-1,3-diazol-4-yl)
NGF	nerve growth factor
NP	nanoparticle
NTDE	neurotensin-degrading enzyme
OCT	organic cation transporter
P-gp	p-glycoprotein
PBCA	poly(butyl cyanoacrylate)
PBS	phosphate-buffered saline
PDI	polydispersity index
PE	phosphatidylethanolamine
PEG	polyethylene glycol
PET	positron emission tomograpy
pI	isoelectric point
PK	pharmacokinetic
PLGA	poly(lactic-co-glycolic acid)
PS product	permeability-surface area product
RAP	receptor associated protein
SATA	N-succinimidyl-S-acetylthioacetate
SLN	solid lipid nanoparticle
SPECT	single photon emission computed tomograpy
Tf	transferrin
TfR	transferrin receptor
TGFβ	transforming growth factor-β
TJ	tight junction
TU	transducing unit
UPLC	ultra-performance liquid chromatography
VLDL	very-low-density lipoprotein
ZO	zonula occludens
γ-GT	γ-glutamyl transpeptidase

List of Publications

Publications from this thesis

I. van Rooy, S. Cakir-Tascioglu, P.O. Couraud, I.A. Romero, B. Weksler, G. Storm, W.E. Hennink, R.M. Schiffelers, E. Mastrobattista. Identification of peptide ligands for targeting to the blood-brain barrier, Pharm.Res. 27 (2010) 673-682.

I. van Rooy, S. Cakir-Tascioglu, W.E. Hennink, G. Storm, R.M. Schiffelers, E. Mastrobattista. In Vivo Methods to Study Uptake of Nanoparticles into the Brain, Pharm.Res. 28 (2011) 456-471.

I. van Rooy, E. Mastrobattista, G. Storm, W.E. Hennink, R.M. Schiffelers. Comparison of five different targeting ligands to enhance accumulation of liposomes into the brain, J.Control.Release. 150 (2011) 30-36.

I. van Rooy, S.Y. Wu, G. Storm, W.E. Hennink, H. Dinter-Heidorn, R.M. Schiffelers, E. Mastrobattista. Preparation and characterization of liposomal formulations of neurotensin-degrading enzyme inhibitors, Int.J.Pharm. (2011), in press.

I. van Rooy, W.E. Hennink, G. Storm, R.M. Schiffelers, E. Mastrobattista. Attaching the phage display-selected GLA peptide to liposomes: factors influencing target binding. Submitted for publication.

Other publications

R.M. Schiffelers, **I. van Rooy**, G. Storm. siRNA-mediated inhibition of angiogenesis, Expert Opin.Biol.Ther. 5 (2005) 359-368.

S. Oliveira, **I. van Rooy**, O. Kranenburg, G. Storm, R.M. Schiffelers. Fusogenic peptides enhance endosomal escape improving siRNA-induced silencing of oncogenes, Int.J.Pharm. 331 (2007) 211-214.

R.M. Schiffelers, H.K. de Wolf, **I. van Rooy**, G. Storm. Synthetic delivery systems for intravenous administration of nucleic acids, Nanomedicine (Lond). 2 (2007) 169-181.

Podium presentations

36th Meeting of the Controlled Release Society (2009) Copenhagen, Denmark.
11th Edition of the FIGON Dutch Medicines Days (2009) Lunteren, The Netherlands.
11th European Workshop on Particulate Systems (2010) Paris, France.

Patent application

I. van Rooy, W.E. Hennink, E. Mastrobattista, R.M. Schiffelers, H. Dinter-Heidorn, R.P. Brinkhuis, J.C. van Hest, F.P. Rutjes. Peptide ligands for targeting to the blood-brain barrier. WO/2011/005098.

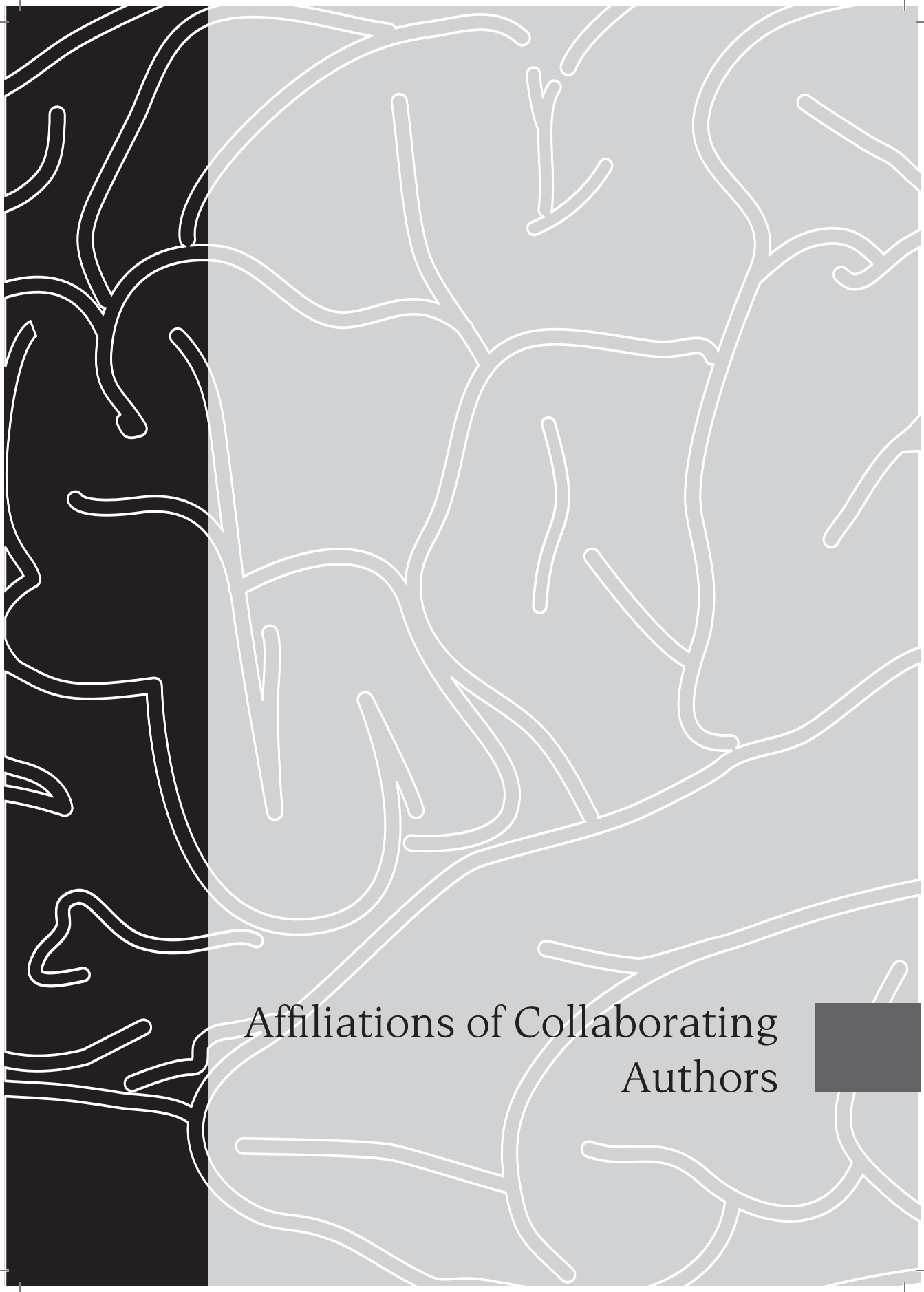

Affiliations of Collaborating Authors

Enrico Mastrobattista
Department of Pharmaceutics, Utrecht Institute for Pharmaceutical Sciences (UIPS), Utrecht University, P.O. Box 80082, 3508 TB Utrecht, The Netherlands

Raymond M Schiffelers
Department of Pharmaceutics, Utrecht Institute for Pharmaceutical Sciences (UIPS), Utrecht University, P.O. Box 80082, 3508 TB Utrecht, The Netherlands

Wim E Hennink
Department of Pharmaceutics, Utrecht Institute for Pharmaceutical Sciences (UIPS), Utrecht University, P.O. Box 80082, 3508 TB Utrecht, The Netherlands

Gert Storm
Department of Pharmaceutics, Utrecht Institute for Pharmaceutical Sciences (UIPS), Utrecht University, P.O. Box 80082, 3508 TB Utrecht, The Netherlands

Serpil Cakir-Tascioglu
Unilever R&D, Olivier van Noortlaan 120, 3133 AT Vlaardingen, The Netherlands

Heike Dinter-Heidorn
Abbott Products GmbH, Hans-Böckler-Allee 20, 30173 Hannover, Germany

Pierre-Olivier Couraud
Institut Cochin, Université Paris Descartes, CNRS (UMR 8104), Paris, France.

Ignacio A Romero
Department of Biological Sciences, The Open University, Milton Keynes, United Kingdom

Babette Weksler
Department of Medicine, Weill Medical College, New York, NY

Curriculum Vitae

Inge van Rooy was born on December 20th 1982 in Waalre, The Netherlands. In 2001, she graduated from the Sondervick college secondary school in Veldhoven, after which she started studying biomedical sciences at Utrecht University. In 2004, she started a Master's program in drug innovation at Utrecht University. During her Master's, she performed a 9-month research project in the department of pharmaceutics at Utrecht University, to study the knockdown of a mutated form of the K-Ras protein in colon carcinoma cells. This was accomplished using RNA interference. After this, she performed a 6-month research project at N.V. Organon (now MSD) in Oss, to study the effect of haptoglobin on the immune system, using a haptoglobin-knockout mouse. In 2006, she obtained her Master's degree and started her PhD project at Utrecht University under the supervision of prof. dr. ir. Wim Hennink, prof. dr. Gert Storm, dr. Enrico Mastrobattista and dr. Raymond Schiffelers. This project was a collaboration with Abbott Healthcare Products B.V. (formerly Solvay Pharmaceuticals B.V.). The results of this PhD project are presented in this thesis.

Dankwoord

Mijn ontdekkingsreis naar de bloed-hersenbarrière is voorbij. Deze periode van ruim vier jaar was een hele speciale tijd, waarin ik veel heb geleerd over het doen van onderzoek en vele bijzondere mensen heb leren kennen. Alle mensen die voor mij iets betekend hebben in deze periode wil ik hier graag bedanken.

Op de eerste plaats dank aan mijn begeleiders.

Beste Wim, tijdens werkbesprekingen hield je er altijd goed de vaart in. Ook al sloot mijn biologisch georiënteerd onderzoek niet altijd aan bij je kennis, je deed er alles aan om mijn project tot een succesvol einde te brengen. Nagekeken artikelen of andere emails stuurde je vaak nog na 11 uur 's avonds (en dan was je de dag erna om 8:30 verbaasd dat ik je email niet gezien had!). Bedankt voor de zinvolle werkbesprekingen en je begeleiding.

Beste Gert, je was minder betrokken in mijn project dan Wim, maar je was altijd bereikbaar (per email) voor een vraag of advies over liposoom samenstellingen, circulatietijden, of radioactieve labels. Heel erg bedankt!

Beste co-promotoren, als ik in een dipje zat over teleurstellende resultaten, dan was er niets wat me meer kon opvrolijken dan een werkbespreking met jullie! Met een nespressootje erbij werd aan de resultaten altijd een positieve draai gegeven. Ook werden nieuwe ideeën in een mum van tijd gecreëerd, waardoor ik altijd een stukje vrolijker weer verder ging.

Beste Enrico, gedurende mijn tijd als aio ben jij degene geweest die zich het actiefst bezig heeft gehouden met mijn begeleiding. Je toonde altijd interesse en kwam met vele goede ideeën, daar ben ik je enorm dankbaar voor.

Beste Ray, ook al had je het vaak veel te druk; op de momenten dat ik je het meest nodig had was je er. Je uitgebreide kennis over in vivo experimenten hebben me erg geholpen. Ook als het op de praktijk aankwam draaide jij je hand niet om voor een dissectie of iv injectie. Of het nu 8 uur 's ochtends was of 9 uur 's avonds, die 200 µl was altijd raak!

In het lab heb ik veel waardevolle hulp gehad van onze analisten. Louis, bedankt voor je behulpzaamheid en het delen van je liposomenkennis. Mies, met name bedankt voor je hulp bij de HPLC. Ebel, ontzettend bedankt voor je hulp bij dissecties en iv injecties.

Ik heb het genoegen gehad om twee Master studenten voor 9 maanden te begeleiden en te laten werken aan mijn project.

Serpil, jouw inzet en enthousiasme waren groot, ik vond het ontzettend leuk om met je samen te werken! Samen hebben we denk ik wel duizend agar platen gegoten! Bedankt voor je bijdrage aan hoofdstuk 2 en 4 van dit proefschrift.

Shin-Ying, the plan was that you were going to do in vitro studies, but things turned out differently and you ended up working on liposomal formulations. It turned out well because most of your work resulted in chapter 6 of this thesis! Thank you for your contribution!

Conny, jij was niet mijn studente, maar in de maanden dat je op de 6e stage liep zijn we wel goede vriendinnen geworden. Superleuk dat we elkaar nog steeds zien! Bedankt voor alle gezelligheid!

Ik heb altijd met veel plezier gewerkt in het goede oude Wentgebouw. Deze aangename sfeer werd met name bepaald door mijn labgenootjes! Daarom wil ik in het bijzonder de mensen waarmee ik in z505 gezeten heb bedanken: Ethlinn, Ellen, Bart, Maria, Joris, Afrouz en Grzegorz, ontzettend bedankt voor de leuke sfeer op het lab! Ook bedankt voor de leuke conversaties tijdens de lunches en de activiteiten die we ondernomen hebben.

Verder wil ik heel (ex-)biofarmacie bedanken voor de aangename sfeer in de groep! Dankjewel Maryam, Rolf, Amir, Isil, Steffen, Frits, Roy, Pieter, Marina, Amir, Hajar, Sima, Negar, Kim, Alex, Sylvia, Albert, Markus, Marcel, Sabrina, Chiara, Barbara, Lidija, en de rest!

Buiten het Wentgebouw heb ik samengewerkt met een TI Pharma consortium. Hiervoor wil ik in het bijzonder Daan bedanken. Ook dank aan Heike en alle andere consortium leden, met name de mede-aio's: Julia (we had great times in Groningen and Utrecht!), Katica, René, Hanneke, Joost en Hans.

Terwijl ik dit schrijf komt mijn promotiedatum dichterbij. Ik ben ontzettend blij dat ik tijdens mijn promotie zal worden bijgestaan door twee geweldige paranimfen!

Lieve Emmy, met jouw promotiedatum 2 maanden na de mijne zitten we bijna tegelijkertijd in hetzelfde schuitje! Gelukkig kunnen we bij elkaar onze frustraties kwijt over artikelen schrijven en het afgewezen worden door sponsors! Ook al zit het soms tegen, we weten allebei dat het allemaal goed komt. Fantastisch dat jij mijn paranimf bent! 2011 is ons jaar!

Dear Melody, I was proud to be your paranimf last year, and I'm so happy that you will be mine! I love how you always come up with great things we can do for fun: drinking cocktails, film festivals, museum nights, comedy nights, sunday brunches, and so on. I always enjoy the time we spend together, and I hope there are many more great times to come!

Ook wil ik mijn familie bedanken.

Lieve pap en mam, jullie hebben me altijd m'n eigen gang laten gaan en me gesteund in de studiekeuzes die ik maakte. Ik heb veel aan jullie te danken! Ontzettend bedankt voor jullie warmte, steun en interesse, jullie zijn fantastische ouders!

Lieve Lonneke en Niels, bedankt voor de leuke tijden en gezelligheid wanneer we met z'n allen samen zijn! Nielie, succes met de Mangerie! Lon, succes met je carrière, misschien wel in Barcelona!

Beste opa, zelfs op jouw leeftijd ben je nog altijd nieuwsgierig naar nieuwe technologieën en mijn onderzoek! Bedankt voor je interesse!

Lieve Mike, tenslotte wil ik jou bedanken. Als ik na een drukke werkdag thuis kom dan ben jij daar en dat maakt me vrolijk. Als ik bij jou ben kan ik alles om me heen vergeten en helemaal mezelf zijn. Met jouw liefde, humor en gezelligheid kan ik alles aan en dat betekent heel veel voor me! Je behulpzaamheid bij het maken van vele figuren en de omslag van dit proefschrift was fantastisch! Bedankt voor alles liefje, ik hou van je.

Inge